MASTERARBEIT | MASTER'S THESIS

Titel | Title

Long-range signalling mediated by extracellular vesicles in hepatocellular carcinoma

verfasst von | submitted by

Leila Djerlek BSc

angestrebter akademischer Grad | in partial fulfilment of the requirements for the degree of

Master of Science (MSc)

Wien | Vienna, 2024

Studienkennzahl lt. Studienblatt | Degree programme code as it appears on the student record sheet:	UA 066 834
Studienrichtung lt. Studienblatt | Degree programme as it appears on the student record sheet:	Masterstudium Molekulare Biologie
Betreut von | Supervisor:	ao. Univ.-Prof. Mag. Dr. Wolfgang Mikulits

Acknowledgement

I extend my deepest gratitude to Ao.Univ.-Prof. Mag. Dr. Wolfgang Mikulits for his invaluable guidance, patience and support throughout my master's journey. His expertise and mentorship were instrumental in shaping my research and academic skills.

I am also profoundly thankful to my team members, whose collaboration and insights enriched my thesis work immeasurably. Especially I want to thank Ing. Heidemarie Huber, Dr. Viola Hedrich, Dr. Kristina Breitenecker and Denise Heiden for all the laughs and the good times during my masters. Also, I want to thank Dr. med. univ. Gregor Ortmayr for supporting my experimental work.

I want to thank Dr. Sibylle Madlener, Lab Manager of the Molecular Neuro-Oncology Laboratory at the University Clinic for Pediatrics and Adolescent Medicine, for all the NTA measurements she made at any time and for her useful advice and support. I would also like to express my gratitude to the Faculty of Chemistry, specifically the Department of Analytical Chemistry under the supervision of Univ.-Prof. Dr. Christopher Gerner, for their technical support and provision of resources.

I must also acknowledge my parents Alija and Safeta, my brother Elmer, my boyfriend Alen and my family and friends for their enduring support as well as their encouragement; their belief in my abilities sustained me during this challenging and rewarding journey.

Thank you all for being part of this significant phase of my academic life.

CONTENTS

Abstract

Hepatocellular carcinoma (HCC) represents a significant global health challenge with increasing incidence and mortality rates. HCC is largely influenced by risk factors such as chronic viral infections with hepatitis B or C virus, alcohol, and metabolic dysfunction-associated steatotic liver disease. The development of HCC often involves chronic liver damage leading to fibrosis and cirrhosis, setting the stage for malignancy. Current therapeutic strategies include surgical resection, liver transplantation, and systemic therapies, yet resistance and recurrence continue to pose major challenges.

In this study, we focused on the metastatic abilities of HCC cells. We hypothesized that long range signals from HCC cells are sent through extracellular vesicles (EVs) to establish a pre-metastatic niche (PMN) that is essentially involved in the colonization of spreading HCC cells. In particular, we examined the impact of transforming growth factor (TGF)-β signalling on EV secretion and the composition of the EV cargo as well as on the fusion with target cells.

We show that EVs derived from TGF-β-treated HCC cells exhibited a larger size and increased release compared to those from untreated cells. Blocking TGF-β signalling with LY2109761 did not alter the cargo of EVs. Notably, HCC-derived EVs tagged with CD63-green fluorescent protein or stained with PKH67 fused with stromal target cells, thus showing their potential to circulate through the bloodstream and generate a PMN. Our data further suggest that EVs could serve as crucial mediators of cell-to-cell communication between mesenchymal and epithelial HCC cells, leading to changes in epithelial plasticity. Together, these data point to the importance of EV-driven long range signalling in HCC progression. Despite promising preliminary findings, further studies are required to validate these results and to understand the mechanisms underlying long-range signalling by EVs in response to TGF-β signalling.

Zusammenfassung

Das hepatozelluläre Karzinom (HCC) stellt aufgrund steigender Inzidenz- und Sterblichkeitsraten eine bedeutende globale Gesundheitsherausforderung dar, die maßgeblich durch Risikofaktoren wie chronische Infektionen mit Hepatitis B oder C Viren, Alkoholabusus und steatotische Lebererkrankungen beeinflusst wird. Die HCC Entwicklung umfasst häufig chronische Leberschäden, die zu Fibrose und Zirrhose führen und den Weg für eine Malignität bereiten. Gegenwärtige therapeutische Strategien umfassen chirurgische Resektion, Lebertransplantation und systemische Therapien, jedoch stellen Behandlungsresistenz und Rückfälle weiterhin große Herausforderungen dar.

In dieser Studie haben wir uns auf die metastatischen Fähigkeiten von HCC Zellen konzentriert. Wir haben angenommen, dass Langstreckensignale von HCC Zellen über extrazelluläre Vesikel (EVs) gesendet werden, damit eine prämetastatische Nische (PMN) für die Kolonisierung von sich ausbreitenden HCC Zellen etabliert werden kann. Speziell untersuchten wir den Einfluss des transformierenden Wachstumsfaktors (TGF)-β auf die EV-Sekretion, die Zusammensetzung der EV Fracht sowie auf die Fusion mit Zellen der Tumorumgebung.

Wir zeigen, dass EVs, die von TGF-β-behandelten HCC Zellen stammen, eine zunehmende Größe und eine erhöhte Freisetzung im Vergleich zu EVs aus unbehandelten Zellen aufweisen. Die Blockade des TGF-β Signalwegs mit LY2109761 verändert die Beladung der EVs nicht. Durch die Markierung mit CD63/grün fluoreszierenden Protein oder mit PKH67 konnte nachgewiesen werden, dass EVs von HCC Zellen mit stromalen Zellen der Tumorumgebung fusionieren. Diese Beobachtung zeigt das Potenzial der EVs auf, durch den Blutkreislauf zu zirkulieren und eine PMN zu bilden. Unsere Daten deuten außerdem daraufhin, dass EVs als entscheidende Vermittler der Zell-Zell Kommunikation zwischen mesenchymalen und epithelialen HCC Zellen dienen können, was zu Veränderungen der epithelialen Plastizität führt. Zusammengenommen unterstreichen diese Daten die Bedeutung von EV-gesteuerten Langstreckensignalen bei der HCC Progredienz. Trotz vielversprechender vorläufiger Ergebnisse sind weitere Studien erforderlich, um diese Ergebnisse zu validieren und die Mechanismen zu verstehen, die der

weitreichenden Signalübertragung durch EVs als Reaktion auf den TGF-β Signalweg zugrunde liegen.

1 Introduction

1.1 Hepatocellular Carcinoma – Prevalence, Epidemiology and Etiology

In 2020, liver cancer was the third leading cause of cancer deaths globally [1]. It shows a high mortality rate with 830,200 deaths [1]. 905,700 new cases were reported globally [1]. Hepatocellular carcinoma (HCC), making up 75%-85% of these cases, is the most prevalent form of liver cancer, indicating a significant health challenge with poor outcome [2]. The number of cases has been rising and is expected to grow by 55% by 2040, reaching 1.4 million new cases [3]. Currently, HCC represents a significant global health concern and is projected to become increasingly burdensome in the future [3].

Risk factors for HCC includes hepatitis B (HBV), hepatitis C (HCV) and hepatitis D virus (HDV) infections, chronic alcohol consumption, metabolic dysfunction-associated steatotic liver disease (MASLD), often leading to metabolic dysfunction associated steatohepatitis (MASH) [4]. The incidence and mortality rates of HCC vary globally due to regional risk factors [4]. HBV infections are most prevalent in Asia, while HCV is more frequent in Western countries [4]. Alcohol abuse is a worldwide problem regarding HCC development with a prevalence in Central/Eastern Europe [4]. Obesity, type 2 diabetes, and fatty liver disease are more present in wealthier countries [4]. Notably, East Asia and Africa report the highest HCC incidence and mortality, with a noticeable increasing trend in Europe and North America [4]. HCC cases are lower in developed countries excluding France, Japan, and Italy [5]. The liver is prone to cancer because it's constantly exposed to harmful substances that it filters from the blood, leading to chronic inflammation and damage [5]. Chronic liver disease exhibits a higher incidence in males compared to females, which may be attributed to the greater prevalence of HBV, HCV, and alcohol consumption among the male population [5].

1.1.1 Chronic Liver Injury and Cirrhosis as Risk Factors for HCC Development

The path to HCC often involves progressive liver damage, starting from fibrosis to cirrhosis – a condition marked by necrosis of hepatocytes and subsequent fibrotic scarring as shown in Figure 1 [5, 6]. Notably, liver cirrhosis precedes HCC in approximately 80–90% of cases, positioning cirrhosis as the primary risk factor for the emergence of HCC [5]. Among the aetiologies of cirrhosis, HBV and HCV infections are identified as major contributors [5]. In the pathogenesis of HCC, cirrhosis represents a critical juncture wherein the continuous necrosis of hepatocytes leads to the accumulation of fibrotic tissue, significantly altering liver architecture and function [5]. The molecular pathogenesis of HCC is complex and involves multiple genetic and epigenetic alterations that drive the transformation of normal hepatocytes into cancer cells [5, 7]. It can be categorized into two distinct etiological groups: those of viral origin and those arising from non-viral causes [5]. In the adult liver, telomerase is generally inactive, which leads to telomere shortening, hepatocyte senescence, and the potential development of cirrhosis [8]. It happens due to chronic inflammation and exposure to carcinogens which induce repeated cycles of cell necrosis followed by proliferation [9]. Reactivation of the TERT gene and abnormal telomerase expression initiate malignancy in mouse models [6]. The reactivation of TERT occurs through multiple mechanisms, with promoter mutations being the most frequent, present in approximately 40–60% of cases [6, 9]. This is considered a key early mutational event in the development of HCC [6]. Persistent liver damage leads to chronic inflammation due to an imbalance between pro-inflammatory and anti-inflammatory signals [10]. This ongoing inflammation causes tissue remodelling in the liver, characterized by the accumulation of extracellular matrix (ECM) components and the development of fibrous scars. This process is recognized as a premalignant stage, setting the stage for further liver disease progression [10].

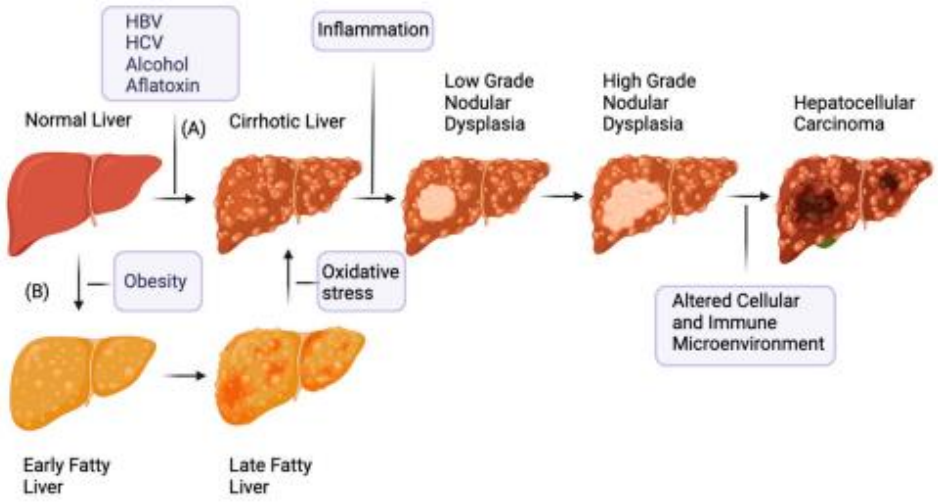

Figure 1: HCC development.

The pathogenesis mechanism of HCC induced by A) chronical exposition of viruses and toxins. This exposure results in cirrhosis, which over time promotes the formation of low-grade dysplastic nodules through chronic inflammation (LGDN), leading to the progression of high-grade dysplastic nodules (HGDN). The altered cellular and immune microenvironment of the cirrhotic liver causes development of HCC. The alternative pathway B) induces HCC through fatty liver disease, initiated by obesity and by oxidative stress as the disease progresses. This leads to cirrhosis, followed by chronic inflammation which promotes LGDN and HGDN and eventually HCC as in pathway A. Picture taken from Coffin, P., et. Al. 2023.

1.1.2 Viral Causes of HCC

The etiological association between HBV, HCV, and HDV with the development of HCC is well-established, reflecting the correlation between the global incidence of HCC and the prevalence of these viral infections [5]. HBV plays a central role in HCC oncogenesis, in the presence or absence of cirrhosis [5]. HCC can happen through chronic HBV infection in which the viral genetic material integrates into the host DNA of hepatocytes, disrupts normal cell function and potentially initiates oncogenic transformation [5, 9, 11, 12]. HBV genome fragments are often found in hepatocarcinoma cells [5]. Such conditions support the generation of mutations in the host genome, resulting in genetic changes by chromosomal rearrangements, inactivation of tumour suppressor genes, and activation of oncogenes [5]. HCC development in the absence of cirrhosis is a rare event mostly due to viral infection followed by viral insertion near a cancer gene that can modify the expression or function of the gene and promote malignant transformation [5]. Genes targeted by HBV insertions are: TERT, MLL4, CCNA2 and CCNE1 [9]. Furthermore, an HBV

infection with co-exposure to aflatoxin B1 (AFB1) noticeably escalates the risk of developing HCC up to 70% [13, 14]. Notably, the high incidence of HCC in Guatemala can potentially be explained by an AFB1 signature mutation (R249S) in the TP53 gene [13]. Nearly 50% of both sample variants identified a TP53 mutation, with 25% of samples showing the AFB1-signature mutation [13]. The absence of overlap between the R249S mutation and HBV infection in the cohort indicates a unique mutation profile in Guatemalan HCC cases [13]. AFB1 metabolites cause DNA damage by forming covalent and promutagenic DNA adducts, particularly inducing G→T transversions at codon 249 of the TP53 gene, leading to a p53-R249S mutation [15, 16]. This mutation is present in 50% of HCC patients in Africa and up to 90% in Qidong, China, both regions with high AFB1 exposure, and is not detected in other TP53 hotspot regions [15, 16]. *In vitro* studies suggest that the AGG sequence context is a favourable site for AFB1 adducts [15]. This specificity indicates that the p53-R249S mutation may confer a selective advantage in liver cancer development [15]. HBV infection may increase the formation of AFB1-induced mutations at codon 249 of TP53 due to chronic inflammation and oxidative stress in hepatocytes [15]. This process potentially raises the mutation load at TP53's codon 249 [15]. This synergistic interaction underscores the multifactorial nature of HCC pathogenesis, where both viral and environmental carcinogens contribute to the disease progression [4].

Individuals infected with HCV exhibit a 15- to 20-fold increase in the risk of developing HCC [5]. HCV is as an RNA virus, which does not integrate into the host genome [5]. Epidemiological evidence indicates that co-infection with HBV and HCV substantially increases the risk of HCC progression [4, 5]. HDV, which is an RNA virus, requires the presence of HBV surface antigens for its replication and subsequent infectivity [4]. In a large study, patients with HBV and acute HDV infection had a significantly higher risk of developing HCC [17]. Similarly, those with chronic HDV infection also faced an elevated risk, with an RR of 3.9 (95% CI 1.6–7.2), compared to individuals with only HBV infection [17]. This highlights the severe impact of HDV co-infection compared to HBV monoinfection in patients regarding HCC development [17]. Such dual infections are correlated with a heightened risk of fibrosis development, accelerated

cirrhosis progression, and serve as an independent prognostic factor for the progression of HCC [4, 5].

1.1.3 Non-viral Causes of HCC

Non-viral etiologies of HCC encompass pathogenetic mechanisms primarily associated with lifestyle factors like excessive alcohol consume, high caloric Western diet, and tobacco intake [4, 5]. They have been identified as potential carcinogenic factors, highlighting the diverse molecular mechanisms underlying HCC pathogenesis [4, 5]. MASLD is a metabolic disorder linked to HCC which affects more than 200 million people worldwide [18]. It can progress from a less severe state called steatosis to a more serious condition known as MASH in about 10–20% of people [18]. The progression involves the activation of the body's immune system, increased levels of certain metabolites, and stress on the cellular machinery, leading to ongoing liver damage and repair that may eventually result in HCC [18]. MASH, particularly in people with diabetes or obesity, is becoming a key risk factor for developing liver cancer [18]. With the rise in obesity rates, MASH is now the leading cause of severe liver scarring, and cirrhosis in many parts of the world [4]. Empirical research suggests a correlation between metabolic syndrome, such as obesity and diabetes mellitus, and an elevated incidence of HCC [5]. Interestingly, individuals presenting with a Body Mass Index (BMI) exceeding 25 kg/m^2 are predisposed to an increased risk of primary liver cancer [5].

1.2 Tumour Evolution and Classification

Three principal hypotheses have been postulated to elucidate the evolutionary dynamics of tumours [7]. *The Clonal Evolution Model*, conceptualized in 1976, hypothesizes that tumour progression is initiated from a singular cellular progenitor [7]. Mutations that happen in this original cell give it certain advantages, leading to the creation of new groups of cells with different characteristics [7]. Research supporting this idea has shown that tumours have two types of mutations, called "trunk" and "branch" mutations, found at the tumour’s genetic material from different areas [7]. Trunk mutations are found throughout the tumour and are probably early signs of cancer development [7].

Branch mutations are found in specific parts of the tumour and appear in later stages of the tumour's growth [7]. *The Big Bang Model*, proposed in 2015, suggests that tumours grow in a single, large burst where mutations keep adding up without any particular selection, depending only on time [7]. *The Evolution Model* suggests that there is no specific selection in how tumours develop; instead, random mutations just build up gradually over time [7].

Also, the immune system may facilitate rather than inhibit tumour development, allowing tumours to evade immune detection [19, 20]. Cancer immunoediting consists of three phases: i) elimination (immunosurveillance), ii) equilibrium (a dormant state), and iii) escape (immune evasion) [19, 20]. Research has enhanced the understanding of the complex interplay between the immune system and tumour cells [19, 20]. Notably, the evasion of immune system by cancer cells is now recognized as a hallmark of cancer [19, 20].

Liver cancer is complex and varies in three main ways: i) differences between patients (interpatient), ii) differences between tumours in the same patient (intertumoral), and iii) differences within a single tumour (intratumoral) [7]. HCC patients presenting with multiple tumour lesions, may have them developed due to intrahepatic metastasis (IM) or multi-centric occurrence (MC) [21]. This occurs probably due to the strong cancerogenic background in the liver [21]. The distinction between IM and MC remains difficult during routine clinical examination due to the biologically different behaviour and the unreliable diagnosis of them via morphological and clinicopathologic criteria (time interval, vessel infiltration, tumour size) [21]. Before choosing a treatment for someone with multiple liver tumours, it's beneficial to understand the differences between these tumours, especially when figuring out if they spread within the liver or started independently [21]. IM tumours show in their latent period malignant progression, while MC tumours are mostly in early stages when diagnosed [21]. Whole genome and RNA-sequencing analyses of 49 tumours from 23 HCC patients enabled the accurate diagnosis of MO and IM using somatic single nucleotide variation (SNV) information, without explicitly providing the ratio of IM and MC in the paper [21]. Yamamoto, *et al.* analysed in 2020 41 HCC tumours, where 18 patients were diagnosed with genomic IM and 23 patients were diagnosed with genomic MO [22]. The analysis showed that patients with IM exhibited common mutations between HCC tumours, with the primary tumour

being more aggressive than those with MO [22]. Clinical diagnosis based on liver lobe and segment was accurate in 68.3% and 78.0% of cases, respectively [22]. Patients diagnosed with clinical IM had significantly shorter survival compared to those with clinical MO, emphasizing the need to differentiate between these two types of multiple HCC for better prognosis and treatment planning [22]. Intertumoral heterogeneity means that different tumour lesions in the same patient can vary a lot, often because each one might start from a different malignant cell, especially in patients with cirrhosis or cancer spread within the liver [7]. Intratumoral heterogeneity, however, is about how even within one tumour lesion, different parts can be quite different from each other [7]. Both processes, IM and MO, lead to the generation of genetically and phenotypically diverse subclones, enhancing intratumoral heterogeneity [23].

1.2.1 Molecular Classification and Prognosis of HCC

HCC´s genomic variability led to several non-uniform classification systems as presented in Table 1 [6]. There are two main types in many liver cancer cases: the one with rapid proliferation, and the non-proliferative one [6]. The proliferative class is often associated with HBV infections, activations of TGF-β, MET, AKT and IGF2, as well as with mutations in genes such as TP53, RAS, and mTOR, leading to a worse prognosis [6]. The non-proliferation class is usually linked to alcohol abuse as well as HCV infections and tends to have better outcomes compared to the proliferative class [6]. Both classes appear equally often [6, 24].

Table 1: Major classification system of HCC adapted from Coffin, P., et al 2023 [6]. AFP=α-fetoprotein

	Subclasses	
Major Subclasses	***Proliferative***	***Non-proliferative***
Lee 2004	Cluster A	Cluster B
Boyault 2006	G1, G2, G3	G4, G5, G6
Chiang 2008	Proliferation	CTNNB1, Polysomy 7, Interferon

Hoshida 2009	S1, S2	S3
TCGARN 2017	iCluster1, iCluster2	iCluster 3
Shared clinical features	Poor survival, High vascular invasion, women, Asian, high AFP, HBV, normal body weight, poorly differentiated hepatocyte	Improved survival, Low vascular invasion, alcohol, HCV, lower AFP, well-differentiated hepatocyte, smaller tumor size

While the subclassification system aims to categorize HCC based on molecular, genetic, or phenotypic characteristics, the Barcelona Clinic Liver Cancer (BCLC) staging system (Figure 2) is widely utilized for prognosis and treatment of HCC patients [25]. It categorizes patients into five stages (0, A-D) based on tumour attributes (e.g., number, size, vascular involvement, extrahepatic spread) and liver function (Child-Pugh score) [25, 26]. Stage 0 denotes "very early stage" with a single, small (<2 cm) lesion, no vascular invasion, and intact liver function [25]. Management varies based on potential access to liver transplantation (LT) and specific clinical profiles [25]. Due to high risk of recurrence, LT is considered if criteria are met, with resection being the first choice for eligible patients [25]. Pathology indicating higher recurrence risk (e.g., microscopic vascular invasion) may shift preference towards LT [25]. Stage A represents "early HCC" with either a single lesion >2 cm or up to three lesions <3 cm, both stages being eligible for curative treatments with surgical resection or liver transplantation [25]. Stages B also known as “intermediate stage” involves a more advanced disease stage [25]. The current BCLC version divides the BCLC-B stage into 3 groups of patients corresponding to tumour burden and liver function [25]. Standard procedures for HCC treatment are surgical resection, LT, radio-frequency ablation (RFA), transarterial chemoembolization (TACE), and systemic therapy [25, 26]. An individualised patient profile may guide the choice between LT, TACE or systemic therapy [25].

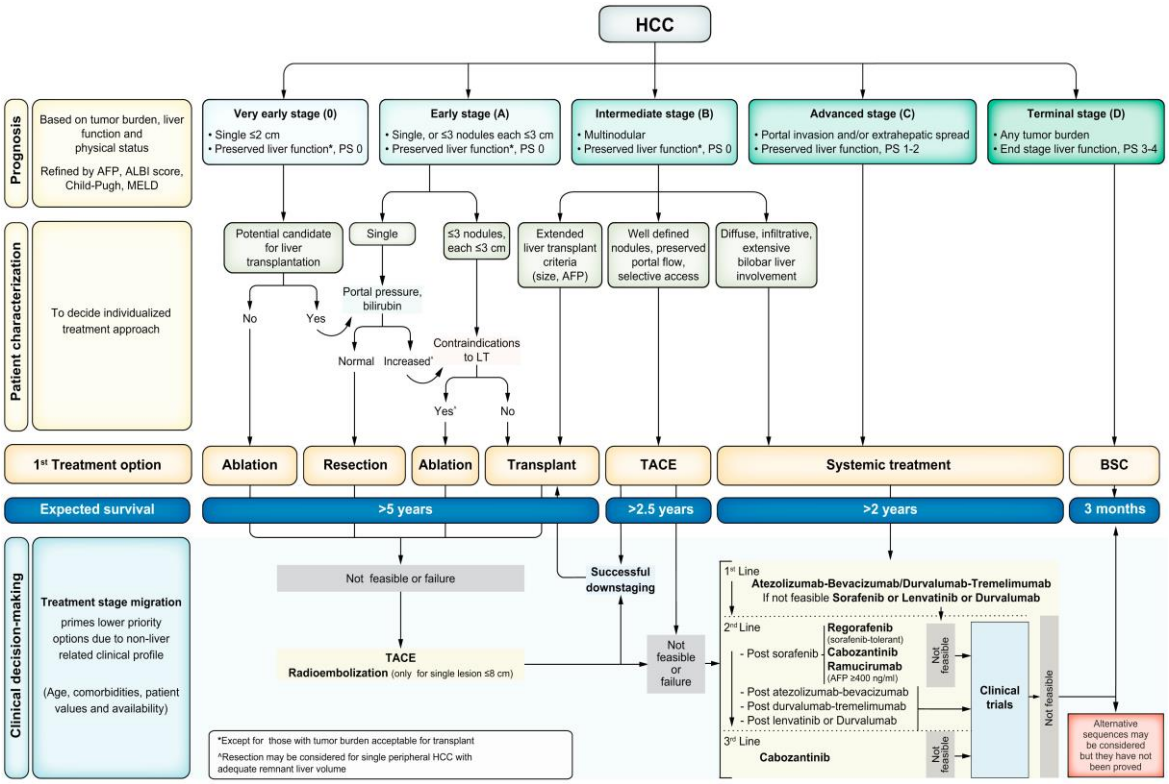

Figure 2: BCLC staging system in 2022. Picture taken from Reig, M; et al. 2022.

BCLC-C stage, also known as “advanced stage”, includes patients with vascular invasion or extrahepatic spread with preserved liver function. These patients should be evaluated for systemic therapy [25]. BCLC-D stage represent patients with impaired liver function, owing to chronic liver disease, and treatment of HCC will not change expected survival [25]. In such cases, palliative care is essential [25].

Prognosis of HCC patients remain poor due to the high rate of diagnosis at advanced stages. The expected median survival of patients with HCC, according to the BCLC proposal, is more than 5 years for BCLC 0/A, 2.5 years for BCLC B, 2 years for BCLC C, and 3 months for BCLC D [25]. The main goal of the various classification and staging systems for HCC is to improve understanding of the disease and to find molecular targets for new treatments [6, 21, 26, 27].

1.3 HCC Therapy and Resistance

1.3.1 Multi-Kinase Inhibitor and Monoclonal Antibodies

The complexity of precision oncology in HCC is significantly due to its high genetic diversity and molecular heterogeneity [28]. The introduction of multiple first-line and second-line systemic therapies since 2017 marks a significant advancement in HCC treatment [28]. Of particular importance are receptor tyrosine kinases (RTKs) facilitating intercellular communication and regulating various critical biological processes such as cell proliferation, movement, differentiation, and energy metabolism [28]. Until 2017, Sorafenib - a multi kinase inhibitor targeting RAF/MEK/ERK pathway in tumour cells and vascular endothelial growth factor receptor (VEGFR)/platelet-derived growth factor receptor (PDGFR) in tumour vasculature - was the only systemic therapy approved by the US food and drug administration (FDA) for advanced HCC, underscoring the need for more precise treatments [6]. In 2018, Lenvatinib emerged as an alternative first-line treatment, broadening the options for patients [6]. Lenvatinib, like Sorafenib, is a multi-kinase inhibitor which, targets a wider range of receptors, including VEGFR1-3, and fibroblast growth factor receptor (FGFR1-4) [6]. Its approval was based on a phase III trial (titled REFLECT) that demonstrated its noninferiority to Sorafenib in terms of overall survival, with Lenvatinib patients showing a median survival of 13.6 months compared to 12.3 months for those by Sorafenib [6]. The REFLECT trial also highlighted Lenvatinib's superiority over sorafenib in secondary outcomes like progression-free survival, time to progression, and quality of life [6, 29]. Notably, a subgroup analysis revealed that patients who responded to Lenvatinib had a significantly longer median overall survival than non-responders [6]. However, the study suggested that Lenvatinib's efficacy might be underestimated due to imbalances in baseline prognostic factors, like α-fetoprotein (AFP) levels [6].

Beyond first-line therapies, significant progress has been made in second-line treatments for HCC [6]. Regorafenib extends the survival of patients who no longer respond to Sorafenib, with an overall survival increase to 10.6 months from 7.8 months with placebo [6]. This trial also suggested that sequential treatment with multi-kinase inhibitors might have an additive effect, potentially due to an impact on the tumour's inflammatory microenvironment [6].

Cabozantinib and Ramucirumab have expanded treatment options for patients previously treated with Sorafenib, offering improved survival benefits in specific patient subgroups as demonstrated in the CELESTIAL trial [6]. Recent advancements in HCC treatments highlight a shift towards personalized medicine, yet these findings do not translate into clinical outcomes [6]. Combining tyrosine kinase inhibitors with monoclonal antibodies such as Ramucirumab (anti VEGFR2) offers promise but faces challenges like adverse events and resistance [6, 30].

1.3.2 Immune Checkpoint Inhibitors

Recently, immune checkpoint inhibitors (ICIs) targeting PD-1, PD-L1, and CTLA-4 have been approved for treating various cancers [6]. The approval of ICIs like Nivolumab and Pembrolizumab for inoperable HCC marks a significant advancement in cancer therapy [6]. The IMbrave150 study highlighted the efficacy of combining Atezolizumab and Bevacizumab as a first-line treatment for advanced HCC [6]. The interplay between anti-angiogenic drugs and immunotherapy shows potential in therapy as front-line setting [31]. Actual data highlights the importance of novel combination strategies since HCC is not just a “one drug disease” [31]. Resistance to anti-PD-1 therapy as well as non-responders in cancer treatments is a problem [32]. New strategies are needed to overcome these hurdles and to enhance the effectiveness of immunotherapies [32].

1.3.3 Molecular Adaptions and Therapy Resistance

Jiang *et al* investigated tumour samples collected before and after anti-PD-1 treatment by analysing cell interactions through single-cell RNA sequencing (scRNA-seq) and identified several interactions that may affect the efficacy of anti-PD-1 therapy [32]. Extensive studies have focused on understanding the cellular and molecular mechanisms that contribute to the development of resistance in tumour cells [33]. Autophagy plays a crucial role in fostering resistance in liver cancer cells, with numerous factors like TGF-β, MAPK, NRF2 and NF-κB contributing to this process [33]. These elements, together with others such as epithelial-mesenchymal-transition (EMT) and cancer stem cells, enhances treatment resistance in HCC, complicating therapeutic approaches

[33]. EMT contributes to therapy resistance in cancer models by inducing a stem-like phenotype [34]. The challenges of HCC treatment include the side effects of drugs, the genetic complexity of HCC, and the need for more impactful therapies [34].

1.4 The role of TAM receptors and TGF-β in HCC

The TAM family of receptor tyrosine kinases, which includes Tyro3, Axl, and MerTK, was expanded upon discovering their ligands, Gas6 and Protein S (Pros1). These ligands function as bridges, connecting phosphatidylserine residues on apoptotic cells, platelets, or viruses to the TAM receptors through their amino-terminal domains, and attaching to the receptors themselves at the carboxy-terminus (Figure 3) [10]. TAM receptors, which are closely associated with EMT-promoting signals, play a crucial role in this resistance [34]. Specifically, Axl signalling within the TAM receptor family is identified as a key mechanism behind the development of chemoresistance, as it allows cancer cells to evade the effects of drugs by circumventing the targeted pathways [34, 35]. In the context of liver disease, the presence of soluble Axl, generated by the cleavage of Axl by the metalloproteinase ADAM10/17, is a biomarker for diagnosing liver cirrhosis and the progression of HCC from early to late stages [10]. Axl works in collaboration with TGF-β signalling, where its expression is key in switching TGF-β from anti-oncogenic to pro-oncogenic functions in HCC by activating target genes, including those involved in autocrine TGF-β signalling [36].

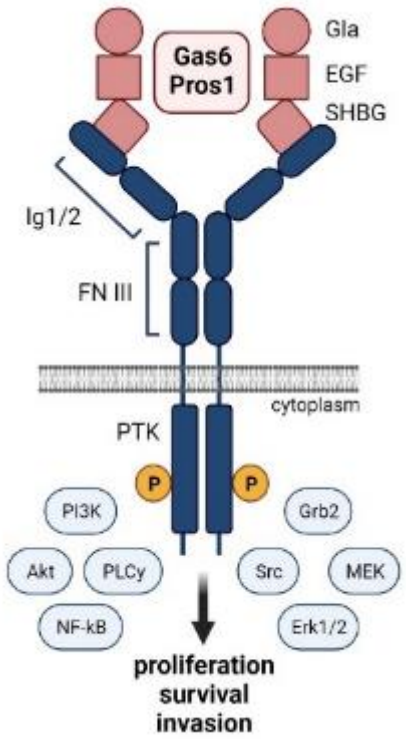

Figure 3: Gas6-Pros1/TAM receptor.

Binding of the ligands to the TAM receptor causes homodimerization which activates the intracellular protein kinase domain (PTK) by phosphorylation. Picture taken from Hedrich, V., et al. 2021

1.4.1 Transforming Growth Factor β (TGF-β)

The TGF-β superfamily comprises cytokines including TGF-β1-3, bone morphogenetic proteins (BMPs), as well as growth and differentiation factors (GDFs) which plays critical roles in cellular processes vital for tissue homeostasis [37]. Its dysregulation is linked to various diseases [37]. TGF-β is produced and secreted by nearly all cells, initially as a pro-peptide consisting of a large N-terminal fragment named latency associated peptide (LAP) and a C-terminal mature TGF-β [37]. In the Golgi network it is processed to form a small latent complex (SLC) as depicted in Figure 4 [37]. The LAP of the SLC prevents premature receptor binding [37]. This complex is secreted as a large latent complex after binding to the large latent TGF-β binding protein (LTPB) and stored in ECM until activated, predominantly through integrin αv-mediated forces [37].

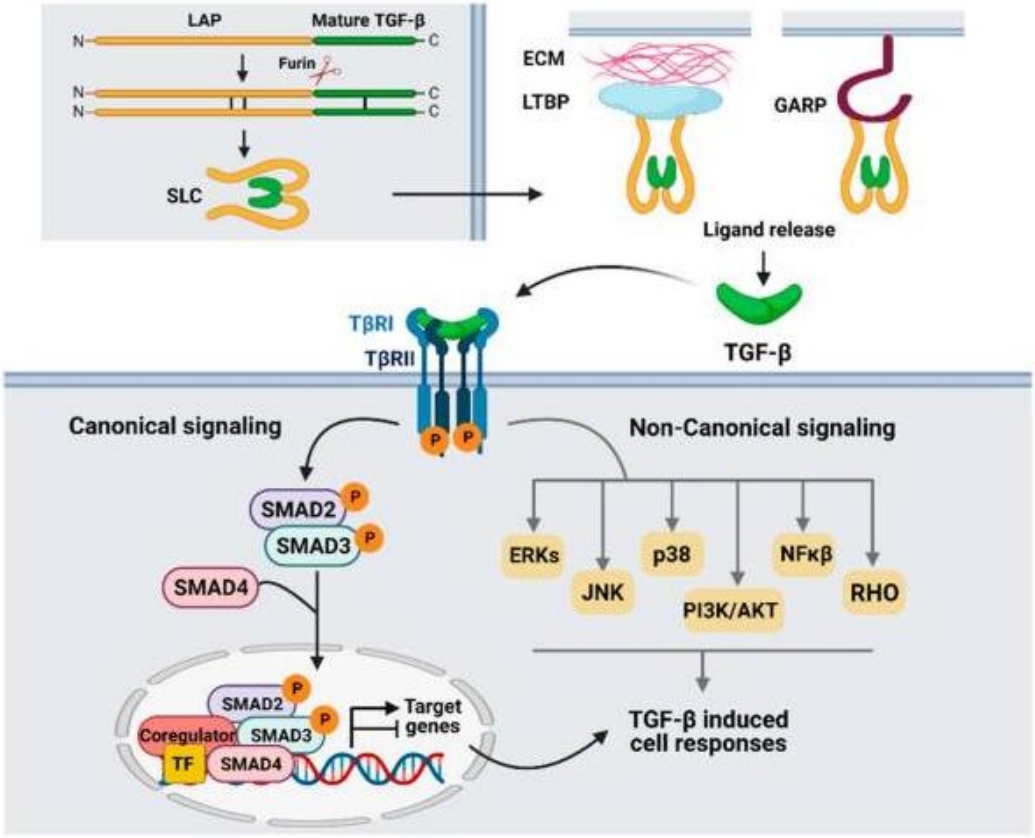

Figure 4: Processing of the TGF-β peptide (upper panel) and TGF-β mediated signalling (lower panel). Picture taken from Gonzalez-Sanchez, E., et al.2021

TGF-β is a crucial cytokine involved in fibrogenesis and is mainly produced by mesenchymal cells activated after chronic liver damage [37]. It initiates

signalling by binding to a heterotetrameric complex of type I and II serine/threonine kinase receptors [37]. This binding triggers canonical signalling pathways through the phosphorylation of Smad2 and Smad3 and their association with Smad4 [10]. These activated Smad complexes then move into the nucleus to regulate the transcription of various target genes as shown in Figure 4 [10, 37, 38]. Besides its Smad-dependent pathways, TGF-β can also activate several Smad-independent or non-canonical signalling pathways, such as the ERK/MAP, JNK, p38 MAPK, NF-κB and the phosphoinositide 3 kinase (PI3K)/Akt signalling, through the direct phosphorylation of downstream effectors [37, 38].

TGF-β initially acts as a tumour suppressor in early HCC development by inhibiting cell proliferation and growth [10, 37-40]. However, as HCC progresses, TGF-β shifts its role to promote oncogenic activities, such as invasion and metastasis [10, 37-40]. This transformation is partly facilitated by its interaction with Axl, leading to the secretion of CXCL5, which attracts neutrophils into the HCC tissue [10, 37-40]. This Axl-dependent shift towards a metastatic HCC phenotype involves changes in the phosphorylation of the Smad3 linker region, leading to increased expression of Snail, Slug, MMP9, and Pai1 [10, 37-40]. Studies involving long-term TGF-β treatment on cellular HCC models has revealed that the effects of TGF-β on cell migration are duration and concentration-dependent [40]. This process is linked to advanced tumour stages and decreased survival rates in HCC patients, highlighting a critical "switch" in TGF-β's function from tumour suppression to tumour promotion as illustrated in figure 5 [10, 37-40]. This suggests that targeting the TGF-β/Axl/CXCL5 pathway could offer a novel therapeutic approach for managing TGF-β-positive HCC patients [29, 37-40]. The goal of targeted therapy is to navigate the "double-edged sword" of TGF-β by inhibiting its pro-oncogenic activities in advanced cancer stages while restoring its anti-oncogenic effects during early tumour development [29, 37-40].

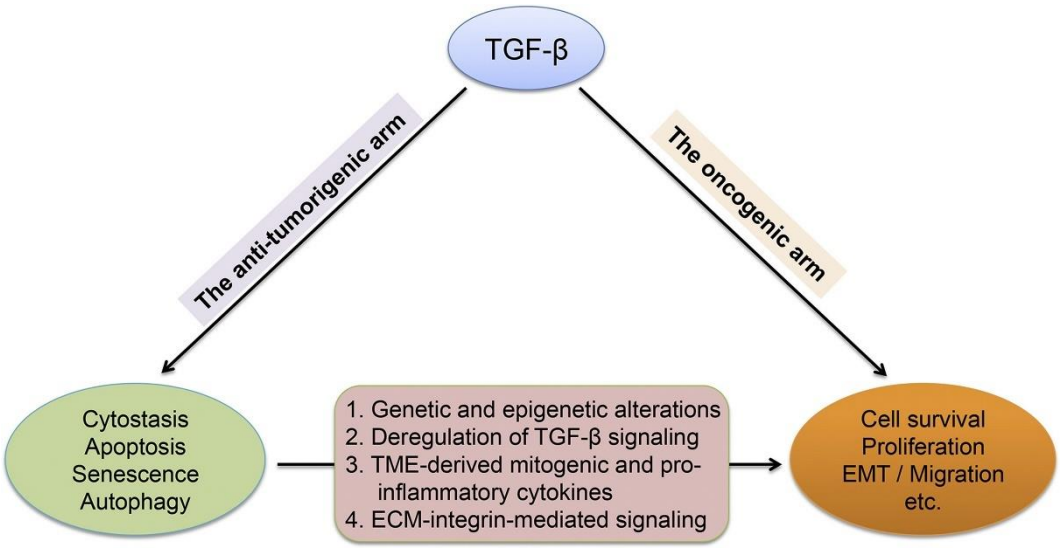

Figure 5: TGF-β switch from tumour suppressor to tumour promotion in HCC. Picture taken from Zhang, K., et al. 2020

1.4.2 Signalling Pathway Dysregulations in HCC

A study using whole exome sequencing of 243 tumours identified 161 potential driver mutations and found 11 key pathways that were frequently mutated in at least 5% of the cases, including TERT (promoter), Wnt/β-catenin, PI3K/AKT/mTOR, TP53/cell cycle, Ras/Raf/MAPK, JAK/STAT, and TGF-β with a frequency of 60%, 54%, 51%, 49%, 43%, 9% and 5% in tumours, respectively [6]. Aberrant activation of these pathways can promote cell proliferation, angiogenesis, metastasis, and resistance to cell death [6]. Activation of common potential drivers such as TGF-β and Wnt, is believed to happen later in oncogenesis [6]. A median rate of approximately 70 proteins altered by mutations per tumour were identified on a genomic landscape of HCC [9]. Most of them are passenger mutations, i.e. they accumulate randomly and are not involved in carcinogenesis. Some of them are considered as “driver” mutations which alter signalling pathways leading to a selective advantage [9]. Most frequent mutated genes are TERT (promoter), TP53, CTNNB1, AXIN1, ARID1A and ARID2, making these genes key targets for therapeutic treatment [9, 27].

1.5 Microenvironment Interactions in Injured Liver

The tumour microenvironment (TME) in HCC includes various cell types such as immune cells, fibroblasts, resident macrophages (Kupffer cells), HSCs/myofibroblasts, and liver sinusoidal endothelial cells as shown in Figure 6 [10]. This complex cellular landscape influences tumour behaviour, disease

progression, and the efficacy of therapies, including targeted and ICI treatments [10]. Upon liver injury, Kupffer cells respond to IL-1α from damaged hepatocytes by releasing pro-inflammatory cytokines TNF-α and IL-6, which induce hepatocyte proliferation [10, 41].

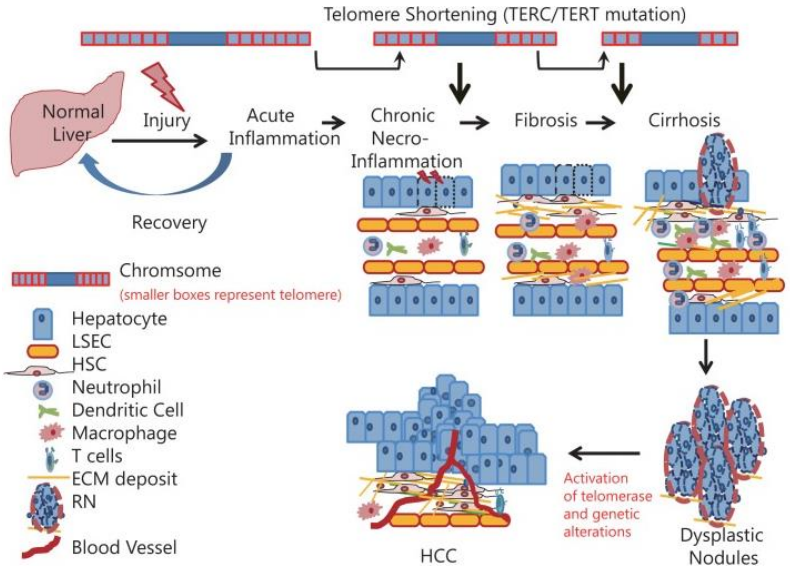

Figure 6: Progression of liver disease through various pathological changes. Picture taken from Ramakrishna, G., et al. 2013

Some neutrophils, known as tumour-associated neutrophils, create an immunosuppressive environment by secreting arginase-1 or indoleamine 2,3-dioxygenase, hindering T cell activity against tumour cells [10]. Dendritic cells in the liver produce type 1 interferon (IFN) and present antigens to activate T cells, while cytotoxic CD8+ T cells target tumour cells through the secretion of perforin and granzymes, inducing apoptosis [10]. Kupffer cell-derived TGF-β activates HSCs, transforming them into ECM-producing myofibroblasts, which contribute to a pro-fibrotic and anti-inflammatory environment that suppresses the activity of CD8+ T cells and NK cells, thereby facilitating tumour growth [10]. The inflamed TME of the liver serves as substrate for the development of recurrent HCC primary tumours in a phenomenon termed the “field effect” [6].

1.6 EMT as a Contributor to Tumor Growth and Metastasis in HCC

In carcinoma, the process of epithelial to mesenchymal transition (EMT) is crucial for tumour development [42, 43]. EMT involves the transformation of cells from an epithelial state, characterized by cell-cell adhesion and a structured epithelial arrangement, to a mesenchymal state, where cells gain mobility and invasive properties (Figure 7) [42, 43]. This transition is marked by the loss of the epithelial marker E-cadherin and the gain of mesenchymal markers such as e.g. vimentin [43]. Epithelial cells that acquire some mesenchymal traits while retaining epithelial characteristics, allowing them to maintain a hybrid epithelial/mesenchymal state, are in partial EMT [42]. They experience a partial loss of polarity while maintaining intercellular adhesion, which is essential for coordinated collective migration [42]. These cells dynamically transit between epithelial polarity (characterized by apical-basal orientation) and mesenchymal polarity (front-rear organization) [42]. In the hybrid stages of EMT, cells display both epithelial and mesenchymal markers, which enhances their plasticity, allowing them to invade

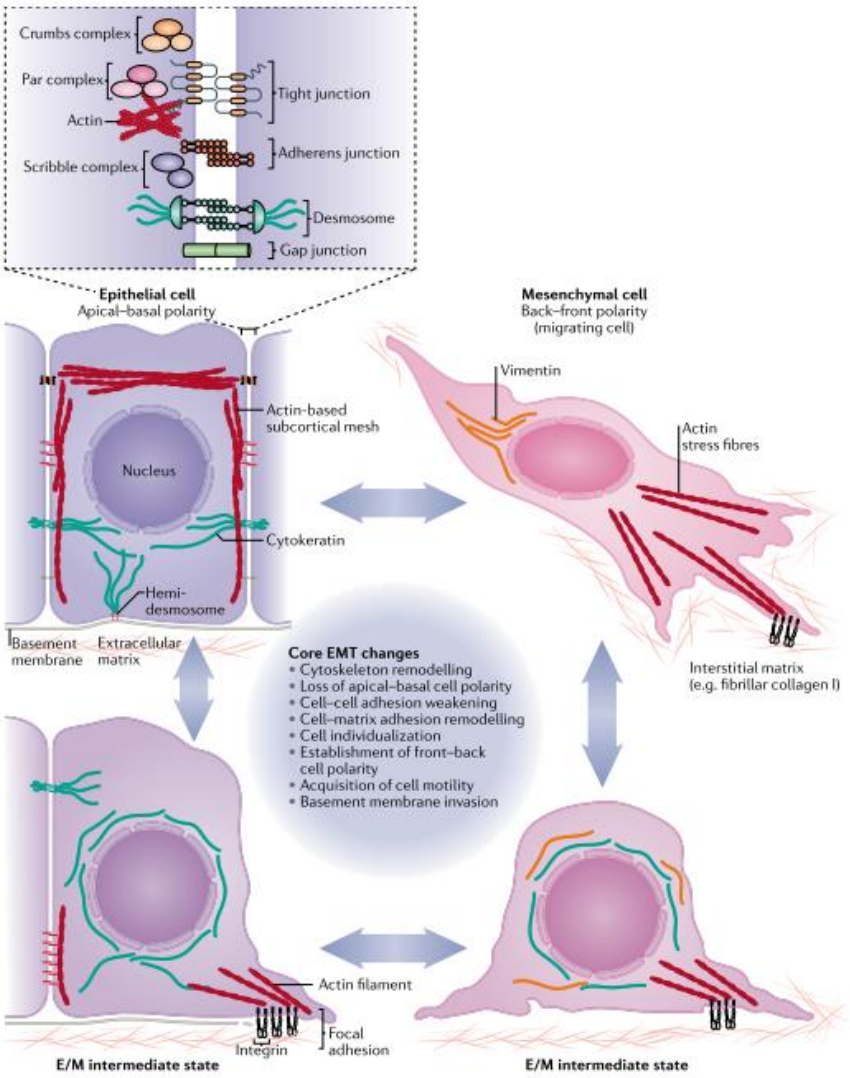

Figure 7: Epithelial-mesenchymal plasticity model. Picture taken from Yang, J., et al. 2020

and metastasize while preserving the capacity to revert to a fully epithelial state when needed [42]. This plasticity supports tumor initiation, growth, the development of stem cell-like features, cell migration, intravasation, and metastasis [42]. The progression of HCC in cancer cell models often involves EMT which is propelled by transcription factors like Snail, Slug, Twist, and Zeb1/2 [44]. These transcription factors reduce the expression of epithelial genes while simultaneously increasing the expression of genes associated with a mesenchymal-like phenotype [44]. TGF-β, which is often overexpressed in various cancers, has been identified as a strong inducer of EMT in cultured cells [45]. Initial studies, such as one showing that silencing Twist1 in breast cancer cell lines reduces lung metastasis, supported EMT's role in promoting metastasis [42].

Figure 8 illustrates the epithelial cell plasticity involved in metastasis, where EMT facilitates initial invasion and MET supports colonization at secondary sites [43]. First, epithelial tumour cells lose their cell-cell junctions, dissociate, and invade surrounding tissues, undergoing EMT to acquire migratory and invasive abilities [43]. The tumour cells enter the bloodstream (intravasation) and travel to distant organs, exiting the vasculature (extravasation) to seed new locations [43]. After extravasation, tumour cells may remain dormant or form micrometastases [43]. Eventually, they undergo MET to regain epithelial traits, allowing proliferation and macrometastasis formation [43].

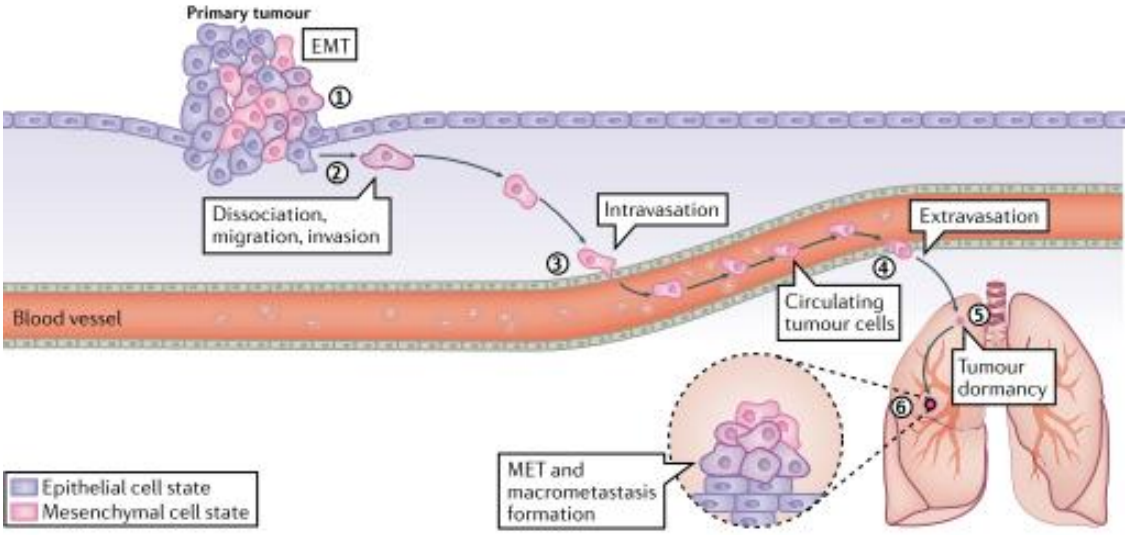

Figure 8: Epithelial cell plasticity of carcinoma cells upon metastatic cell dissemination.

1) Invasion; epithelial tumour cells lose cell-cell junctions. 2) Dissociation of epithelial cell contacts, and invasion into surrounding tumour tissue. 3) Intravasation; tumour cell invades blood vessel. 4) Extravasation; exit of disseminating tumour cells into the circulation system through the capillary endothelium of distant organs. 5) Tumour dormancy of solitary tumour cells or small groups of tumour cells known a micrometastasis. 6) Mesenchymal to epithelial transition (MET) and macrometastasis formation; proliferating of secondary tumours. Picture taken from Yang, J., et al 2020

However, some cancers appear to metastasize without undergoing EMT [42]. Reports suggested that EMT might not be essential for metastasis, as shown in mouse models of pancreatic and mammary tumorigenesis where key EMT regulators were manipulated [42]. Notably, deleting Zeb1 in a pancreatic cancer mouse model significantly reduced tumour cell invasiveness and metastasis, indicating that the suppression of EMT, through Zeb1 deletion, can have an impact on tumour behaviour and metastatic abilities [42]. Albeit the role of EMT is complex and not always required for metastasis, it plays a significant role in the aggressiveness and spread of certain cancers [42]. The role of EMT, in liver fibrosis is somehow inconsistent [46]. Contrary to earlier beliefs that hepatocytes undergo EMT to become collagen-producing myofibroblasts. However, recent evidence suggests that hepatocytes do not typically undergo EMT *in vivo* [46]. Instead, the transdifferentiation of HSCs into myofibroblasts is identified as the primary source of collagen production in liver fibrosis, accounting for the majority of the myofibroblast population in transgenic mouse studies [46]. Despite these findings, there are reports indicating that EMT might still play a role in liver fibrosis [46]. For example, HSC have been shown to secrete collagen I, which induces EMT of hepatoma cells [46]. Additionally, inhibition of TGF-β signalling suppresses fibrosis, and microRNAs can modulate EMT of hepatocytes through TGF-β inhibition [46]. Notably, the deletion of the EMT-related transcription factor Snail in hepatocytes has been shown to attenuate liver fibrosis, suggesting a potential involvement of hepatocyte-EMT in the fibrotic process [46].

The reverse process of partial and complete EMT, known as MET, involves cells losing their migratory capabilities and gaining characteristics typical of epithelial tissues [43, 46]. This is essential for the outgrowth of metastatic tumours to build metastasis in distal organs [43, 46]. During MET, cells undergo apico-basal polarization and start expressing junctional complexes, which are key features of epithelial cells [43, 46]. Inhibition of EMT-associated changes could potentially

reduce the spread of cancer cells in early-stage carcinoma, while preventing the reverse process in disseminated tumour cells may hinder their ability to form metastases in distant organs [43]. Both experimental and clinical research has established a strong link between the development of resistance to various cancer treatments, such as chemotherapy and immunotherapy, and EMT phenotypes [43]. These findings indicate that strategies to target EMT could be effective in addressing therapy resistance [43].

1.7 Extracellular Vesicles

1.7.1 Classification and Communication

Extracellular vesicles (EVs) play a significant role in cancer development and progression [47-49]. EVs are membrane-enclosed particles released by cells that can carry various signalling factors and bioactive molecules, such as nucleic acids (DNA, RNA and miRNA), proteins (receptors, transcription factors, enzymes and, ECM components), and lipids, termed as “cargo” [47-49]. The definition of EV is that any type of membrane particle that can be released by any type of cell, into the extracellular space, regardless of differences in biogenesis and composition [48, 50]. EVs are classified into several categories, including exosomes, microvesicles (MVs), and large oncosomes, each varying in size and origin [48, 50]. Exosomes are the smallest, with diameters ranging from 30 to 100 nanometres [48, 50]. MVs are larger, ranging in size between 50 and 1000 nm [48, 50]. Apoptotic bodies, arising from cell apoptosis, are also considered as EVs, and larger than MVs [51]. Large oncosomes, spanning 1 to 10 μm in diameter, are specifically derived from cancer cells, indicating their significant role in cancer biology and the potential for cancer therapies [48]. Evidence is emerging that cancer cells may release different subtypes of EVs, together with those derived from normal cells [48]. Because of their atypical size (>100 times larger than exosomes), oncosomes may have unique properties and may present new opportunities for tumour profiling [48]. They can travel through body fluids and mediate communication between cells [48]. Intercellular communication is essential for the coordination and regulation of various cellular functions within an organism [48]. Autocrine communication is a process where the target and secreting cells are the same, allowing a cell to respond to signals

it produces itself, which is crucial for functions like cell growth [48]. In contrast, paracrine communication involves signalling between cells that are nearby one another, with the secreted molecules acting locally to modulate the behaviour of neighbouring cells [48]. Endocrine communication enables the transmission of signals over long distances within the body [48]. In this system secreted factors, like hormones, travel through the bloodstream to reach target cells that are located far from secretion site, facilitating a coordinated systemic response [48]. Juxtacrine communication requires direct physical contact between cells and is a mode of signalling often observed in scenarios involving highly migratory or amoeboid tumor cells [48]. Another mode of intercellular communication is through EVs, which represent a complex and evolutionarily conserved system [48]. EVs have been found in various bodily fluids such as pleural effusion, breast milk, ascites, semen, salivary gland fluid, cerebrospinal fluid and urine [51]. These EVs carry functional substances that can have positive or negative effects on the body [51]. One example of a negative effect is the presence of beta-amyloid proteins associated with Alzheimer's disease in exosomes and their release into the extracellular space [51].

1.7.2 Exosome Biogenesis and Composition

Exosome biogenesis is a process starting with the invagination of clathrin-coated domains on plasma membrane, leading to early endosome (EE) formation [49]. After interaction of EEs with the Golgi apparatus and the endoplasmatic reticulum (ER), the EEs mature into late endosomes [49]. Exosomes emerge from the inward folding of endosome membranes to form intraluminal vesicles (ILV) [49]. The binding and incorporation of exosomal cargoes into ILVs happens through a well-coordinated process that involves the inward budding and fission of vesicles to form multivesicular bodies (MVBs) [52]. MVBs can either fuse with lysosomes for degradation or fuse with the plasma membrane as depicted in Figure 9 [49]. Sorting of cargo molecules during internal budding of the membrane is an important step in exosome formation, and the endosomal-sorting-complex-required for transport (ESCRT) is responsible for this sorting [48, 49]. This machinery consists of sequential protein complexes (ESCRT-0, -I, -II, -III) and accessory proteins [49].

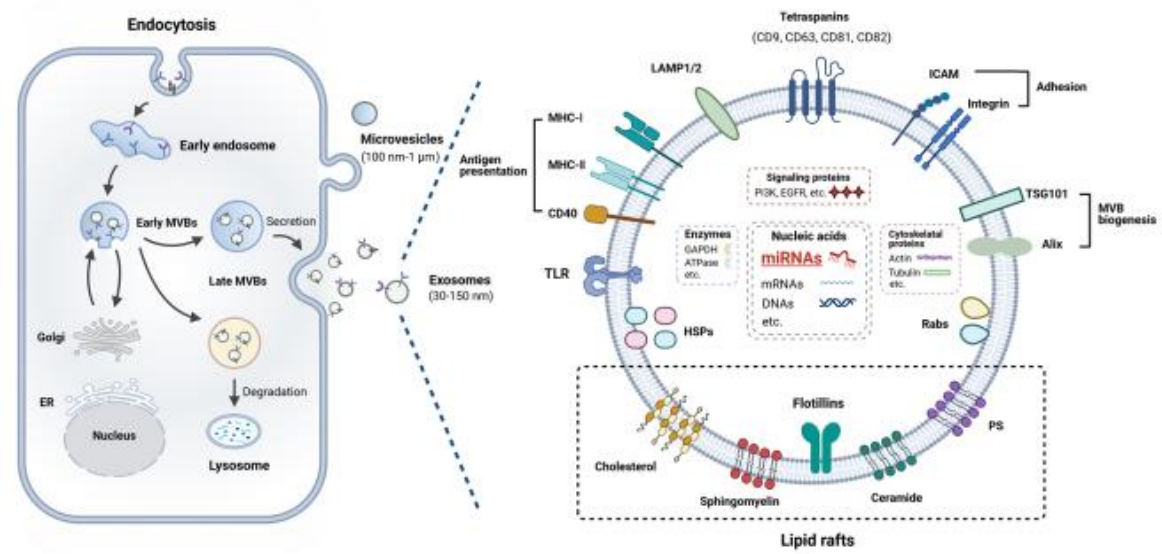

Figure 9: Biogenesis and composition of exosome. Picture taken from Wenqian, W., et al. 2021

Depletion of certain ESCRT-family members can change the protein content and release rate of exosomes from cancer cells [48]. Proteins like Alix and Tsg101 play a role in the formation of ILVs [48]. Inhibiting Alix affects the ability of dendritic or muscle cells to release exosomes enriched with CD63 [48]. Proteins like Tsg101 are often used as markers for exosomes, as they are frequently involved in exosome formation of cancer cells [48, 52]. Exosome secretion is also influenced by the intracellular calcium concentration and stress exposure [48]. The uptake of exosomes involves the interaction between phosphatidylserine (PS) on the exosome membrane and T-cell immunoglobulin-and-mucin-domain-containing molecule (Tim4) [51]. This process is called fusion and endocytosis [51]. Fusion involves the merging of the exosome membrane and the recipient cell membrane, while endocytosis is an active process [48]. MVs are plasma membrane-derived vesicles, distinct from exosomes, formed through outward membrane budding and release into the extracellular environment [48]. This process needs significant membrane reorganization, including alterations in lipid and protein composition and calcium levels [48]. MVs marked by phosphatidylserine externalization and lipid raft domains, have regulated cargo sorting mechanisms that reflect the donor cell but are not solely determined by the donor cell's composition [48]. Another study points out that annexins rather than integrins are crucial for the cellular uptake of EVs [53]. Especially annexin A1 significantly influences EV aggregation and act as an adhesion agent, positioning annexin A1 as a central figure in EV

biology [54]. In addition, tetraspanins like CD9, CD81, and CD63 are always known to play a significant role in EV biogenesis and trafficking [48]. Various biochemical and cell biology methods assess the involvement of these tetraspanins in EV-mediated transfer of molecular cargo [48]. A recent study showed that CD63 and CD9 do not play significant roles in the content delivery function of EVs, indicating that other mechanisms or molecules might be responsible for this critical aspect of EV biology [55].

1.7.3 EVs Supporting Cancer Progression

Exosome research is conducted in various disease areas, including cancer, regenerative medicine, and disorders of the immune, nervous, endocrine, as well as cardiovascular systems [51]. Tumor-derived EVs can affect the TME by targeting different cells and altering the ECM [48]. Fibroblast-derived EVs can induce EMT in cancer cells through microRNAs [48]. Studies showed that exosomal microRNA derived from liver cancer (miR-1247-3p) induce conversion of fibroblasts into cancer-associated fibroblasts (CAFs) which contribute to the promotion of lung metastasis of liver cancer [56]. The involvement of EVs in drug resistance and the potential role in creating a metastatic niche are novel areas of research and are still limited in evidence from *in vivo* studies [48]. Large oncosomes can transfer the oncoprotein EGFRvIII to tumor cells lacking this receptor, thus promoting tumor growth [48]. The relationship and differences between tumor-derived MVs and large oncosomes, particularly in their role in cancer progression, remain largely undefined [48]. Further research to elucidate their specific functions and markers is needed [48]. There is evidence that Nidogen 1-enriched EVs play an important role in promoting the extrahepatic metastasis of liver cancer cells [57]. The study demonstrates that these vesicles activate pulmonary fibroblasts to secrete tumor necrosis factor receptor 1 (TNFR1), which is crucial for the metastatic process [57]. This study provides significant insights into the molecular mechanisms underlying liver cancer metastasis and highlights the potential of targeting Nidogen 1-enriched EVs and their interactions with pulmonary fibroblasts as a therapeutic strategy to inhibit the progression of liver cancer [57]. Also, tumour-derived exosomes containing TGF-β convert fibroblasts into myofibroblasts, contributing to vascularization, tumour growth, and local invasion [58]. EVs secreted by oral cancer cells can

induce EMT, under the influence of TGF-β, leading to the destabilization of endothelial barriers [59]. This process is critical as it enhances the permeability of blood vessels, facilitating cancer cell invasion and metastasis [59]. The study highlights the potential of targeting such interactions to maintain endothelial integrity and prevent cancer progression [59].

1.7.4 EVs as Potenial Biomarkers

EVs derived from cancer cells have been shown to facilitate angiogenesis, enhance coagulation processes, modulate immune responses, and induce the remodelling of the surrounding tissue [47]. EVs circulate in the bloodstream of cancer patients which could lead to metastasis [47]. Circulating tumour-derived EVs show a potential as biomarkers for tracking cancer progression and pinpointing metastatic sites [60]. Specific integrin patterns on EVs, such as a6b4 for lung, avb5 for liver, and avb3 for brain metastases, indicate organ-targeted metastasis [60]. Consequently, these vesicles hold a significant potential as diagnostic and prognostic biomarkers, in addition to serving as viable targets for therapeutic intervention [47].

1.8 Long Range Signalling and the Preparation of the Premetastatic Niche

The pre-metastatic niche (PMN) hypothesis proposes that exosomes released by tumours may play a crucial role in building PMN and facilitating the transition of cancer cells to new environments [47, 51]. Exosomes have been observed to prepare the secondary site before the arrival of cancer cells, creating a hospitable microenvironment in which cancer cells can thrive and establish metastatic lesions [51]. These exosomes are believed to transport proteins and nucleic acids to prime the secondary site, promoting angiogenesis, immune evasion and organ-specific adaptations for metastases [51]. Vascular leakiness is a critical aspect of distal organ colonization, facilitating the spread of cancer cells to distant organs (Figure 10) [47]. Specifically, miR-105-expressing metastatic breast cancer cells have been shown to disrupt the integrity of endothelial barriers by targeting the tight junction protein ZO1, thereby increasing vascular permeability [61]. Another study demonstrates a novel mechanism by which CAFs, activated by EVs derived by high-metastatic lung

cancer cells, enhance metastasis through mitochondrial DNA transfer, suggesting a potential therapeutic target for lung cancer [62]. However, the precise mechanisms by which EVs affect endothelial barrier integrity, and their organ-specific targeting remain areas for further investigation [47]. A study demonstrates that the PMN influences MET dynamics, particularly via TGF-β signalling [63]. In lung metastasis models, myeloid cells secreting ECM components and activated fibroblasts, promote MET and cell proliferation while reducing TGF-β-mediated EMT [63]. This highlights the intricate relationship between environmental cues and TGF-β in regulating cancer metastasis [63]. These findings elucidate the complex interplay between tumour-derived exosomes and the vascular system in promoting metastasis [61]. The interactions between EVs and the ECM are complex and play a significant role in cellular migration and the formation of PMNs [52]. These interactions are facilitated through multiple mechanisms [52]. Firstly, ECM molecules that are bound to integrins on the surface of EVs can be released in an autocrine manner, creating an adhesive substrate that enhances the speed of cell migration [52]. Additionally, integrins present on EVs can bind to specific ECM components like laminin-332 and fibronectin [52]. This binding is crucial for the potential establishment of PMNs in tissues, providing a fertile ground for metastasizing tumour cells [52]. Moreover, EVs carry matrix metalloproteinases (MMPs), which can degrade ECM components [52]. This degradation facilitates the remodelling of tissues, thereby promoting increased invasion and migration capabilities of tumour cells [52]. Collectively, these interactions show the pivotal role of EVs in modulating the ECM, influencing cellular behaviour, and contributing to the metastatic process [52].

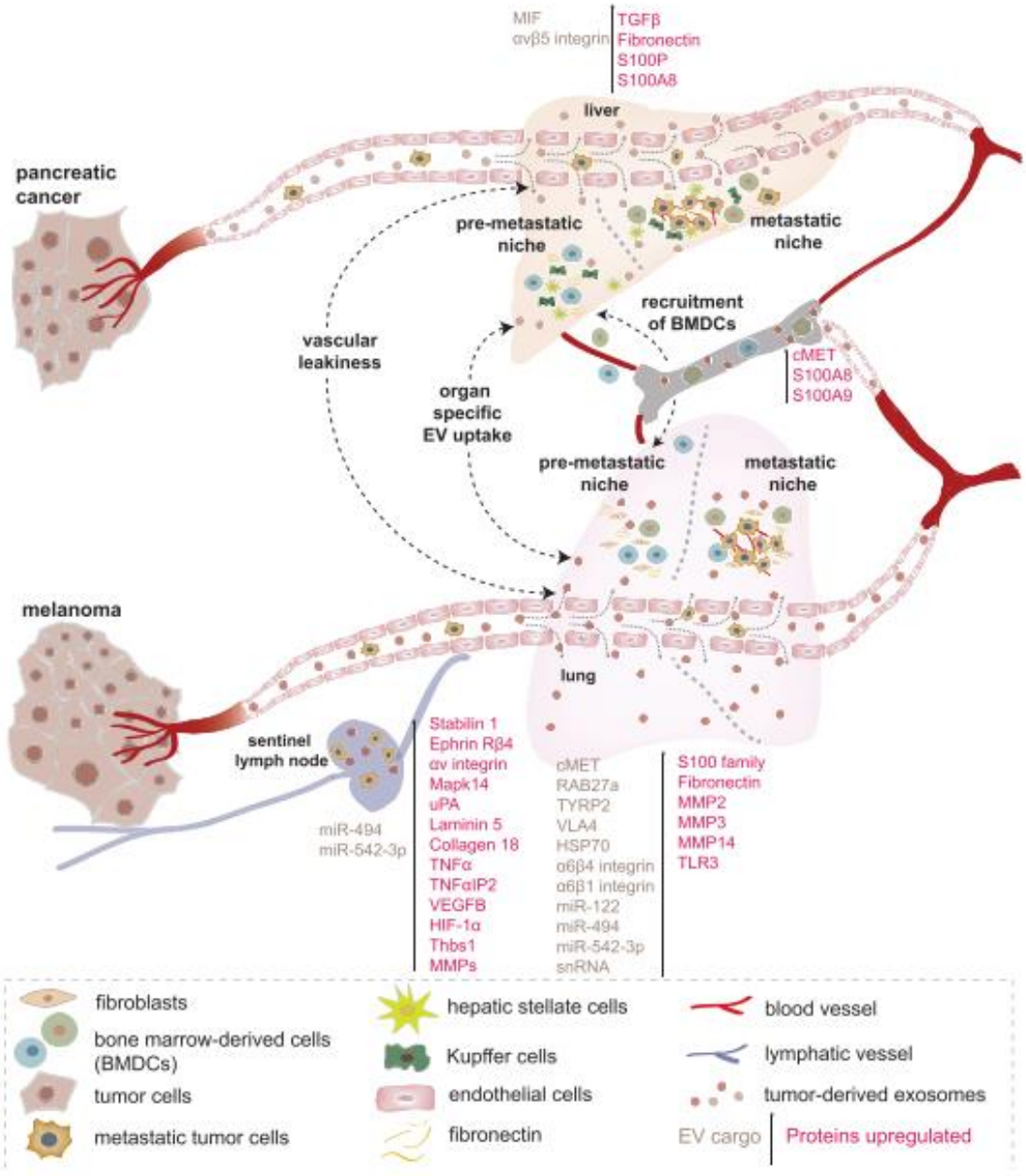

Figure 10: Pre-metastatic niche Formation and Metastasis via tumor-derived EVs.

Originating from various cancer cells, EVs travel via blood and lymphatic systems to initiate PMNs by mechanisms that are not yet fully understood. They can cause vascular leakiness and modulate distant organ environments by targeting specific resident cells through membrane components such as exosomal integrins. EVs also influence local cells to express inflammatory mediators and remodel stromal cells, facilitating bone marrow-derived cells' (BMDCs) recruitment to PMNs. Picture taken from Becker, A., et al. 2016.

It was observed that Kupffer cells in the liver internalize EVs containing migration inhibitory factor (MIF), which then triggers the secretion of TGF-β [64]. This leads to the activation of HSCs to produce fibronectin [64]. This protein is a key matrix component that facilitates the localization of bone marrow cells and neutrophils, which are crucial steps in the establishment of the PMN [64]. An interesting finding is the detection of EVs with high levels of MIF in the circulation of mice with pancreatic ductal adenocarcinoma (PDAC) even before the formation of PDAC lesions, suggesting the potential of MIF as an early biomarker for PDAC metastasis formation [64, 65]. Moreover EVs from the non-malignant TME, such as astrocyte-derived EVs carrying PTEN-inhibiting miRNA, also play significant roles in shaping metastatic niches by targeting metastatic tumour cells and enhancing their ability to recruit myeloid cells from the bone marrow [64]. These findings underscore the complex interplay between various cell types mediated by EVs in the formation of the PMN, with TGF-β being a key molecular player in this process [64]. Furthermore, the potential of using exosomal components like MIF as prognostic markers are highlighted for early detection and treatment of metastatic cancer [64].

1.9 EV Isolation and Characterization

Standard protocols for EV isolation in clinical practice are still lacking, although differential centrifugation is commonly used [48]. However, this method may result in heterogeneous preparations, and other techniques, such as centrifugation gradients may provide better purity [48]. Specific markers for exosomes and other types of EVs are still being identified [48]. Electron microscopy is required to visualize nano-sized EVs and MVs, while larger EVs can be observed by confocal or optical microscopy [48]. Flow cytometry analysis is commonly used to detect EVs, but it is limited in its ability to analyse particles smaller than 500 nm [48]. However, a recent study found that nano-sized particles can be accurately quantified using flow cytometry [48]. This approach can also be used to categorize different subsets of heterogeneous EVs by using a multicolour labelling strategy [48]. An innovative approach to detect EVs is tagging of key EV components by green fluorescent protein (GFP) [48]. This method significantly enhances the visibility and traceability of EVs, facilitating more efficient and accurate analysis and manipulation in various

biotechnological applications [48, 66]. Other studies have shown that nano-sized EVs can be counted using flow cytometry with the help of antibody-coated beads larger than exosomes [48]. Nanoparticle tracking analysis (NTA) is another method frequently used to study nano-sized EVs [48]. It captures and analyses the light scattered by the particles through computer software, allowing for the measurement of EV size distribution and concentration in samples [48]. However, NTA is not suitable for quantitative analysis of EVs larger than 400 nm [48]. EVs have the potential to provide valuable information from body fluids through non-invasive methods [48].

In exosome research, scientists typically use three basic approaches. The first approach involves isolating exosomes and analysing their contents [51]. The second approach introduces exosomes to other cells to observe how the cells respond [51]. The third approach labels exosomes and studies their release into cellular environments or examines their release in a co-culture system [51]. The isolation method used is crucial as the results obtained from subsequent experiments may be influenced by it [51]. However, there is currently no consensus among researchers on the definitions of certain terms and the detection and isolation of exosomes, making interpretation of experimental data and reproducibility challenging [51]. For studies focusing on exosome recovery and experiments involving EVs, such as MVs, the standard methods are ultra-centrifugation or the density-gradient technique [51]. However, distinguishing between exosomes derived from endosomes and MVs derived from the plasma membrane is challenging with ultracentrifugation [51]. Currently, there is no standardized method for isolating exosomes. In addition, the understanding of the physiological functions of exosomes and the underlying mechanisms of their secretion and uptake is limited [51].

2 Hypothesis and Aims

EVs represent a communication system implicated in cancer progression [67]. They have the potential to transfer various biomolecules and alter the TME. Understanding the pathology of EVs could provide valuable insights into the tumour development and therapeutic strategies [51, 67]. This project hypothesized that EVs are central in cancer cell dissemination of HCC. Cancer-derived EVs – regulated by TGF-β signalling - are crucially involved in long range signalling by fusion to target cells and micro-environmental alterations at secondary sites which facilitate colonization of HCC cells [52]. In particular we propose that long range signals from HCC are sent through EVs to establish a PMN that is essentially involved in intra- and extrahepatic colonization of spreading HCC cells [52, 67].

In order to verify this hypothesis and make relevant progress, several tasks were performed as described below:

1. Analyse the cargo of EVs regulated by TGF- signalling via proteomics. Validation of proteomics data by immunological methods with a particular focus on cell attachment and cell signalling.
2. Examine the involvement of TGF-β signalling in the release of EVs and cargo loading by pharmacologic intervention *in vitro.*
3. Study the modulation of cargo proteins in CD63-GFP-tagged EVs/exosomes derived from HCC cells and their phenotypical consequences after fusion to HSCs, and endothelial cells *in vitro.*

3 Materials and Methods

3.1 Cell Lines and Cell Culture Conditions

The mesenchymal like human HCC cells termed HLF were used as EV donors. In addition, we employed HLF cells either treated for long-term with TGF-β1 (HLF-T) or exogenously expressing CXCL5 (HLF-CXCL5). For EV tracking HLF-CD63-GFP cells, generated by the former master student Adriana Martinez Turtos in her master's thesis entitled, "Extracellular vesicles and their impact on the epithelial plasticity of hepatocellular carcinoma cells." In particular, HLF cells were transduced with a lentiviral vector encoding a CD63-GFP fusion gene. The pLVX-CD63-GFP plasmid was generously provided by Paola Martinelli and Sonia Melo from the University of Texas MD Anderson Cancer Center [68]. All cell lines were cultivated in DMEM supplemented with 10% fetal calf serum (FCS; Sigma Aldrich, St. Louis, USA) and 1% antibiotics (50 U penicillin and 50 µg/mL streptomycin) at 37°C and 5% CO_2. The medium was referred to as D10. TGF-β signalling was stimulated in HLF-T cells every second day with 1 ng/mL TGF-β (R&D Systems, Minneapolis, USA) for > 10 days. To inhibit TGF-β signalling, the low molecular weight compound LY2109761 (Ly; Santa Cruz, Dallas, USA) antagonizing TGF-β receptors I/II was used at a concentration of 10 µM for 24 hours. Cells treated with TGF-β were maintained for a period not exceeding 30 days upon initiation of TGF-β1 treatment. The human HSC line LX2 and human umbilical vein endothelial cells (HUVECs) were used as EV-acceptor cells. LX-2 cells were cultured in DMEM supplemented with 5% heat inactivated FCS and 1% antibiotics. HUVECs were propagated in Endothelial Cell Growth Medium with supplement mix including 2% FCS and 1% antibiotics (PromoCell, Heidelberg, Germany).

3.1.1 Freezing of Cells

Cells were trypsinized at 80% confluency. The resulting cell suspension was centrifuged at 200 g for 6 minutes at room temperature. The cell pellet was resuspended in 3 mL of FCS containing 5% dimethyl sulfoxide (DMSO). The cell suspension was divided into three pre-cooled freezing vials, each containing 1 mL of the cell suspension. The cells were chilled on ice for 10 minutes before

being transferred to a -80°C freezer. After one week, the cells were transferred to a liquid nitrogen container for long-term storage.

3.1.2 Thawing of Cells

Frozen cells were thawed in a 37°C water bath and resuspended in 10mL culture medium. Cells were centrifuged at 200 g for 6 minutes at room temperature. The cell pellet was resuspended in fresh culture medium and plated on a 10 cm culture dish.

3.2 Wound Healing Assay

7.5 x10^5 cells were seeded on a 6-well-plate. Prior to seeding, vertical lines were drawn at 3 mm intervals on the outer bottom of the wells to aid in capturing accurate images using microscopy and in quantifying the migration rate. Horizontal scratches were made in the cell monolayer 24 hours after seeding, using a blue 1 mL pipette tip (2 scratches per well), and the culture medium was replaced with fresh medium to remove detached cells. At the time of scratching (0 hr-scratching) and 24 hours post-scratching, images were captured using a Nikon Eclipse Ti-S/L100 microscope (Nikon, Tokyo, Japan) and NIS-Elements version 4.30.01 imaging software. Cell migration was assessed by quantifying the gap area of the scratches at 0 hr and 24 hr using ImageJ [69].

3.3 EV Isolation and Characterization

3.3.1 EV Isolation from HCC cells

In Figure 11 the flowchart details the protocol for the isolation of EVs using differential ultracentrifugation [70]. It is structured into sequential steps performed over three days. On “day 1” 1.8x10^7 cells were seeded at a 15 cm plate with 20 mL of culture medium D10. A total of 15 plates were used per cell line, adding up to 2.7x10^8 cells. On “day 2” the medium was discarded after 24 hours of incubation. The plate was washed three times with 5 mL of phosphate buffered saline (PBS) at room temperature. Then, 12 mL of FCS free medium with 1% Penicillin/Streptomycin was added, and the cells were starved for 24 hours at 5% CO_2 and 37°C. On “day 3” the protocol continues with the collection of the so-called “conditioned medium” (CM) in 50 mL tubes. This medium was

centrifuged at 400 g for 10 minutes at 4°C to remove debris. Following centrifugation, the medium was filtered using 0.22 µm cellulose acetate filters. The CM was filtered again through centrifugal filter devices with a molecular weight limit of 10 kDa to reduce the volume. The centrifugation was performed in the same centrifuge at 3500 g for 15 minutes at 4°C. The “concentrated conditioned medium” (CCM) did not pass the filter, since EVs are larger than 700 kDa [71].

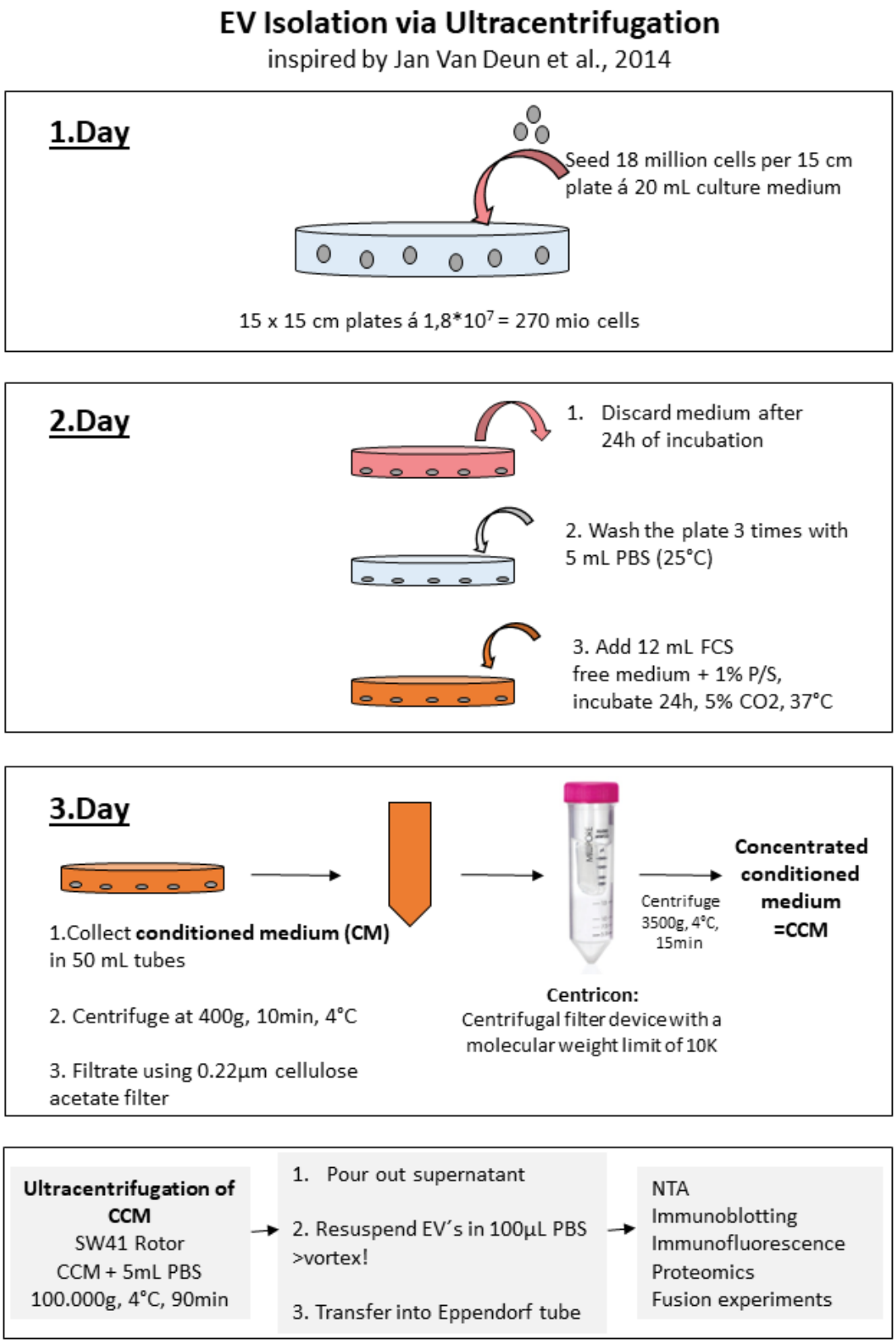

Figure 11: Flow chart of EV isolation from CCM by differential ultracentrifugation. Artwork made by Leila Djerlek

Ultracentrifugation of the CCM was then performed using a SW41 rotor, combining the CCM with 5 mL PBS, and centrifuging at 100.000 g for 90 minutes at 4°C without brakes. After ultracentrifugation, the supernatant was poured out, and the EVs were resuspended in 100 µl sterile filtered PBS through pipetting and vortexing. Finally, the resuspended EVs were transferred into Eppendorf tubes. EVs were either immediately processed for further analysis including nanoparticle tracking analysis (NTA), immunoblotting, proteomics, immunofluorescence, and cell fusion experiments. Eppendorf tubes containing EVs were immediately frozen at -80°C for storage. To prevent aggregation, it is recommended to process EVs prior to freezing. For all experiments except NTA and cell fusion assays, EVs were lysed for protein concentration determination. Frozen samples were thawed and stored until needed at 4°C. Freshly isolated EVs and lysed EVs were stored at -80°C.

3.3.2 Nanoparticle Tracking Analysis

Nanoparticle tracking analysis (NTA) was performed using a NanoSight NS500 instrument (Malvern, UK) equipped with a 532 nm laser. The device was configured with specific parameters: a detection threshold set at 5, camera level at 14, and screen gain maintained at 1, utilizing the NTA 3.1 software suite. The established standard operating procedure mandated the acquisition of six consecutive image captures for each sample, with each capture lasting 30 seconds. Prior to analysis, samples were diluted in PBS at a ratio of 1:100. This dilution was optimized to achieve a measurement concentration ranging between $1x10^7$ and $1x10^8$ particles per mL, equating to approximately 10 to 100 particles per frame in the visual field. PBS without any EVs served as the blank control. The particle concentration and size data were reported as the mean ± standard error of the mean. In order, to provide a comprehensive analysis, size distribution plots were generated.

3.4 Western blotting

3.4.1 Sample Preparation

EV samples of HCC cell lines, reconstituted in PBS, underwent lysis using a 1:1 ratio of PBS to RIPA buffer, facilitated by three freeze/thaw cycles at -196°C

(liquid N_2). Their protein concentrations were quantified with a Micro BCA Protein Assay kit (Thermo Fischer Scientific, Massachusetts, USA) according to the manufactor´s protocol. Cellular lysates of the corresponding cell line prepared in RIPA buffer with a protease inhibitor cocktail were centrifuged at 9.600 g for 10 min at 4°C after snap-freezing in liquid N_2 and subsequent thawing. The protein concentrations in supernatants were determined via the Bradford assay, as described by the manufacturer (Protein Assay Dye Reagent Concentrate, BioRad, USA). In the process of Western blot analysis, specimens were homogenized in a sodium dodecyl sulfate (SDS) loading buffer, modified to accommodate both non-reducing and reducing conditions. Under reducing conditions, a 5x SDS-loading buffer was employed, comprising 250 mM Tris-HCl at pH 6.8, 10% SDS, 5% β-mercaptoethanol (β-ME), 100 mM dithiothreitol (DTT), 3 mg/mL bromophenol blue, and 30% glycerol. In contrast, both β-ME and DTT were omitted from the SDS-loading buffer composition to achieve non-reducing conditions. Prior to conducting SDS-polyacrylamide gel electrophoresis (SDS-PAGE), the samples were heated at 95°C for 5 minutes, followed by rapid cooling on ice.

3.4.2 Immunoblotting

The apparatus for Western blotting was set up using polyacrylamide (PAA) gels of 1 mm thickness and with concentrations of 7.5% or 10% PAA. An electrophoresis buffer composed of 25 mM Tris, 192 mM glycine and 0.1% SDS was utilized. Equivalent protein quantities from EV lysates and cellular lysates were loaded onto the gels, alongside a protein molecular weight marker ranging from 10 to 250 kDa (PageRuler Plus Prestained Protein Ladder, Thermo Fisher Scientific). The electrophoresis was conducted at a constant current of 25 mA for a minimum duration of one hour. Subsequently, proteins were transferred onto a nitrocellulose membrane (Amersham Protran 0.2µm, GE Healthcare Life Sciences, USA) using a 'sandwich' blotting technique in a chilled blotting buffer (25 mM Tris, 192 mM glycine, 15% methanol, 0.02% SDS) at 100 V for one hour. Successful transfer was checked using Ponceau S staining (0.1% Ponceau S in 5% acetic acid). Post staining, the membrane was rinsed with double-distilled water and then blocked using either 4% bovine serum albumin (BSA) or 5% milk in TBS-T (0.1% Tween-20 in Tris-buffered saline (20 mM Tris,

150 mM NaCl, pH 7.5)) depending on the primary antibody. The selection of the primary antibody is listed in Table 2 based on literature review and preliminary unpublished data. Table 3 describes the conditions and concentrations needed for the experiments. The membranes were incubated in the primary antibody dilution overnight at 4°C, followed by three washes with TBS-T buffer each lasting 15 min. Peroxidase-labelled horse anti-mouse and goat anti-rabbit secondary IgG antibodies (Vector Laboratories Inc, USA) were used at dilutions described in Table 3 and were incubated at room temperature for 1 hr. Subsequently, blots were washed three times with TBS-T buffer each for 15 min.

Table 2: List of primary antibodies used for Western blotting.

	Target	Clone	Host	molecular weight [72]	Vender	Cat#
Primary Antibodies	actin	polyclonal	rabbit	42	Sigma	A2066
	annexin A1	polyclonal	rabbit	37	Proteintech	21990-1-AP
	annexin A2	D11G2, monoclonal	rabbit	38	Cell signaling	#8235
	CD63	TS63, monoclonal	mouse	30-60 smear	abcam	ab59479
	GRP78	Clone 40/BiP, monoclonal	mouse	78	BD	610979
	integrin a5	EPR7854, monoclonal	rabbit	150	abcam	ab150361
	integrin β1	TS2/16, monoclonal	mouse	130	Invitrogen	MA2910
	TSG101	Clone C-2	mouse	45	Santa Cruz	sc-7964

Table 3: Concentrations and dilutions of primary antibodies for Western blotting.

	Target	Clone	Host	Western Blot			
				Condition	Blocking Buffer (BB)	Prim. AB dilution in BB	Sec. AB dilution in BB
Antibodies	actin	polyclonal	rabbit	reducing	4% BSA in TBS-T	1:3000	1:10000
	annexin A1	polyclonal	rabbit	reducing	5% milk in TBS-T	1:500	1:10000

	annexin A2	D11G2, monoclonal	rabbit	reducing	4% BSA in TBS-T	1:1500	1:10000
	CD63	TS63, monoclonal	mouse	non-reducing	4% BSA in TBS-T	1:1000	1:1000
	GRP78	Clone 40/BiP, monoclonal	mouse	reducing	5% milk in TBS-T	1:1000	1:500
	integrin a5	EPR7854, monoclonal	rabbit	reducing	4% BSA in TBS-T	1:1000	1:10000
	integrin β1	TS2/16, monoclonal	mouse	non-reducing	5% milk in TBS-T	1:4000	1:200
	TSG101	Clone C-2	mouse	non-reducing	5% milk in TBS-T	1:1000	1:100

The blotted membranes were developed utilizing a self-made enhanced chemiluminescence (ECL) reagent composed of 0.1 M Tris pH 8.8, 13.07 mg/L para-coumaric acid in DMSO, 44.3 g/L luminol in DMSO. 3µL H_2O_2 were added per mL working solution and incubated on the membrane for 1 min prior to exposition on an X-ray film. For some EV samples the Select Western Blotting Detection Reagent (Amersham, GE Healthcare Life Science) was used with an incubation time of 5 min.

3.5 Immunofluorescence Microscopy

To image cells, sterilized cover slips were placed in a 12-well plate and coated with 120µl of 0.1 mg/mL poly-L-lysine for 15 minutes at room temperature, after which the solution was removed. HLF, HLF-T and HLF-CXCL5 cells were each added at a density of $1x10^5$ cells per well and incubated for 24 hrs at 37°C with 5% CO_2. Following incubation, the media was discarded, and the cells were washed with PBS and fixed with Histofix (Carl Roth) for 15 minutes at 37°C. The fixed cells underwent three washes with PBS, were subsequently permeabilized with 0.25% Triton-X in PBS for 5 minutes, and then washed again three times with PBS. For blocking, 5% horse serum in 1% BSA/PBS was used for 40 minutes at room temperature, followed by another series of three PBS washes. Cells were then incubated with primary antibodies, as listed in Table 4. After 1 hour at room temperature, they were washed three times with PBS, and

subsequently incubated with secondary antibodies (Alexa Fluor 488, Thermo Fisher) and DAPI, 1:1000 (Sigma Aldrich) in 1% BSA/PBS for 1 hour in the dark. After a final set of three PBS washes, the cover slips were mounted upside down on microscope slides using an anti-fade reagent (Prolong Gold Antifade Reagent, Molecular probes (Invitrogen), USA) and allowed to dry for two days at 4°C. Finally, immunofluorescence microscopy was performed using a 63x magnification oil immersion lens on a Confocal Laser Scanning Microscope (Zeiss, Germany) to visualize cells.

Table 4: Concentrations and dilutions of primary antibodies for immunofluorescence analysis.

Target	Clone	Host	Immunofluorescence	
			prim AB dilution in 5% horse serum	**sec AB dilution in 5% horse serum**
annexin A1	polyclonal	rabbit	1:200	1:200
annexin A2	D11G2, monoclonal	rabbit	1:100	1:200
CD63	TS63, monoclonal	mouse	1:100	1:200
integrin a5	EPR7854, monoclonal	rabbit	1:100	1:200
integrin β1	TS2/16, monoclonal	mouse	1:100	1:200

3.6 EV to Cell Fusion

EVs stably expressing CD63-GFP or EVs labelled with PKH67 were used to monitor cell fusion. The use of labelled EV´s allows tracking via fluorescence microscopy. EVs from both HLF and HLF-T cells were stained with PKH67, following the protocol outlined in section "3.7.1 PKH67 Membrane Stain."

Table 5: Experimental set-up for EV-cell fusions

EVs | Timepoints	0h (no EVs)	1h	2h	4h	12h	24h
control (unlabelled EVs)	LX-2 / HUVEC	LX-2 / HUVEC	LX-2 / HUVEC	LX-2 / HUVEC	LX-2 / HUVEC	LX-2
HLF-CD63-GFP	LX-2 / HUVEC	LX-2 / HUVEC	LX-2 / HUVEC	LX-2 / HUVEC	LX-2 / HUVEC	LX-2

HLF-T-CD63-GFP	LX-2 / HUVEC	LX-2 / HUVEC	LX-2 / HUVEC	LX-2 / HUVEC	LX-2 / HUVEC	LX-2
HLF-PKH	LX-2 / HUVEC	LX-2 / HUVEC	LX-2 / HUVEC	LX-2 / HUVEC	LX-2 / HUVEC	LX-2
HLF-T-PKH	LX-2 / HUVEC	LX-2 / HUVEC	LX-2 / HUVEC	LX-2 / HUVEC	LX-2 / HUVEC	LX-2

Collagen-coated wells of chambered cover slips with 8 wells each (µ-Slide 8 Well, ibidi) were utilized. 6 x 10^4 LX-2 or HUVEC cells were seeded on each well as described in Table 5. Both cell lines were subjected to identical experimental conditions, except for the incubation period. HUVECs did not undergo a 24 hours incubation as previous findings indicated no significant difference between 12 and 24 hours of incubation (unpublished data). Following seeding, the cells were incubated for 24 hrs, after which the media was changed, and approximately 6 x 10^8 Particles (~5 µg of EVs) were added to each well. The EV amount was adapted from existing literature [73, 74]. Subsequent to the designated timepoints, the cells were fixed with Histofix for 15 min at 37°C and washed three times with PBS. The chambers were then stored at 4°C in PBS until all timepoints were completed. After the fixation of all samples, the same procedure as described in section "2.7 Immunofluorescence Microscopy" was followed. The cells were permeabilized using 0.25% Triton-X, washed three times in PBS, blocked in 1% BSA in PBS, and then incubated for 1 hour in the dark with phalloidin (R415, Invitrogen, diluted 1:1700 in 1% BSA/PBS) and DAPI (Sigma-Aldrich, diluted 1:100 in 1% BSA/PBS). After three further PBS washes, the stained cells were stored in PBS in the dark and examined using the IXplore Spinning Disk Confocal system (Olympus, Tokyo, Japan).

3.6.1 PKH67 Membrane Stain

For staining EVs, we used the membrane staining dye PKH67 (Fluorescent Cell Linker Kit, Sigma Aldrich) to ensure that the GFP-CD63 construct in the EVs did not interfere with the uptake of the recipient cells. 5 µg protein of EVs were utilized per well. Initially, a minimum of 10 µL of EVs, with a particle concentration of at least 6x10^8 particles/mL solved in PBS, were diluted to 1000µL with Diluent C in a centrifuge tube. In parallel, an equivalent volume of DMEM to that of the EVs, was prepared in a separate tube, diluted up to 1000µL

with Diluent C, and 6 µL of PKH was added. This mixture was then combined with the EVs in the centrifuge tube and mixed thoroughly for 30 seconds us-ing a pipette. The mixture underwent a 5 minute incubation period in darkness to allow the staining reaction to occur. Subsequently, 2 mL of 10% BSA in PBS and 4.5 mL of DMEM without antibiotics were added to the mixture and combined well. To facilitate the subsequent centrifugation step, 1.5 mL of 0.971 M sucrose solution was carefully layered on the bottom of the tube. The centrifugation was carried out for 2 hr at 4°C with a force of 100,000 g, after which the supernatant was discarded, leaving approximately 1 mL in the tube. The EV pellet obtained was resuspended in 15 mL of PBS and transferred to a 10 kDa filter device tube. A final centrifugation step at 3000 g and 4°C for 50 min without brakes concentrated the EVs in the filter device. 200µL of concentrated PKH-labelled EVs were then transferred to an Eppendorf tube for storage. The EVs could be stored for up to one week at 4°C.

3.7 Transcriptome Profiling by RNA-Sequencing

Total RNA of HLF and HLF-T cells were extracted using the Monarch total RNA miniprep kit (New England Biolabs, Ipswich, MA, USA) in three independent experiments. Isolated RNA was quantified via Nanodrop (Thermofisher, Waltham, MA, USA). Library preparation and sequencing were performed by Lexogen (Greenland, NH, USA). QuantSeq 3′ mRNA-seq (fwd) library, suitable for Illumina sequencing containing Unique Molecular Identifiers (UMIs), was prepared using the quantified RNA. The QuantSeq 3′ (fwd) library underwent SR76 high-output QuantSeq 3′ mRNA sequencing using the Illumina NextSeq 500. Spike-In RNA Variant Controls (SIRVs), which are synthetic unique RNA transcripts, were included as controls for the RNA sequencing.

3.8 Proteomics

As outlined in section "3.3 EV Isolation from HCC Cells" the cell plating procedure remained consistent, with the exception that a total of $1.6x10^8$ cells from both HLF and HLF-CXCL5 were seeded, which are in total 6 plates per cell line. Three plates of each cell line were treated with the TGF-β inhibitor LY2109761 at a concentration of 10 µM starting from day one. For the HLF-T, less cells were seeded, i.e. a total of $1.08x10^8$ cells distributed on 6 plates. 3

plates of HLF-T also received the LY2109761 treatment, while the remaining cells were subjected to TGF-β1 exposure. All groups treated with the inhibitor are referred to as the LY-group.

Cells without TGF-β inhibition served as control groups. In these controls, 20µL of DMSO was added per plate. Following 24 hours incubation period, the medium was discarded, the cells were washed twice with PBS and starvation was initiated. An additional dose of 10 µM LY2109761 was administered to all LY-groups during the starvation phase. TGF-β was not added to HLF-T groups during starvation. Subsequent to the starvation, the protocol was repeated as described in section 2.3. In total, 18 samples were analysed, including HLF, HLF-LY, HLF-T, HLF-T-LY, HLF-CXCL5, and HLF-CXCL5-LY cells, each with 3 replicates. These samples were subjected to the analysis using liquid chromatography-mass spectrometry (LC-MS/MS) in collaboration with Christopher Gerner (Department of Analytical Chemistry, University of Vienna, Austria).

Isolated EVs were lysed using the S220 focused ultrasonicator from Covaris, employing Adaptive Focused Acoustics® (AFA®) technology (Covaris, Woburn, USA). The lysed EVs underwent tryptic digestion following the S-trap protocol [75]. After digestion, the peptides were eluted, dried, and stored at -20°C until ready for liquid chromatography (LC)-mass spectrometry (MS)/MS analysis. The peptide samples, once reconstituted, were injected into the Dionex Ultimate 3000 nano high-performance liquid chromatography (HPLC) system (Thermo Fisher Scientific, Waltham, USA). Peptides were concentrated on a pre-column (2 cm × 100 µm C18 Pepmap100; Thermo Fisher Scientific, Waltham, USA) before being separated on an analytical column (25 cm × 75 µm, 1.6 µm C18 Aurora; Ionopticks, Middle Camberwell, Australia). The MS analysis was conducted using the TimsTOF Pro mass spectrometer (Bruker, Billerica, USA) with a captive spray ion source set at 1600 V, operating in the Parallel Accumulation-Serial Fragmentation mode. Data from LC-MS/MS was analysed and quantified using software packages such as MaxQuant and MSFragger [76, 77]. For statistical evaluation, the Perseus software package and Skyline will be utilized [78, 79].

3.9 Statistical analysis

The comparative analysis of migration rates between HLF and HLF-T cells was conducted using an unpaired Student's t-test with a two-tailed p-value. Statistical significance was established at $p < 0.05$. The obtained data, with at least three technical replicates, was expressed as the mean ± standard deviation (SD). For multiple comparison analyses of means across multiple groups a one-way ANOVA testing was performed. Data was first tested for normal distribution via Kolmogorov-Smirnov test. Significance levels were considered when $p>0.05$. All analyses were carried out utilizing Microsoft Excel (Windows 365) or GraphPad Prism software, version 5.01.

4 Results

4.1 Preliminary data

A study of Costa Silva et al in 2015 suggests that TGF-β signalling is involved in EV-mediated long-range signalling initiating PMN formation in the liver [65]. Our preliminary work showed that HCC cells exposed to long-term TGF-β release higher numbers of EVs as compared to parental cells (unpublished data). Notably, EVs derived from long-term TGF-β treated HCC cells (HLF-T) induced changes in cell plasticity of epithelial HCC cells by downregulation of E-cadherin (unpublished data). Furthermore, EVs isolated from HLF-T cells and analysed by liquid chromatography-mass spectrometry (LC-MS/MS) revealed a TGF-β-specific cluster containing 53 proteins (Figure 12A; unpublished data). Functional classification of the protein cargo from HLF-T derived EVs allowed us to identify four categories involved in (i) cell attachment and signalling, (ii) inflammation and immune modulation, (iii) glycolysis and metabolism as well as (iv) vesicle biogenesis (Figure 12B). Since the working hypothesis proposes that long-range signals from HCC are sent through EVs to establish a PMN, proteins from the category “cell attachment and signalling” were of great interest (in collaboration with Mgr. Eva Řezníčková, Ph.D., Olomouc).

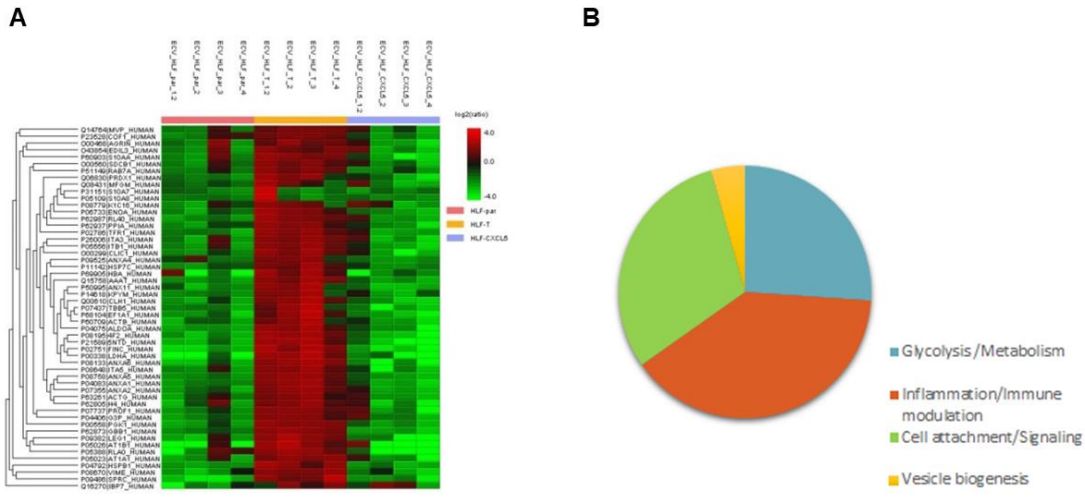

Figure 12: Analysis of EV proteins derived from TGF-β exposed and CXCL5 expressing HCC cells.

A) Heatmap of proteins identified in EVs of HCC cells. EVs were isolated from parental HLF cells (HLF-par), TGF-β exposed HLF cells (HLF-T), and CXCL5-expressing cells (HLF-CXCL5). EVs were analysed by LC-MS/MS. Data were further evaluated using Spectrum Mill MS Proteomics Workbench software

(version A03.03; Agilent, Santa Clara, USA and SwissProt Database). Green, low expression; red, high expression. B) The cargo of EVs from TGF-β exposed HLF-T cells show four categories of proteins.

4.2 Selection of Extracellular Vesicles (EV) Cargo

Based on the functional classification of the EV content and insights from the literature, we have selected candidate proteins from the EV cargo of the HLF-T cluster for further studies (Figure 12A). In particular, the cargo proteins upregulated in the HLF-T cluster were filtered for proteins involved in HCC development, PMN formation and TGF-β signalling. Table 6 shows the proteins, and the literature found that can be assigned to these aspects.

Table 6: Summary of HLF-T cargo proteins and available data in the literature. Green, referenced literature.

Protein	HCC	PMN	TGF-β	EV marker
annexin A1		71, 72, 73	72	
annexin A2	74	75, 76	77, 78	
intergrin α-5	79, 80		81	
integrin β-1	82	83	84	
CD63				85, 86
TSG101				87
GRP78				88

Annexin A1 (ANXA1) was identified as a PDAC-specific exosome cargo compared to healthy controls [80]. ANXA1 promotes metastasis formation by enhancing TGF-β/Smad signalling and actin reorganization, facilitating an EMT-like switch which enables efficient cell migration and invasion in metastatic breast cancer cells [81].

ANXA1 KO cell lines exhibit reduced migratory and invasive potential, which can be restored by stimulation with EVs from wild-type (WT) cells. Additionally, WT exosomes enhance the migratory and invasive behaviour of HUVECs, indicating that exosomal ANXA1 promotes angiogenesis [82].

Phosphorylation of Annexin A2 (ANXA2) at tyrosine 23 is associated with highly metastatic HCC cells and poor prognosis [83]. Serum exosomal ANXA2 from breast cancer patients promotes angiogenesis in Matrigel plug assays. Its expression correlates with a bad prognosis [84]. Knockdown of ANXA2 in EVs

reduces the metastatic potential of breast cancer cells in "exosome-primed" mice. Following injection of WT exosomes, elevated levels of TNFα and IL-6 were observed, and lungs showed increased staining for phospho-NF-kB, phospho-p38, and phospho-STAT3. ANXA2 interacts with pro-cathepsin B on recipient cells [85]. In colorectal cancer (CRC), ANXA2 and TGF-β signalling cooperate to induce EMT and invasion [86]. ANXA2 expression correlates with tumour staging, metastasis and poor prognosis [86]. TGF-β upregulates ANXA2 and decreases E-cadherin expression, while silencing of ANXA2 expression reduces TGF-β-induced invasiveness and inhibits the Src/ANXA2/STAT3 axis in CRC [86]. In PDAC patients, tenascin C (TNC) and ANXA2 expression increase with disease progression [87]. TNC, as a component of the extracellular matrix, interacts with fibronectin and cell surface receptors ANXA2, showing a synergistic role in the development of PDAC [87].

Inhibition of integrin α5β1 has been shown to reduce liver metastasis rates in mouse models of ovarian cancer [88]. A recent study found that treatment with the MEK inhibitor selumetinib suppressed liver metastasis in melanoma by reducing integrin α5 levels, highlighting the potential of integrin α5 as a therapeutic target for liver metastasis in melanoma [88, 89]. Furthermore, TGF-β1 co-stimulates the growth of CD8+ T cells by activating the α5 beta 1 integrin and/or its ligand, and supports sustained growth partly by providing α5-β1-mediated protection against apoptosis [90].

Higher levels of integrins α6 and β1 are secreted via EVs derived from aggressive tumour progenitor cells, indicating the potential of circulating integrins for early detection and prediction of aggressive cancers [91]. Activated integrin α4β1 promotes lymphatic endothelium expansion in lymph nodes and captures VCAM-1+ metastatic tumour cells, facilitating lymph node metastasis [92]. Additionally, integrin β1 signalling is essential for TGF-β activation of p38MAPK and epithelial plasticity [93]. The tetraspanin member CD63, as well as tumour susceptibility gene 101 protein (TSG101) were chosen as exosome markers as reported [94-96]. Furthermore, GRP78 was used as a negative control for EVs as it is only present in the endoplasmatic reticulum rather than in EVs [97].

4.3 RNA-Sequencing versus Mass Spectrometry Analysis

RNA sequencing (RNA-seq) of HLF and HLF-T cells demonstrated significant differences at the transcript level of fibronectin and integrin α5, with p-values of <0.0004 and <0.0286, respectively (Figure 13A). These results suggest that fibronectin and integrin α5 are upregulated at mRNA level in HLF-T cells. The other candidate genes showed similar transcript expression in HLF and HLF-T cells, indicating no significant changes. In contrast, protein levels in EVs derived from HLF-T were found to be elevated (Figure 13B). These findings suggest that TGF-β directly regulates the levels of fibronectin, ANXA1, ANXA2 and integrin β1 in the protein cargo of EVs derived from HLF cells. Further experiments are required to confirm these results.

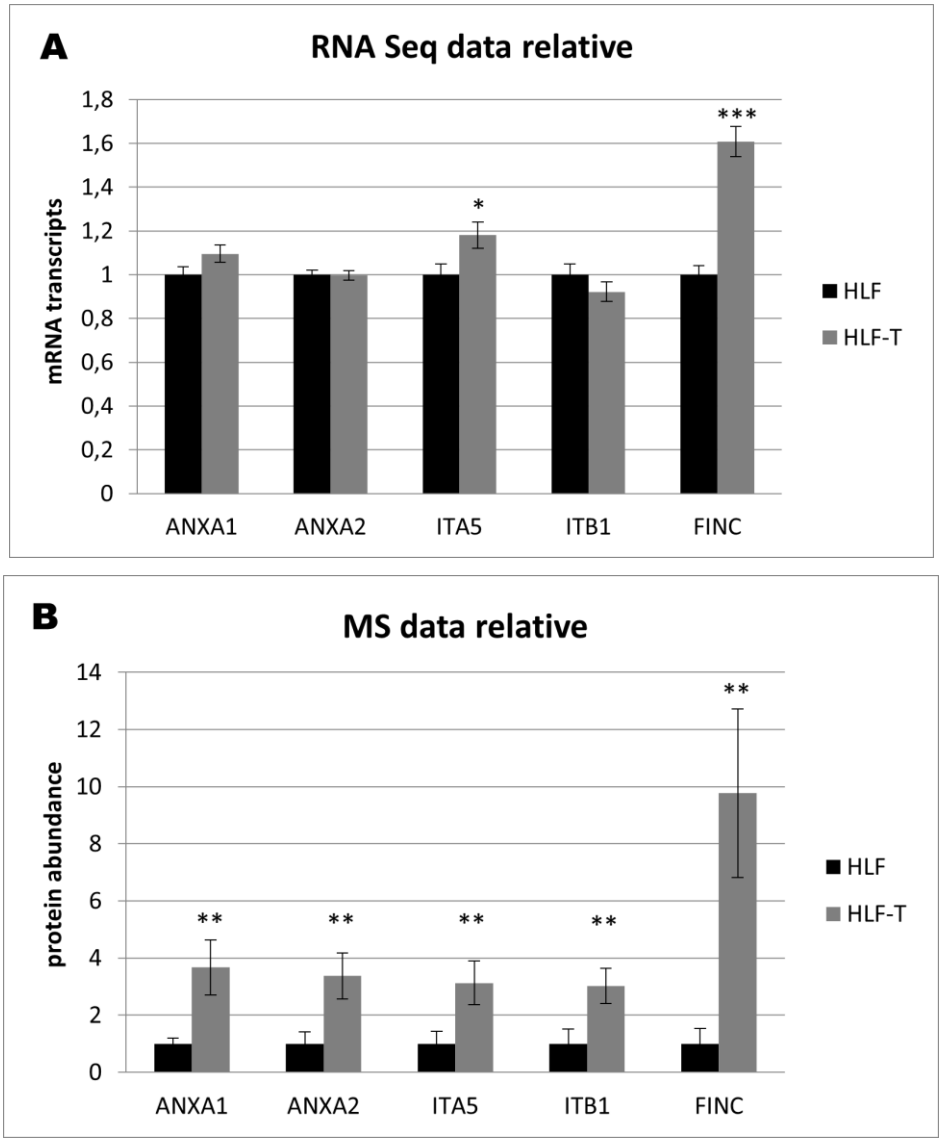

Figure 13: RNA-seq vs LC-MS/MS analysis.

*A) RNA-seq analysis of transcripts of interest in total cell lysates of HLF and HLF-T cells. B) Quantification of the EV cargo proteins derived from HLF and HLF-T cells and analyzed by LC-MS/MS (Figure 12A; data quantified by Viola Hedrich). FINC, fibronectin, ANXA1, annexin A1; ANXA2, annexin A2; ITA5, integrin α5; ITB1, integrin β1. The values of parental cells were set to 100%. Data are expressed as mean +- SD. P-values were calculated with t-test for 2 independent groups, * P < 0.05, ** P < 0.01, *** P < 0.001.*

4.4 Characterization of EVs derived from HCC cells by NTA

We performed nanoparticle tracking in order to prove the successful isolation of EVs for each cell line. The NTA profile revealed the concentration of EV particles per mL and the mean particle size of EVs (Figure 14).

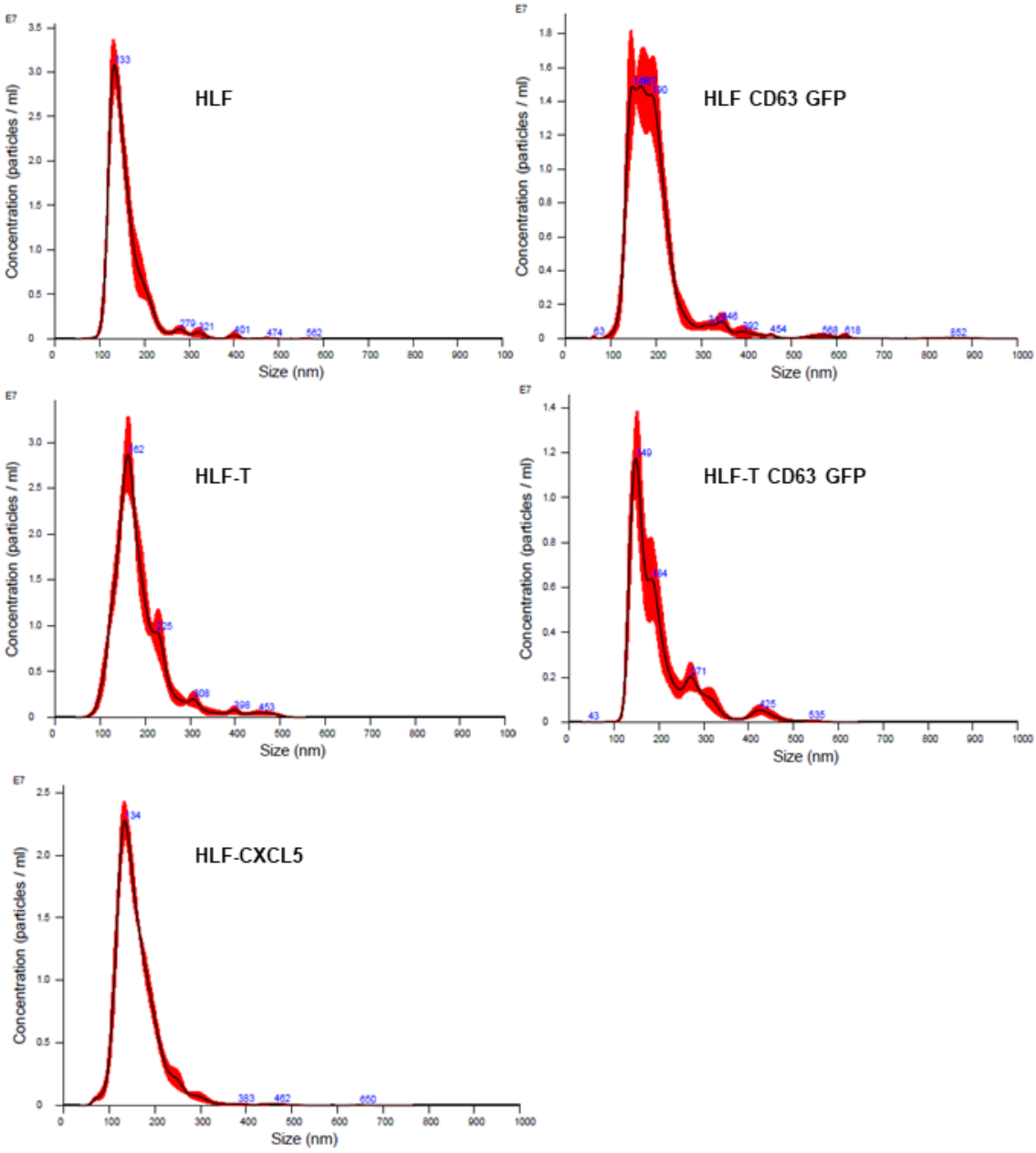

Figure 14: Characterization.of EVs by NTA.

NTA profiles of EV´s derived from HLF, HLF-T, HLF-CXCL5, HLF CD63-GFP, and HLF-T CD63-GFP after enrichment via 10K filter device and DUC isolation. The samples were measured in a 1:100 dilution in PBS.

The NTA peaks at maximum intensity revealed in all samples a size range of 130-190 nm. Consequently, all groups contained mostly micro vesicles, which are 50 nm to 1000 nm bis in size. NTA profile of HLF-CD63-GFP and HLF-T-CD63-GFP derived EVs displayed wider peaks and therefore a wider size distribution as compared to those EVs isolated from HLF, HLF-T and HLF-CXCL5 cells. The peak intensity and the peak width reflect the concentration of a particular size, concluding that especially HLF CD63 GFP has a high EV yield of 140 nm to 190 nm sizes. Also, EVs derived from a cell line expressing a CD63-GFP construct show more peaks in the range of 300 nm to 600 nm, therefore larger EV sizes suggesting aggregate formation.

NTA analysis allowed us to further evaluate the influence of TGF-β stimulation on the production of EVs. In order to monitor the phenotypical changes of HLF cells induced by TGF-β, the induction of the TGF-β switch in HLF following long-term TGF-β treatment was confirmed by the increased migration (Figure 15) [40]. This test was conducted after subjecting the cells to long-term treatment with TGF-β over a period of at least 10 days. EVs were only isolated if the oncogenic phenotype of HLF-T cells was observed.

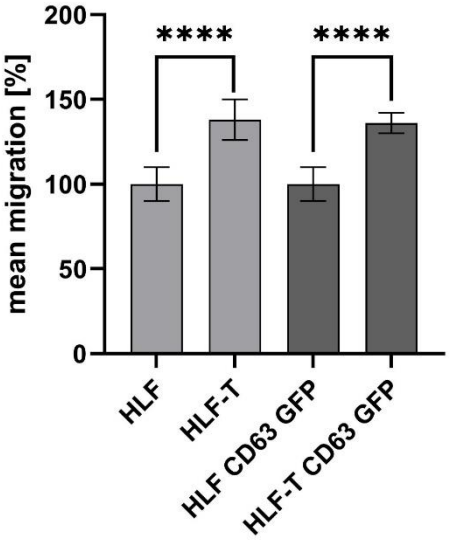

Figure 15: Long-term TGF-ß treatment causes an increased cell motility of HLF cells as analysed by wound healing assays.

*Light grey: Mean migration areas (n=40) of long-term TGF-ß-treated HLF cells (HLF-T) normalized to parental HLF cells. Dark grey: Mean migration areas (n=24) of long-term TGF-ß-treated CD63-GFP-expressing HLF cells (HLF-T CD63 GFP) normalized to parental CD63-GFP-expressing HLF cells. The mean migration area of parental cells was set to 100%. Data are expressed as mean +- SD. P-values were calculated with Mann-Whitney-U tests for 2 independent groups, **** P < 0.0001.*

As shown in Figure 16A, long-term exposure to TGF-β increased the production of EVs 1.5-fold in comparison to parental HLF (Figure 16 B), although less HLF-

T cells were seeded at the beginning. Notably, this effect was specific for HLF-T cells as only a small increase was observed for HLF-CXLC5 cells. The mean vesicle size of HLF-T derived EVs was 1.3-fold bigger than EVs produced by parental HLF or HLF-CXCL5 cells (Figure 16 C). 33%, 44% and 22% of HLF-derived EVs were in the size range of 50-150 nm, 150-200 nm and >200 nm, respectively (Figure 16 D). Conversely, 17%, 33%, and 50% of HLF-T-derived EVs showed the size range of 50-150 nm, 150-200 nm, and >200 nm, respectively. HLF-CXCL5-derived EVs exhibited a size distribution similar to the one of parental HLF derived vesicles. Together, these data suggest that HLF-T cells show a trend of producing bigger and larger quantities of EVs. ANOVA testing for size and quantities showed no significant differences between all three groups due to high standard deviations.

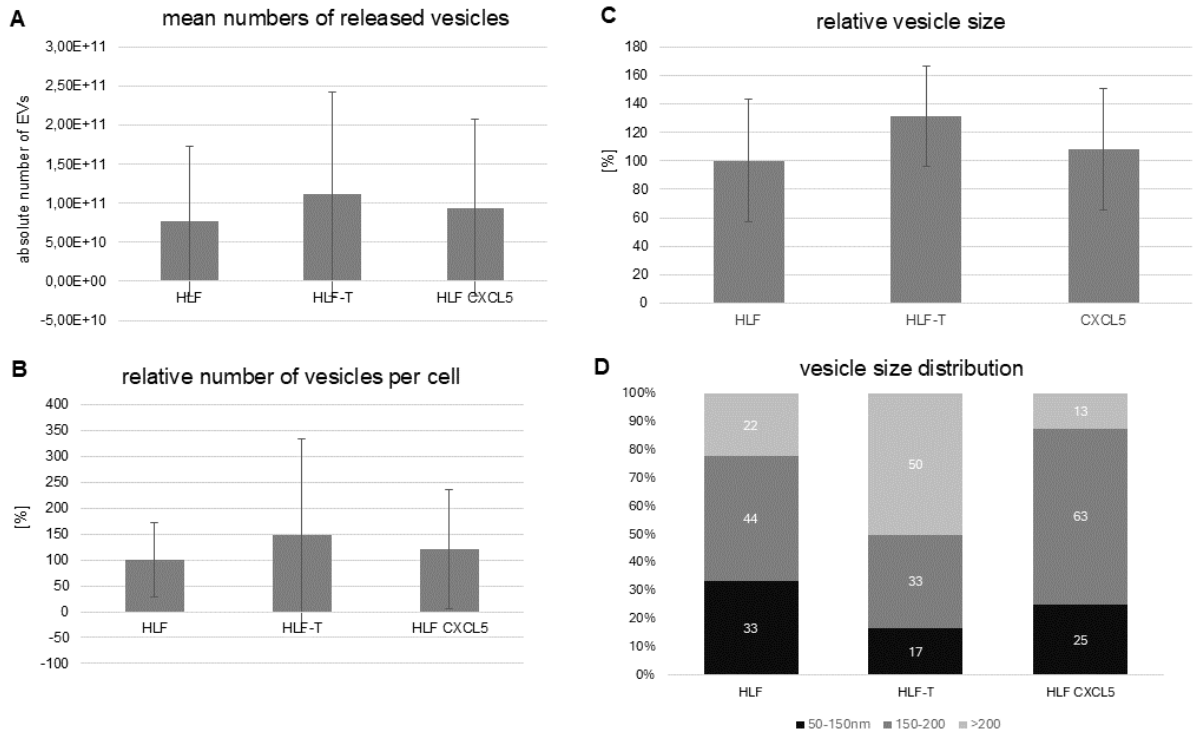

Figure 16: EV production affected by TGF-β.

A) Absolute mean numbers of EVs released from parental HLF, TGF-β exposed HLF (HLF-T) and CXCL5 expressing (HLF-CXCL5) cells. (B) EV numbers were normalized to cell numbers. (C) EV size. The value of parental HLF was set to 100% in B and C. (D) Vesicle size distribution plots. Mean EV number and EV size were determined from $n_{(HLF)}$ = 8 isolations, $n_{(HLF-T)}$ = 10 isolations, $n_{(HLF-CXCL5)}$ = 7 isolations). In all datasets a one-way ANOVA was performed displaying no significant difference in size or vesicle number between the groups (p >0.05).

4.5 Analysis of Selected EV Cargo Immunoblotting and Immunofluorescence Microscopy

After determination of the size and quantities of EVs, the expression of selected proteins was analysed by immunoblotting of HLF-, HLF-T- and HLF-CXCL5-derived EVs and compared to their expression in cell lysates (CL) and in cell lysates of starved cells (CLS). Starved cells were analysed to determine whether changes in protein expression occur following starvation and to assess any potential correlation with EV protein expression. The selection of analysed proteins was based on the results of the EV content obtained by LC-MS/MS (Figure 12) and search in the literature (Table 6). Accordingly, we further examined the expression of ANXA1, ANXA2, integrin α5 and integrin β1 in EVs of various cellular conditions. CD63 and TSG101 were used as exosome markers while GRP78 was employed as a negative control for EVs. β-actin was used as loading control in total cell lysates since it is expressed in all eukaryotic cell types and remains stable in the presence of a wide range of compounds. As a consequence of the limited protein content of EVs following each isolation procedure, which was costly in time as well as complex to implement, only small quantities of protein were loaded onto a gel. To ascertain the most suitable protein load for both cell lysate and EV lysate without compromising the signal, a preliminary assay was conducted. This assay aimed to identify the minimum protein quantity of EVs that can be used while still retaining a detectable signal (Figure 17).

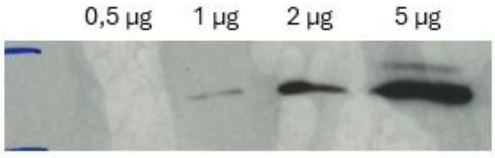

Figure 17: Protein concentration range for signal detection.

β-actin expression at different protein concentrations of the EV cargo. EVs were isolated from HLF cells, and the protein was isolated. 0.5 µg, 1 µg, 2 µg, and 5 µg EV protein were analysed by Western blotting.

The signal intensities increased with protein concentration, indicating that loading at least 5 µg of proteins provides a reliably detectable signal. Prior to the

assay, the specificity of the employed antibodies was evaluated in total cell lysates (data not shown).

The preliminary data revealed a TGF-β specific cluster of HLF-T derived EVs which we aimed to confirm by immunoblotting. Unfortunately, a clear validation of the cluster was not possible, albeit the analysis was repeated several times – at least two times - under the same conditions (Figure 18). Quantification of the signal intensities of immunoblots allowed us to visualize and compare the differences between the groups. The observed trends suggest potential differences in protein expression that warrant further investigation (Figure 19). ANXA1 protein expression was not elevated in EVs derived from HLF-T cells. Here, a polyclonal antibody was used which recognizes the intact (upper band) and the cleaved protein (lower band) (Figure 18) [98]. The protein expression in cell lysates of all three cell lines appeared to be highly similar for all proteins analysed, albeit the cleaved ANXA1 version was increasingly present in all EVs (Figure 18 and 19 A). ANXA1 and ANXA2 seem to have a stronger protein expression in HLF derived EVs. Immunoblotting of integrin α5 was conducted four times, revealing a slight upregulation of protein content in HLF-T-derived EVs. However, quantitative densitometric analysis was hindered by the presence of a smear. Consistent detection of non-specific bands in the same region prompted the exclusion of integrin α5 from further analysis.

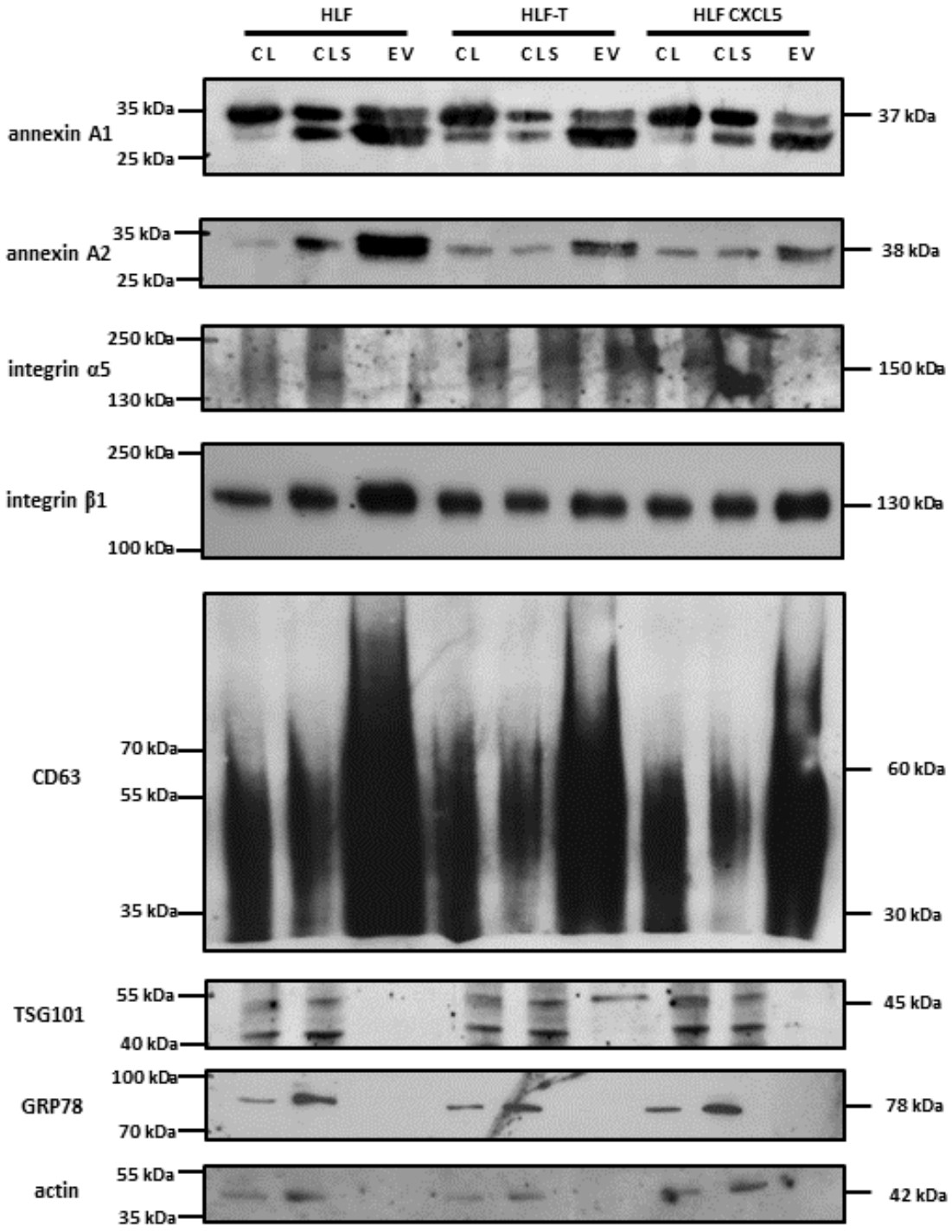

Figure 18: Expression of proteins total cell lysates and in the EV cargo of HLF, HLF-T and HLF-CXCL5 cells as analyzed by immunoblotting.

CL, cell lysate; CLS, cell lysate of starved cells; EV, extracellular vesicle. CD63 and TSG101 was used as exosome markers. GRP78 was a negative control for EVs. Actin was used as a loading control for cellular protein expression.

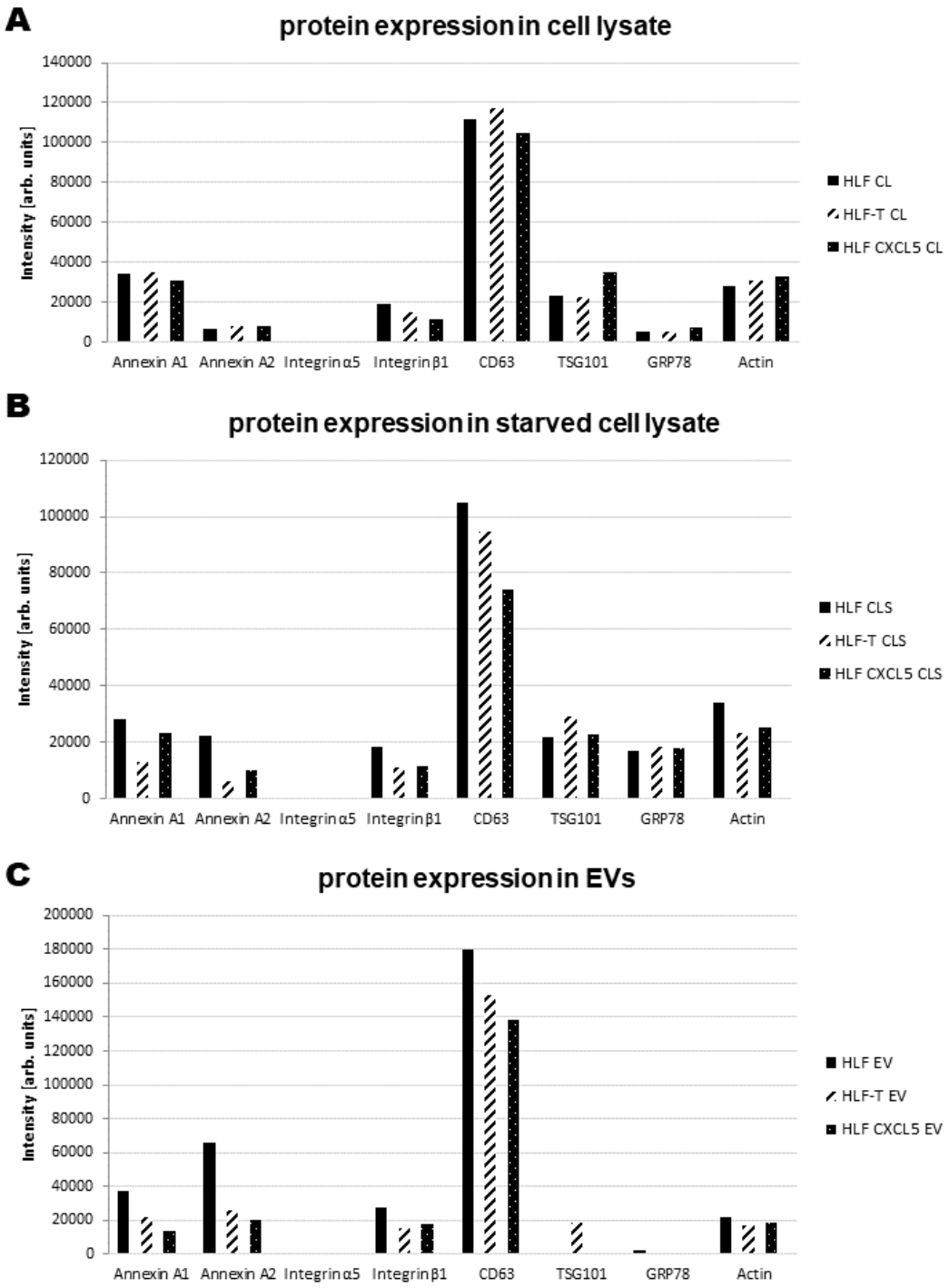

Figure 19: Quantification of signal intensities shown in Figure 18. Signal intensities were analysis of protein expressions of one representative blot in (A) cell lysates, (B) lysates of starved cells, (C) EV lysates.

The protein levels of integrin β1 show a trend of being slightly higher in EVs than in cell lysates (Figure 19 A-C). CD63 expression in all three cell lines was in EVs elevated compared to the cell lysates (Figure 19 C). In all three cell lines the starved cell lysates had a decreased CD63 expression compared to the non-

starved cell lysates, in contrast to the derived EVs which show a notable increase in CD63 expression (Figure 19). TSG101 shows only protein levels in HLF-T derived EVs and is not present in the EV lysates of HLF and HLF-CXCL5. Interestingly, the protein levels of GRP78 in starved cells were elevated in all three cell lines compared to non-starved cell lysates (Figure 19 B). Also, in EVs an similar protein expression as in starved cell lysates was observed. GRP78 is not present in EVs as it is a protein of the endoplasmatic reticulum. However, as this analysis is based on a single experiment, the findings should be interpreted with caution. Further validation via immunofluorescence microscopy confirmed that there were no observable differences in the expression levels of the proteins of interest in the cytoplasm and at cell borders between the groups (Figure 20). From these data we conclude that integrin α5 is suggested to be regulated by TGF-β while other proteins show no changes after TGF- β treatment.

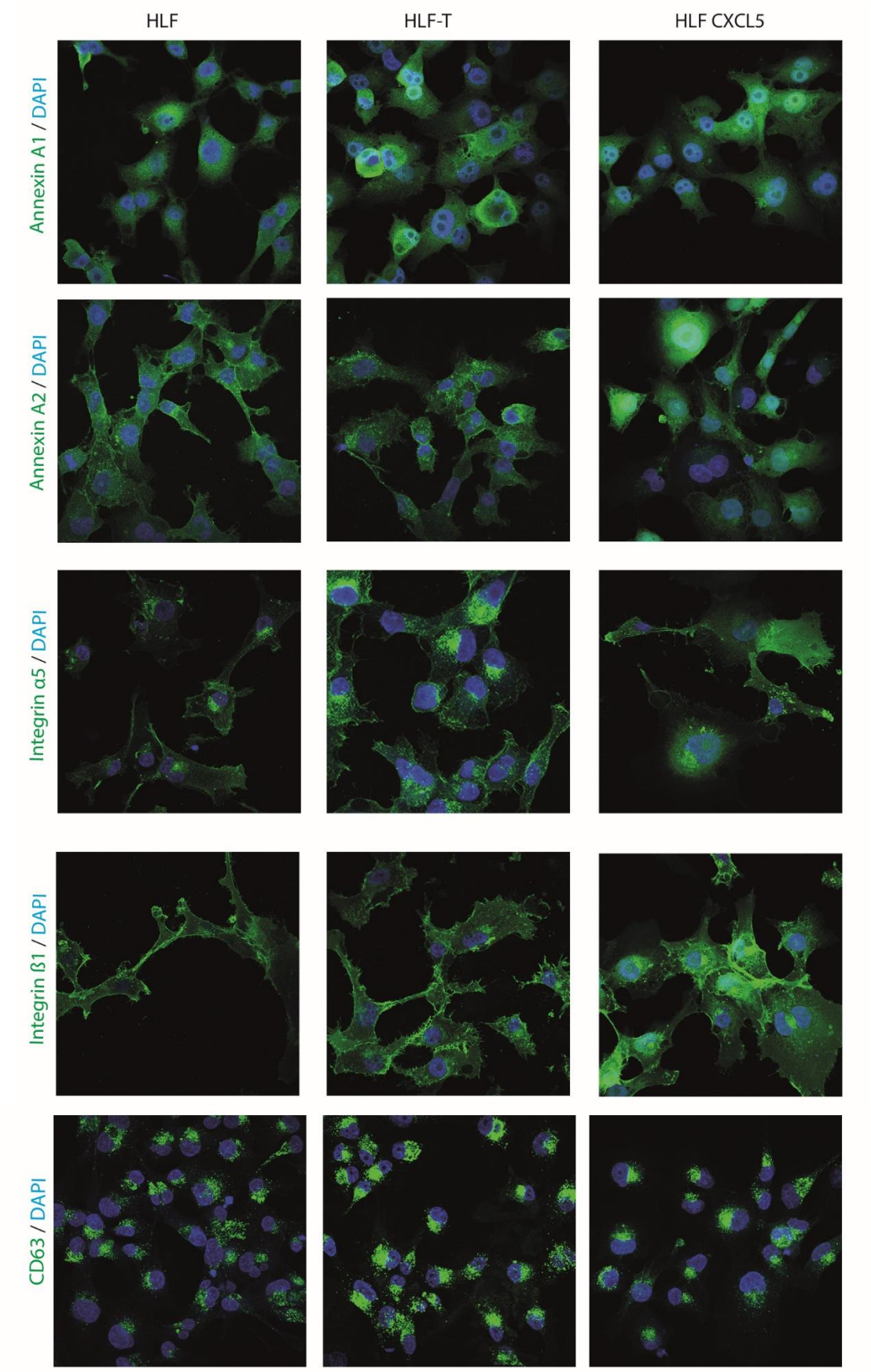

Figure 20: Immunofluorescence microscopy of HLF, HLF-T and HLF-CXCL5 cells. Detection of annexin A1, annexin A2, integrin α5, integrin ß1 and CD63 (green). Nuclear DAPI stain (blue).

4.6 Influence of TGF-β inhibition on selected EV-cargo

Next, we addressed the question whether blocking of the TGF-β signalling affects the loading of the EV cargo. Therefore, we treated cells with LY2109761 which inhibits TβRI/II kinase. Results obtained from experimental liver metastasis models suggest that targeting the activity of TβRI/II kinase on tumour cells and liver microenvironment cells is crucial for suppressing liver metastasis [99]. We were interested whether the inhibition of TGF-β signalling influences the secretion as well as the load of EVs and whether it modulates the identified TGF-β-specific EV cargo cluster (Figure 12). EVs were isolated and LC-MS/MS analysis was performed to identify the content of the vesicles 48 hours of LY2109761 administration. HLF-derived EVs without inhibitor treatment served as control. Unfortunately, no significant differences were observed between the samples with and without LY2109761 administration (Figure 21). Furthermore, immunofluorescence microscopy was conducted on the identical set of samples, however, no visible alterations were observed in the levels of protein expressions (data not shown). The repetition of experiments was not feasible due to time limitations. These data suggest that there are no enhanced levels of at least ANXA1, ANXA2, integrin α5, integrin β1 and fibronectin released from HCC cells by EVs in a TGF-β-dependent manner.

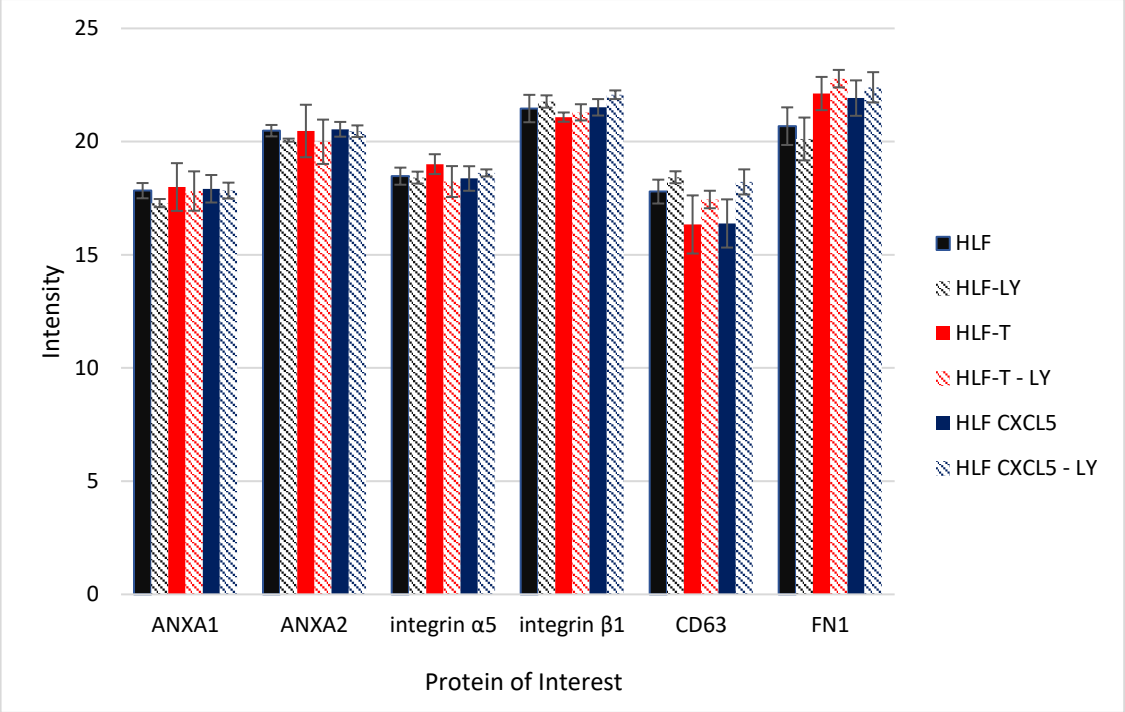

Figure 21: Proteomic analysis of EVs derived from HLF, HLF-T and HLF-CXCL5 cells with and without LY2109761 administration.

LC/MS-MS analysis was performed on EV cargo derived from three different cell types: HLF, HLF-T, and HLF-CXCL5. The samples were tested with and without treatment of LY2109761. Inhibitor-treated samples were indicated with "-LY" marking. The obtained data were expressed as the mean ± standard deviation (SD) of three measurements. ITGA5: integrin α5, ITGB1: integrin β1, ANXA1: annexin A1, ANXA2: annexin A2, FN1: fibronectin.

4.7 EV-fusion with stromal target cells

In the next step, we aimed to investigate whether EVs can fuse with target cells and to visualize this process using spinning disc confocal immunofluorescence microscopy. EVs derived from CD63-GFP-expressing cells incorporate CD63-GFP into their membrane, allowing for their visualization under a microscope at a wavelength of 475 nm.

Target cells include HSCs which play a pivotal role in the progression of hepatic fibrosis due to their capacity to undergo trans-differentiation into collagen-producing myofibroblasts (MFBs). In addition, fusion experiments were conducted using endothelial HUVEC cells. Our hypothesis involves that HCC cell-derived EVs have the ability to circulate via the bloodstream and cross the endothelial barrier to reach other organs. Consequently, the fusion of EVs with endothelial cells holds significant importance. Seeding of both cell types into

dedicated wells was followed by incubation each with 5µg of EVs. Different time durations were selected to investigate the fusion process of EVs with cells. Initially, LX2 cells were co-incubated with EVs for varying time periods of 2, 4, 12 and 24 hours. No significant differences were observed between 12 hours and 24 hours of incubation (Figure 22 and 23). Therefore, the 24 hours' time point of analysis was excluded from the subsequent HUVEC co-incubation experiments. After the predefined time intervals, cells were fixed using 4% Histofix and subsequently stained with DAPI and phalloidin to visualize the cell nucleus and the actin cytoskeleton, respectively. Utilizing the confocal spinning disc microscope, higher resolution imaging was achieved, which is essential for studying vesicles smaller than 1 µm. Most notably, fusion events between EVs and LX-2 cells (Figures 22, 23) as well as HUVEC cells (Figures 24 and 25) were observed. These events were evidenced by the co-localization of EV fluorescence within the cells. Furthermore, no distinction was noticed between parental EVs and those released by TGF-β induced cells. Notably, the staining of EVs with PKH (Figure 23, 25) exhibited greater signal intensities compared to tracking by GFP (Figure 22, 24). While GFP showed a detectable signal only after 4 hours of incubation, PKH already exhibited a signal after 2 hours. The fusion process occurs probably within the initial 2-hour period, although its visibility depends on a strong signal. Prior to fixation, cells were washed, indicating that the EVs must be located within the cells. No signal was observed in the background, i.e. unlabelled control. By tracking EVs with GFP, the signal often appears as if vesicles were aggregated (Figure 22; 12h). In contrast, individual vesicles can be clearly observed with PKH (Figure 25; 12h). Together, these results show that HCC cell-derived EVs fuse with HSCs and endothelial cell in a TGF-β-independent fashion. The fusion of EVs with target cells may play a crucial role in intercellular communication, influencing target cell behaviour and function.

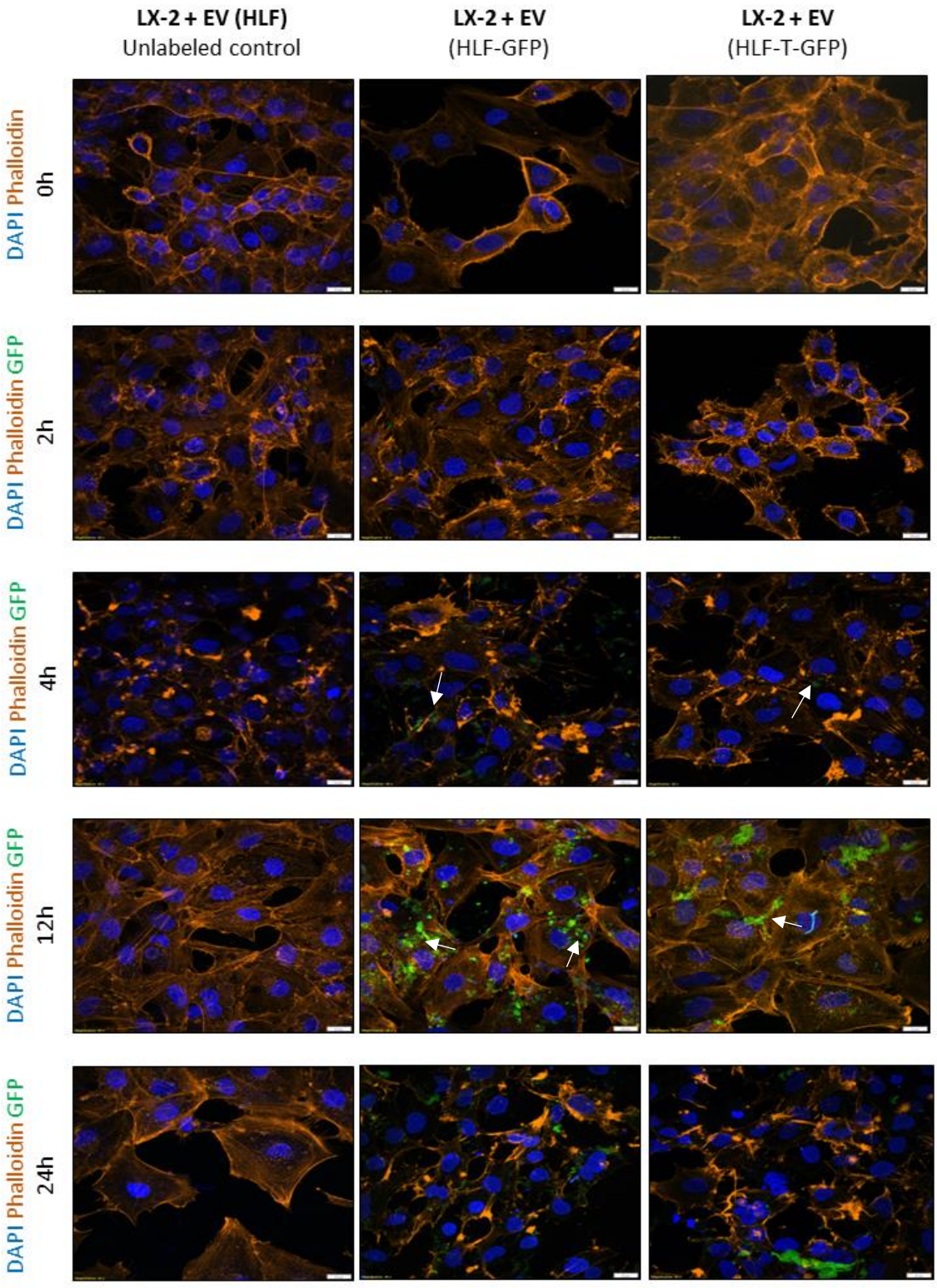

Figure 22: Spinning disc confocal immunofluorescence microscopy of human HSCs (LX2) co-cultivated with EVs generated from HLF and HLF-T cells expressing CD63-GFP (63x magnification in oil). Co-cultures were conducted for different durations of time. Blue, DAPI; orange, phalloidin; green, GFP. White arrow indicates fusion.

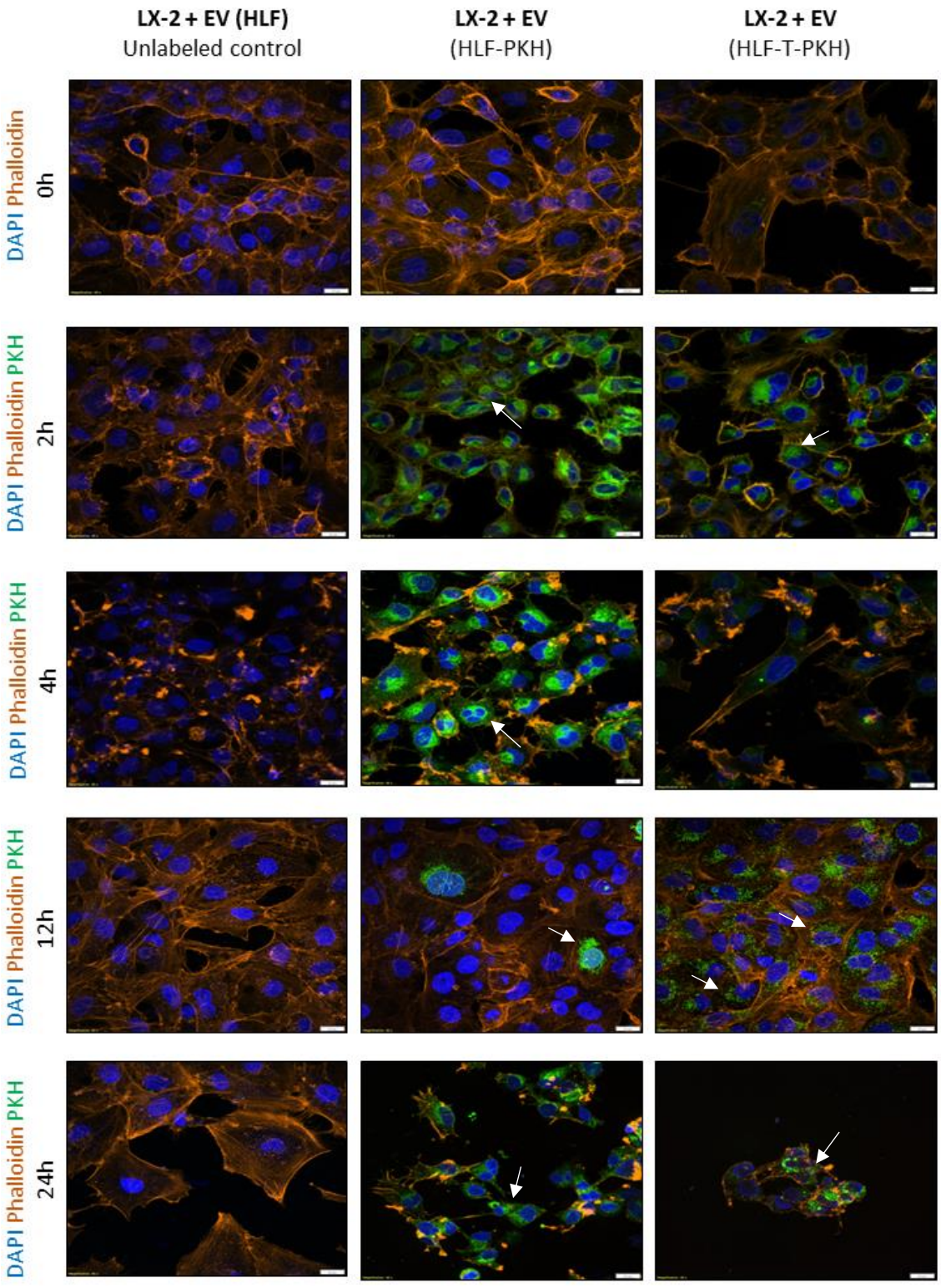

Figure 23: Spinning disc confocal immunofluorescence microscopy of human HSCs (LX2) co-cultivated with EVs generated from HLF and HLF-T cells after staining with membrane dye PKH67. Co-cultures were conducted for different durations of time. Blue, DAPI; orange, phalloidin; green, PKH67. White arrow indicates fusion.

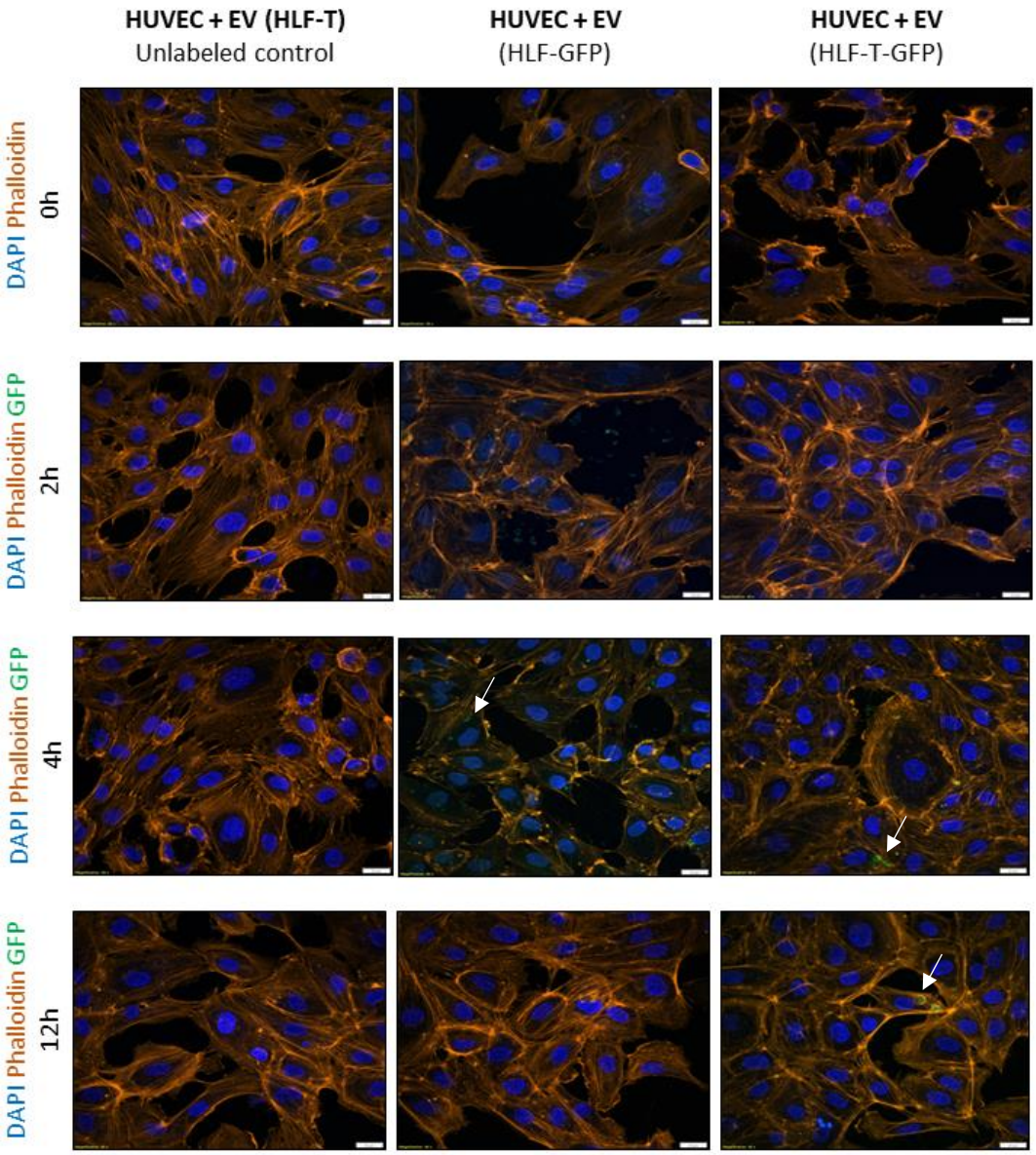

Figure 24: Spinning disc confocal immunofluorescence microscopy of human umbilical vein endothelial cells (HUVECs) co-cultivated with EVs generated from HLF and HLF-T cells expressing CD63-GFP (63x magnification in oil). Co-cultures were conducted for different durations of time. Blue, DAPI; orange, phalloidin; green, GFP. White arrow indicates fusion.

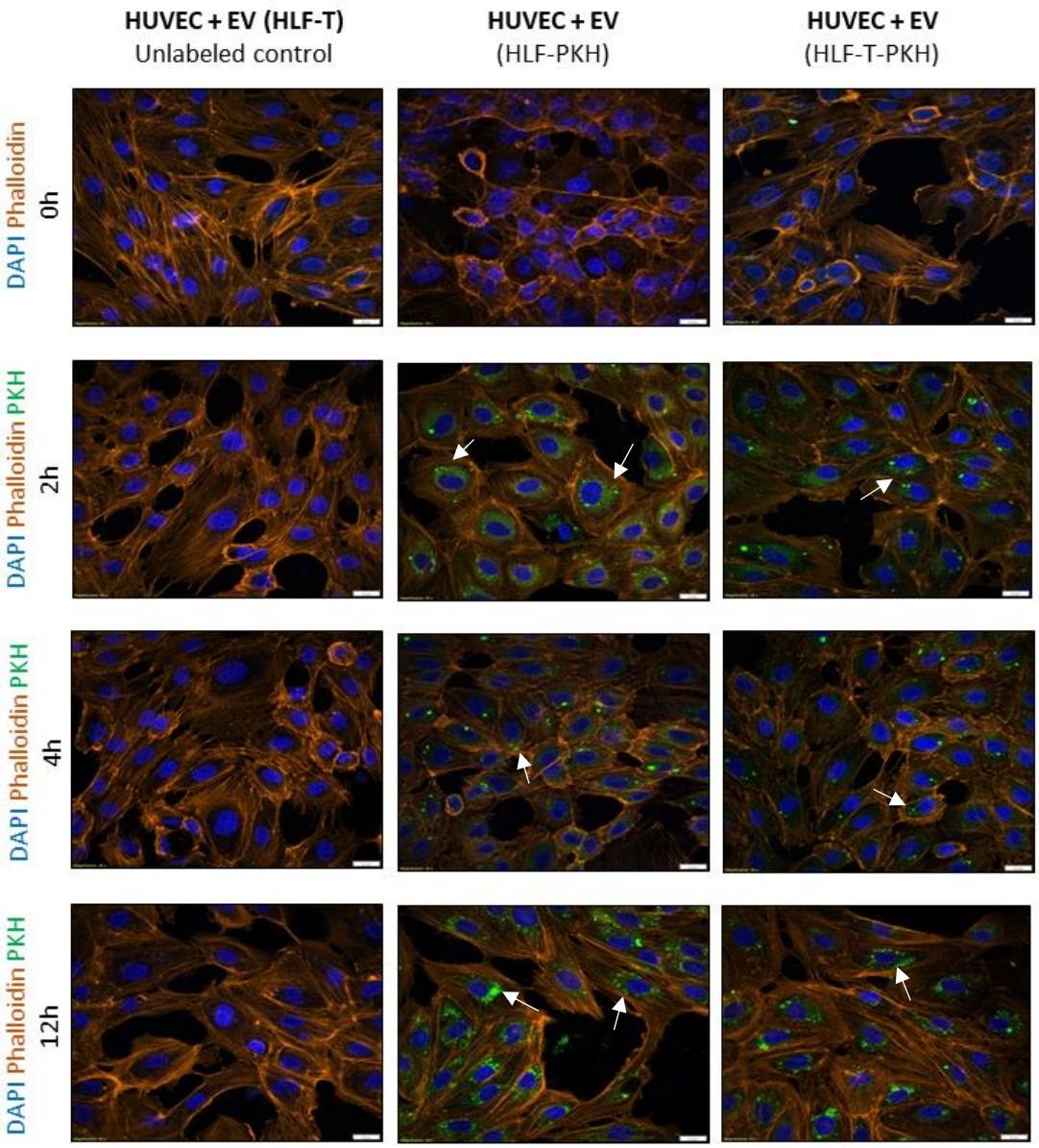

Figure 25: Spinning disc confocal immunofluorescence microscopy of human umbilical vein endothelial cells (HUVECs) co-cultivated with EVs generated from HLF and HLF-T cells after staining with membrane dye PKH67. Co-cultures were conducted for different durations of time. Blue, DAPI; orange, phalloidin; green, PKH67. White arrow indicates fusion.

5 Discussion

We identified a TGF-β-specific cluster of EV proteins in long-term TGF-β treated HCC cells, leading to the hypothesis, that TGF-β signalling may be involved in EV-mediated long-range signalling. RNA sequencing revealed significant upregulation of fibronectin and integrin α5 at the mRNA level in HLF-T cells, indicating a selective transcriptional mechanism, as other proteins remained unchanged. In NTA measurements predominantly microvesicles were represented. EVs from HLF-T cells were larger and more abundant. Immunoblotting suggested that only integrin α5 is regulated by TGF-β, while immunofluorescence microscopy detected no significant differences in protein expression levels. Furthermore, blocking TGF-β signalling did not affect EV cargo or secretion. The ability of EVs to fuse with stromal target cells highlights their role in intercellular communication, potentially influencing the behaviour and function of target cells.

These results suggest a complex contribution of TGF-β in modulating EV cargo and secretion. While the upregulation of fibronectin and integrin α5 at the mRNA level in HLF-T cells points to transcriptional regulation, the lack of corresponding changes in protein expression suggests post-transcriptional regulation or compensatory mechanisms that may balance protein production. The fact that integrin α5 appears to be selectively regulated by TGF-β, as indicated by immunoblotting, supports the idea of a targeted rather than global effect of TGF-β on EV composition. This selective regulation might be linked to the specific role of integrins in mediating EV uptake by target cells, potentially influencing the metastatic niche. Hoshino, et al. stated in 2015 that integrins transported by EVs not only facilitate adhesion to specific organs but also "educate" these organs by modifying their environment, thereby promoting the growth and establishment of metastatic cells and secondary neoplasia [60]. The elevated protein levels in EVs derived from HLF-T cells suggest a differential packaging of these proteins into EVs, which could
have functional implications in the communication to the cellular microenvironment.

The evaluation of EVs via NTA characterization and immunoblotting did not validate the preliminary data. NTA measurements revealed a trend that EVs

generated by HLF-T cells on average were bigger in size as well as larger in quantities than EVs produced by HLF cells. Interestingly, the size and abundance of EVs from HLF-T cells suggest that cellular transformation, perhaps driven by chronic TGF-β exposure, alters the biophysical properties of EVs. The increased size, in a range of 100-1000 nm typical of microvesicles, could reflect a change in EV biogenesis pathways, possibly involving altered membrane dynamics or cytoskeletal changes. This finding is in line with reports that cancer-associated EVs often show unique molecular cargo, which may contribute to their enhanced ability to modulate the TME [100]. 50% of all EV isolations from HLF-T cells had a size greater than 200 nm. All EVs were measured immediately after isolation to prevent aggregation that can occur during freezing. Based on their size, the EVs are likely MVs, as their dimensions exclude exosomes and apoptotic bodies, which are significantly larger. Immunoblot analysis revealed a modest upregulation of GRP78, an endoplasmic reticulum-associated protein and apoptosis marker, in starved cells relative to non-starved controls. This increase may suggest enhanced apoptosis induced by cellular starvation, potentially contributing to the formation of apoptotic bodies. They may account for the small peaks observed in the NTA measurements within the 300 nm to 600 nm range. However, due to the low protein loading concentration of 5 µg on immunoblots, detection was likely hindered by insufficient protein quantity or antibody specificity. Since the markers are not specific enough to identify a particular EV category, these results could correspond to any of the three EV types. The high standard deviations indicate high variations between experimental values. NTA was chosen for EV characterization on the one hand due to its simple sample preparation and fast read-outs, and on the other hand due to its broad routine use for EV analysis. However, it still has some limitations. A study of Vestad, *et al* in 2017 demonstrates that while NTA shows good reproducibility across two different instruments and locations, significant variations in measurements may occur due to differences in instrument settings, technical conditions, and operator influence, demanding stringent standardization to enhance measurement accuracy [101]. Importantly, the gold standard technique for EV characterization is electron microscopy. Thus, operating an electron microscope and interpreting the results requires specialized training and skills provided by

collaborative efforts and expertise. EVs derived from CD63-GFP-expressing cells show a broader size distribution compared to their non-GFP-expressing counterparts. This could suggest that GFP tagging, particularly the CD63-GFP construct, affects vesicle size or heterogeneity. The non-GFP samples have more consistent and narrower size distributions, indicating more uniform populations of EVs. The data suggests that GFP expression, especially in the CD63 context, potentially influence EV size. However, literature supports that CD63-GFP labelling does not significantly alter the composition or physicochemical properties of EVs compared to native vesicles, indicating minimal impact on size due to GFP expression [102].

Larger quantities in TGF-β cluster could be a reason for metastasis progression, which underlines the theory of oncogene-regulated release of EVs. Oncogenes can modify the number, size, and heterogeneity of released vesicles along with altering the ESCRT pathways, crucial for EV production [103]. The MYC and AURKB oncogenes suppress the lysosome pathway, selectively alter the protein and miRNA composition of EVs and influence EV release to sustain cellular homeostasis [103]. Noteworthy, the number of isolations for EVs with CD63-GFP construct is not representative for a significant statement. Due to time limitations more than 2 isolations were not possible.

The inhibitor administration aimed to investigate whether inhibition of TGF-β signalling affects the release and content of EVs, particularly focusing on the previously identified TGF-β-specific EV cargo cluster. However, following 48 hours of LY2109761 administration and subsequent EV isolation together with LC-MS/MS analysis, no significant differences in EV content were observed compared to controls without inhibitor treatment. Additionally, immunofluorescence microscopy showed no visible changes in protein expression levels between treated and untreated samples (data not shown). The inability to repeat experiments due to time constraints further limits the robustness of these findings. Overall, these results suggest that blocking TGF-β signalling with LY2109761 does not significantly alter the EV cargo in the experimental setup used, highlighting the need for further studies to confirm these observations and explore alternative pathways or conditions that might influence EV composition. It is possible that while TGF-ß plays a role in modulating certain EV cargo, such as integrin α5, other signalling pathways are

compensating for the loss of TGF-ß input in maintaining EV production and cargo sorting. TGF-β primarily influences EV cargo by affecting pathways like SMAD-dependent transcriptional regulation or through non-canonical pathways involving various kinases and GTPases [104]. However, studies have shown that other signalling mechanisms, such as the Wnt, ERK, or PI3K/AKT pathways, can take over in modulating EV biogenesis and cargo composition when TGF-β signalling is disrupted [105]. In cancers like PDAC, exosomal miRNAs are known to activate these compensatory pathways, such as PI3K/AKT, to maintain the influence of EVs on the tumour microenvironment, even when TGF-β signalling is blocked [105].

We assumed that the TGF-β-specific cluster of EV cargo proteins is detectable by immunoblotting, suggesting increased protein production in EVs generated by HLF-T. We excluded integrin α5 from further evaluation due to the low antibody specificity or the lack of EV content. ANXA1 and ANXA2 showed higher expression in HLF-derived EVs, suggesting their potential role in EV-mediated functions, albeit independent of TGF-β. ANXA1 was detected in both its intact and cleaved forms, showing higher abundance of cleaved ANXA1 in EVs. A study showed that ANXA1 cleavage occurs on the outer cell surface during apoptosis followed by secondary necrosis in Jurkat cells [106]. However, the results presented starved cells, with and without TGF-β treatment, a stronger ANXA1 signal compared to native cells. This underlines the hypothesis that maybe increased apoptosis due to starvation promotes the formation of apoptotic bodies and influences the packaging of EVs [106]. The exosome markers CD63 confirmed the successful isolation of EVs, particularly displaying elevated CD63 levels in EVs compared to cell lysates. TSG101 was notably present only in HLF-T derived EVs, highlighting a possible specificity in EV content related to TGF-β treatment. GRP78, the negative control for EVs, was not detected in the EV samples, confirming its intracellular localization and the purity of the EV preparations. The data suggest that TGF-β treatment influences somehow the protein composition of EVs [107]. Future studies could focus on improving detection strategies for low-abundance proteins and exploring the functional implications of proteins like ANXA1 and ANXA2 in EV-mediated signalling pathways, particularly in the context of apoptosis and tumour progression.

Given that the findings are based on a single experiment, these results should be interpreted with caution. The absence of error bars in the quantification analysis, attributed to significant variance among replicates, limits the statistical robustness of the conclusions. Multiple Western blot replicates were performed; however, consistent results were not achieved. This inconsistency is likely due to variability in EV isolation processes. EVs have traditionally been purified using ultracentrifugation (UC), as it is stated as the gold standard in the literature [108, 109]. However, UC has several limitations including operator-dependent yields, EV aggregation, altered EV morphology and being time-consuming. Size exclusion chromatography (SEC) offers a time-efficient, reproducible and scalable method for purifying EVs with high yield and similar quality to traditional UC [71, 110]. This underscores the fact that the UC approach could lead to misinterpretation of EV data. Further validation through additional experiments and immunofluorescence microscopy, which did not show observable differences in protein expression levels, supports these observations but also underscores the need for replicative studies. Poor reproducibility of data can significantly contribute to high variance in statistical analysis. When experimental results are inconsistent and lack reproducibility, the variability between repeated measurements or experiments increases, leading to elevated variance. This increased variance obscures true effects and complicate the drawing of reliable conclusions from the data. Furthermore, the protein concentration of EV samples using for EV fusion experiments was not quantified in parallel with NTA estimation of particle concentration as there were not enough EVs in quantities. This dual approach by assessing both proteins and particles, would have allowed consistent EV treatments with same protein/cell and particle/cell ratios. Consequently, additional discrepancies were introduced. The particle concentration of 6×10^8 particles per well, utilized for treating recipient cells, was anticipated to elicit significant effects in stromal cells.

The objective of EV co-incubation with stromal target cells was to investigate the fusion of EVs, produced by HCC cells, with other cell lines, including LX-2 and HUVECs. The presence of CD63-GFP construct in the EV membrane enabled the identification of these EVs as green-fluorescent vesicles under microscopic observation. However, it is worth noting that the GFP protein could potentially interfere with the binding process between the EVs and target cells. Therefore,

the lipophilic membrane stain PKH67 was employed to label EVs by accumulating within their lipid bilayer membrane. This approach allows for the visualization and tracking of EVs without disrupting their natural binding interactions or functional properties. Two cell types were utilized to demonstrate the ability of EVs to fuse with different cells irrespective of their origin. The impact of the GFP-tag and PKH67 dye on internalization processes was found to be negligible. Given the ability of these EVs to fuse with stromal target cells, their potential to influence the TME becomes evident [104]. EVs could act as mediators of long-range signalling, carrying TGF-ß-related cargo that promote changes in stromal cells, facilitating processes such as extracellular matrix remodelling, immune evasion, and angiogenesis [111]. Flow cytometry offers a fast and robust quantitative method for validating the microscopic observations of EV uptake. After labelling EVs and co-incubation with target cells, internalized labelled EVs would exhibit increased fluorescence compared to controls, which are unexposed cells [112]. Dual-labelling techniques, e.g. combining PKH67 with a cell-specific marker, could be employed to discriminate EV-internalized cells from those with surface-bound vesicles [112]. Flow cytometry could separate populations of target cells that have successfully fused with EVs based on their fluorescent signal [112]. Quantification of fusion efficiency could be achieved by measuring the mean fluorescence intensity (MFI) of the target cells, allowing you to compare the efficiency of EV uptake across different cell types or conditions [112].

This technique allows high-throughput analysis, incorporating this technique would provide statistical validation for microscopic observations, ensuring that the fusion or uptake is not restricted to a small population of cells but is reproducible across a broader sample [112]. Future experiments could combine microscopy and flow cytometry. Due to restricted amount of time, we couldn’t confirm the data via flow cytometry. Future research could focus on identifying the specific functional changes induced by EVs in stromal cells, as well as exploring how integrin α5-mediated interactions contribute to EV uptake and downstream signalling cascades in recipient cells [113]. Flow cytometry could help quantify fusion efficiency and phenotypic shifts based on surface markers and intracellular changes [112]. Other methods to observe phenotypical changes post-EV fusion would be a combination of molecular techniques

(qPCR, RNA-seq, proteomics) and functional assays (migration, apoptosis). RNA-seq allows for a global overview of changes in transcriptional activity, identifying upregulated or downregulated genes related to processes like proliferation, apoptosis, or differentiation [114]. qPCR facilitates targeted analysis of specific genes or miRNAs that are known to be carried by EVs or involved in the pathways of interest [114]. By comparing the gene expression profile before and after EV fusion, it is possible to identify which pathways are being modulated. Proteomics detects changes in the protein expression profile of the target cells post-fusion since EVs can deliver proteins directly to target cells, which may alter signalling pathways and downstream phenotypic outcomes [115]. Specific functional changes could be measured by migrations and invasion assays to test if EV fusion enhances the migratory or invasive capabilities of target cells, often relevant in cancer or tissue regeneration studies [116]. Cell death assays determine if EVs induce cell death or protect target cells from apoptosis by staining for apoptotic markers e.g. Annexin V [117]. *In vivo* studies can further validate the phenotypic effects of EV fusion in animal models [118]. Injecting labelled EVs into mice could elucidate their distribution and impact on tissue-specific cells inducing PMNs [118]. The formation of a PMN *in vivo* involves the preparation of distant organs for tumour metastasis and is a multi-step process influenced by the release of EVs from the primary tumour [104, 111]. Integrins on the surface of tumour-derived exosomes have been shown to dictate organotropism by selectively binding to specific cell types in distant organs, such as Kupffer cells in the liver or fibroblasts in the lungs, thereby promoting the establishment of PMNs [104, 111]. These interactions prime the tissue for subsequent tumour cell colonization by remodelling the extracellular matrix and promoting pro-inflammatory environments beneficial for metastasis formation [104, 119]. Furthermore, they have profound impact on the immune system by modulating immune responses and altering cytokine profiles [104, 120]. Tumour-derived EVs are known to carry immunosuppressive molecules such as PD-L1 that bind to PD-1 receptors on CD8+ T cells, leading to T cell exhaustion and immune evasion by tumour cells [104, 120]. Additionally, EVs released from tumours can promote the differentiation of myeloid-derived suppressor cells (MDSCs) and regulatory T cells (Tregs), both

of which further contribute to immunosuppression by inhibiting anti-tumour immune responses [111, 120].

These EVs also carry cytokines and pro-inflammatory molecules like TGF-β, which drive immunosuppressive signalling and alter the cytokine milieu of the PMN [111]. TGF-β, for instance, inhibits the activation of natural killer (NK) cells and reduces the effectiveness of cytotoxic CD8+ T cells, further enhancing immune escape mechanisms [111]. The cytokine environment within the PMN is also reshaped by the recruitment of tumour-associated macrophages (TAMs) and MDSCs, which release pro-tumorigenic cytokines such as IL-10 and VEGF [104, 105]. These cytokines promote tumour growth and angiogenesis, while also suppressing pro-inflammatory cytokines like IFN-γ and TNF-α, which are crucial for anti-tumour immunity [104, 105]. In conclusion, the modulation of the immune system by tumour-derived EVs and the associated cytokine alterations within the PMN create an immunosuppressive and pro-tumorigenic microenvironment that promotes metastasis [105, 111].

5.1 Concluding remarks and future perspectives

The preliminary data identified a TGF-β-specific cluster in long-term treated HCC cells, suggesting that TGF-β signalling may play a role in EV-mediated signalling. RNA sequencing indicated significant upregulation of fibronectin and integrin α5 mRNA in HLF-T cells, potentially contributing to phenotypic changes. Although increased protein levels were observed in EVs, the specific mechanisms of EV content regulation by TGF-β remain unclear, indicating the need for further investigation.

To address these findings, future research should focus on conducting additional replicates to validate initial findings and reduce data variability. Ensuring consistent EV isolation and measurement techniques will enhance the reliability of results. The study's limitations, such as the inability to repeat experiments due to time constraints and the high variability in measurements, highlight the need for rigorous experimental design and standardization. By addressing these issues and expanding the scope of research, future studies can provide a deeper understanding of the role of EVs in HCC and their potential as therapeutic targets.

Furthermore, exploring post-transcriptional regulation and EV biogenesis pathways will help to understand how TGF-β influences EV content. This could involve investigating specific regulatory proteins and pathways involved in EV packaging and secretion. The entire transcriptome could be analysed with RNA sequencing to identify differential expression and splicing variants. This could be useful for identifying post-transcriptional modifications and regulatory RNA elements. CRISPR-Cas9 genomic editing and RNA interference could be used to knocked out or knocked down specific genes involved in EV biogenesis and to elucidate pathway regulation. Utilizing electron microscopy and other high-resolution methods would accurately characterize EV size and morphology. This would provide more detailed insights into the differences between EV subtypes and their functional roles. Additionally, extending the research to *in vivo* models will confirm the relevance of *in vitro* findings and helps to understand the physiological impact of EV-mediated signalling in HCC progression and metastasis. The generation of GFP-tagged CD63-expressing HCC cell lines through stable transduction of a plasmid carrying the fusion gene has proven to be an effective method for producing GFP-labelled EVs without additional processing. This is relevant for future *in vivo* experiments.

Future projects will investigate the potential role of EVs in PMN formation as well as intrahepatic/extrahepatic metastasis in mouse models *in vivo* and study its dependence on TGF-β. GFP-labelled EVs derived from long-term TGF-β treated HCC cells will be administered into immunodeficient mouse models. The optimal experimental procedure needs to be determined to establish a PMN. Peneido *et al* explored in 2017 the concept of PMNs [67]. The study employed syngeneic mouse models, where tumour cells derived from genetically identical mice were injected to examine how primary tumours can release factors like EVs and cytokines, which help "prepare" distant organs for metastasis [67]. These syngeneic models were critical in allowing the researchers to observe the immune system's role in this preparatory phase and how it interacts with the tumour-secreted factors [67]. The findings from this study have provided valuable insights into how metastatic spread is influenced before tumour cells even reach new sites [67]. EVs present potential as both diagnostic and therapeutic biomarkers in HCC [121]. As diagnostic tools, EVs can be non-invasively isolated from body fluids like blood, carrying tumour-specific cargo,

which reflect the molecular characteristics of the primary tumour [121, 122]. This cargo enables early detection of HCC, as well as monitoring of tumour progression and treatment efficacy [121]. Therapeutically, EVs can serve as natural carriers for delivering drugs, small molecules, or gene therapies to target cells due to their biocompatibility and ability to cross biological barriers [121]. This therapeutic use is being explored in cancer treatment, where engineered EVs can deliver specific anti-tumour agents or immune modulators to the TME, enhancing the immune response or directly targeting cancer cells [121]. Furthermore, tumour-derived EVs themselves could potentially be used in vaccines, as they carry tumour antigens that can stimulate an anti-tumour immune response [121]. Thus, EVs offer a dual role as both biomarkers for diagnostic purposes and vehicles for therapeutic interventions in HCC [121].

In conclusion, this study shows the contribution of TGF-β in EV-mediated long range signalling in HCC, particularly through the upregulation of fibronectin and integrin α5 mRNA. However, the precise mechanisms of EV content regulation remain unclear, emphasizing the need for further research. By employing advanced molecular techniques and expanding to *in vivo* models, future studies can uncover deeper insights into how EVs contribute to HCC progression and metastasis. Investigating molecular and cellular changes associated with EV uptake will highlight the impact of EVs as mediators of long-range signalling in HCC progression. These efforts will not only refine the understanding of EV biogenesis but also prepare the foundation for the development of EV-based diagnostic and therapeutic strategies in HCC.

References

1. Rumgay, H., et al., *Global burden of primary liver cancer in 2020 and predictions to 2040.* J Hepatol, 2022. **77**(6): p. 1598-1606.

2. Rumgay, H., et al., *Global, regional and national burden of primary liver cancer by subtype.* Eur J Cancer, 2022. **161**: p. 108-118.

3. Ducreux, M., et al., *The management of hepatocellular carcinoma. Current expert opinion and recommendations derived from the 24th ESMO/World Congress on Gastrointestinal Cancer, Barcelona, 2022.* ESMO Open, 2023. **8**(3): p. 101567.

4. Llovet, J.M., et al., *Hepatocellular carcinoma.* Nat Rev Dis Primers, 2021. **7**(1): p. 6.

5. Jindal, A., A. Thadi, and K. Shailubhai, *Hepatocellular Carcinoma: Etiology and Current and Future Drugs.* J Clin Exp Hepatol, 2019. **9**(2): p. 221-232.

6. Coffin, P. and A. He, *Hepatocellular Carcinoma: Past and Present Challenges and Progress in Molecular Classification and Precision Oncology.* Int J Mol Sci, 2023. **24**(17).

7. Craig, A.J., et al., *Tumour evolution in hepatocellular carcinoma.* Nat Rev Gastroenterol Hepatol, 2020. **17**(3): p. 139-152.

8. Nault, J.C., et al., *The role of telomeres and telomerase in cirrhosis and liver cancer.* Nat Rev Gastroenterol Hepatol, 2019. **16**(9): p. 544-558.

9. Rebouissou, S. and J.C. Nault, *Advances in molecular classification and precision oncology in hepatocellular carcinoma.* J Hepatol, 2020. **72**(2): p. 215-229.

10. Hedrich, V., et al., *Intrinsic and Extrinsic Control of Hepatocellular Carcinoma by TAM Receptors.* Cancers (Basel), 2021. **13**(21).

11. Llovet, J.M., et al., *Immunotherapies for hepatocellular carcinoma.* Nat Rev Clin Oncol, 2022. **19**(3): p. 151-172.

12. Chen, Y. and Z. Tian, *HBV-Induced Immune Imbalance in the Development of HCC.* Front Immunol, 2019. **10**: p. 2048.

13. Alvarez, C.S., et al., *Analysis of TP53 aflatoxin signature mutation in hepatocellular carcinomas from Guatemala: A cross-sectional study (2016-2017).* Health Sci Rep, 2020. **3**(2): p. e155.

14. Kew, M.C., *Synergistic interaction between aflatoxin B1 and hepatitis B virus in hepatocarcinogenesis.* Liver Int, 2003. **23**(6): p. 405-9.

15. Wang, H., et al., *It takes a team: a gain-of-function story of p53-R249S.* J Mol Cell Biol, 2019. **11**(4): p. 277-283.

16. Engin, A.B. and A. Engin, *DNA damage checkpoint response to aflatoxin B1.* Environ Toxicol Pharmacol, 2019. **65**: p. 90-96.

17. Puigvehi, M., et al., *The oncogenic role of hepatitis delta virus in hepatocellular carcinoma.* JHEP Rep, 2019. **1**(2): p. 120-130.

18. Pfister, D., et al., *NASH limits anti-tumour surveillance in immunotherapy-treated HCC.* Nature, 2021. **592**(7854): p. 450-456.

19. McCoach, C.E. and T.G. Bivona, *The evolving understanding of immunoediting and the clinical impact of immune escape.* J Thorac Dis, 2018. **10**(3): p. 1248-1252.

20. Hanahan, D. and R.A. Weinberg, *Hallmarks of cancer: the next generation.* Cell, 2011. **144**(5): p. 646-74.

21. Furuta, M., et al., *Whole genome sequencing discriminates hepatocellular carcinoma with intrahepatic metastasis from multi-centric tumors.* J Hepatol, 2017. **66**(2): p. 363-373.

22. Yamamoto, S., et al., *Spatial and temporal expansion of intrahepatic metastasis by molecularly-defined clonality in multiple liver cancers.* Cancer Sci, 2020. **111**(2): p. 601-609.

23. Evgeny V. Denisov, T.S.G., Marina V. Zavyalova, *Inter- and Intratumor Heterogeneity in Hepatocellular Carcinoma.* Springer, 2016.

24. Panneerselvam, S., et al., *Overview of hepatocellular carcinoma: from molecular aspects to future therapeutic options.* Cell Adh Migr, 2023. **17**(1): p. 1-21.

25. Reig, M., et al., *BCLC strategy for prognosis prediction and treatment recommendation: The 2022 update.* J Hepatol, 2022. **76**(3): p. 681-693.

26. Nevola, R., et al., *Predictors of early and late hepatocellular carcinoma recurrence.* World J Gastroenterol, 2023. **29**(8): p. 1243-1260.

27. Kim, E. and P. Viatour, *Hepatocellular carcinoma: old friends and new tricks.* Exp Mol Med, 2020. **52**(12): p. 1898-1907.

28. Du, Z. and C.M. Lovly, *Mechanisms of receptor tyrosine kinase activation in cancer.* Mol Cancer, 2018. **17**(1): p. 58.

29. He, L., et al., *Differential expression of Axl in hepatocellular carcinoma and correlation with tumor lymphatic metastasis.* Mol Carcinog, 2010. **49**(10): p. 882-91.

30. Caruso, S., et al., *Analysis of Liver Cancer Cell Lines Identifies Agents With Likely Efficacy Against Hepatocellular Carcinoma and Markers of Response.* Gastroenterology, 2019. **157**(3): p. 760-776.

31. Faivre, S., L. Rimassa, and R.S. Finn, *Molecular therapies for HCC: Looking outside the box.* J Hepatol, 2020. **72**(2): p. 342-352.

32. Jiang, Y.Q., et al., *Investigating Mechanisms of Response or Resistance to Immune Checkpoint Inhibitors by Analyzing Cell-Cell Communications in Tumors Before and After Programmed Cell Death-1 (PD-1) Targeted Therapy:*

An Integrative Analysis Using Single-cell RNA and Bulk-RNA Sequencing Data. Oncoimmunology, 2021. **10**(1): p. 1908010.

33. Seydi, H., et al., *Autophagy orchestrates resistance in hepatocellular carcinoma cells.* Biomed Pharmacother, 2023. **161**: p. 114487.

34. Golkowski, M., et al., *Pharmacoproteomics Identifies Kinase Pathways that Drive the Epithelial-Mesenchymal Transition and Drug Resistance in Hepatocellular Carcinoma.* Cell Syst, 2020. **11**(2): p. 196-207 e7.

35. Breitenecker, K., et al., *Synergism of the receptor tyrosine kinase Axl with ErbB receptors mediates resistance to regorafenib in hepatocellular carcinoma.* Front Oncol, 2023. **13**: p. 1238883.

36. Reichl, P., et al., *Axl activates autocrine transforming growth factor-beta signaling in hepatocellular carcinoma.* Hepatology, 2015. **61**(3): p. 930-41.

37. Gonzalez-Sanchez, E., et al., *The TGF-beta Pathway: A Pharmacological Target in Hepatocellular Carcinoma?* Cancers (Basel), 2021. **13**(13).

38. Zhang, K., et al., *The dichotomous role of TGF-beta in controlling liver cancer cell survival and proliferation.* J Genet Genomics, 2020. **47**(9): p. 497-512.

39. Grusch, M., et al., *The crosstalk of RAS with the TGF-beta family during carcinoma progression and its implications for targeted cancer therapy.* Curr Cancer Drug Targets, 2010. **10**(8): p. 849-57.

40. Haider, C., et al., *Transforming Growth Factor-beta and Axl Induce CXCL5 and Neutrophil Recruitment in Hepatocellular Carcinoma.* Hepatology, 2019. **69**(1): p. 222-236.

41. Sakurai, T., et al., *Hepatocyte necrosis induced by oxidative stress and IL-1 alpha release mediate carcinogen-induced compensatory proliferation and liver tumorigenesis.* Cancer Cell, 2008. **14**(2): p. 156-65.

42. Pastushenko, I. and C. Blanpain, *EMT Transition States during Tumor Progression and Metastasis.* Trends Cell Biol, 2019. **29**(3): p. 212-226.

43. Yang, J., et al., *Guidelines and definitions for research on epithelial-mesenchymal transition.* Nat Rev Mol Cell Biol, 2020. **21**(6): p. 341-352.

44. Giannelli, G., et al., *Role of epithelial to mesenchymal transition in hepatocellular carcinoma.* J Hepatol, 2016. **65**(4): p. 798-808.

45. Miettinen, P.J., et al., *TGF-beta induced transdifferentiation of mammary epithelial cells to mesenchymal cells: involvement of type I receptors.* J Cell Biol, 1994. **127**(6 Pt 2): p. 2021-36.

46. Nieto, M.A., et al., *Emt: 2016.* Cell, 2016. **166**(1): p. 21-45.

47. Becker, A., et al., *Extracellular Vesicles in Cancer: Cell-to-Cell Mediators of Metastasis.* Cancer Cell, 2016. **30**(6): p. 836-848.

48. Minciacchi, V.R., M.R. Freeman, and D. Di Vizio, *Extracellular vesicles in cancer: exosomes, microvesicles and the emerging role of large oncosomes.* Semin Cell Dev Biol, 2015. **40**: p. 41-51.

49. Wang, W., et al., *Promising Roles of Exosomal microRNAs in Systemic Lupus Erythematosus.* Front Immunol, 2021. **12**: p. 757096.

50. Schubert, A. and M. Boutros, *Extracellular vesicles and oncogenic signaling.* Mol Oncol, 2021. **15**(1): p. 3-26.

51. Shimasaki, T., S. Yamamoto, and T. Arisawa, *Exosome Research and Co-culture Study.* Biol Pharm Bull, 2018. **41**(9): p. 1311-1321.

52. Maas, S.L.N., X.O. Breakefield, and A.M. Weaver, *Extracellular Vesicles: Unique Intercellular Delivery Vehicles.* Trends Cell Biol, 2017. **27**(3): p. 172-188.

53. Tontanahal, A., I. Arvidsson, and D. Karpman, *Annexin Induces Cellular Uptake of Extracellular Vesicles and Delays Disease in Escherichia coli O157:H7 Infection.* Microorganisms, 2021. **9**(6).

54. Rogers, M.A., et al., *Annexin A1-dependent tethering promotes extracellular vesicle aggregation revealed with single-extracellular vesicle analysis.* Sci Adv, 2020. **6**(38).

55. Tognoli, M.L., et al., *Lack of involvement of CD63 and CD9 tetraspanins in the extracellular vesicle content delivery process.* Commun Biol, 2023. **6**(1): p. 532.

56. Fang, T., et al., *Tumor-derived exosomal miR-1247-3p induces cancer-associated fibroblast activation to foster lung metastasis of liver cancer.* Nat Commun, 2018. **9**(1): p. 191.

57. Mao, X., et al., *Nidogen 1-Enriched Extracellular Vesicles Facilitate Extrahepatic Metastasis of Liver Cancer by Activating Pulmonary Fibroblasts to Secrete Tumor Necrosis Factor Receptor 1.* Adv Sci (Weinh), 2020. **7**(21): p. 2002157.

58. Webber, J., et al., *Cancer exosomes trigger fibroblast to myofibroblast differentiation.* Cancer Res, 2010. **70**(23): p. 9621-30.

59. Kobayashi, M., et al., *Transforming growth factor-beta-induced secretion of extracellular vesicles from oral cancer cells evokes endothelial barrier instability via endothelial-mesenchymal transition.* Inflamm Regen, 2022. **42**(1): p. 38.

60. Hoshino, A., et al., *Tumour exosome integrins determine organotropic metastasis.* Nature, 2015. **527**(7578): p. 329-35.

61. Zhou, W., et al., *Cancer-secreted miR-105 destroys vascular endothelial barriers to promote metastasis.* Cancer Cell, 2014. **25**(4): p. 501-15.

62. Zhou, Z., et al., *Extracellular vesicles activated cancer-associated fibroblasts promote lung cancer metastasis through mitophagy and mtDNA transfer.* J Exp Clin Cancer Res, 2024. **43**(1): p. 158.

63. Bakir, B., et al., *EMT, MET, Plasticity, and Tumor Metastasis.* Trends Cell Biol, 2020. **30**(10): p. 764-776.

64. Zhao, H., et al., *The key role of extracellular vesicles in the metastatic process.* Biochim Biophys Acta Rev Cancer, 2018. **1869**(1): p. 64-77.

65. Costa-Silva, B., et al., *Pancreatic cancer exosomes initiate pre-metastatic niche formation in the liver.* Nat Cell Biol, 2015. **17**(6): p. 816-26.

66. Carrillo Sanchez, B., M. Hinchliffe, and D.G. Bracewell, *GFP-tagging of extracellular vesicles for rapid process development.* Biotechnol J, 2022. **17**(6): p. e2100583.

67. Peinado, H., et al., *Pre-metastatic niches: organ-specific homes for metastases.* Nat Rev Cancer, 2017. **17**(5): p. 302-317.

68. Melo, S.A., et al., *Glypican-1 identifies cancer exosomes and detects early pancreatic cancer.* Nature, 2015. **523**(7559): p. 177-82.

69. Schneider, C.A., W.S. Rasband, and K.W. Eliceiri, *NIH Image to ImageJ: 25 years of image analysis.* Nat Methods, 2012. **9**(7): p. 671-5.

70. Van Deun, J., et al., *The impact of disparate isolation methods for extracellular vesicles on downstream RNA profiling.* J Extracell Vesicles, 2014. **3**.

71. Corso, G., et al., *Reproducible and scalable purification of extracellular vesicles using combined bind-elute and size exclusion chromatography.* Sci Rep, 2017. **7**(1): p. 11561.

72. Global Burden of Disease Cancer, C., et al., *Global, Regional, and National Cancer Incidence, Mortality, Years of Life Lost, Years Lived With Disability, and Disability-Adjusted Life-years for 32 Cancer Groups, 1990 to 2015: A Systematic Analysis for the Global Burden of Disease Study.* JAMA Oncol, 2017. **3**(4): p. 524-548.

73. Boyer, M.J., et al., *Endothelial cell-derived extracellular vesicles alter vascular smooth muscle cell phenotype through high-mobility group box proteins.* J Extracell Vesicles, 2020. **9**(1): p. 1781427.

74. Tabak, S., S. Schreiber-Avissar, and E. Beit-Yannai, *Extracellular vesicles have variable dose-dependent effects on cultured draining cells in the eye.* J Cell Mol Med, 2018. **22**(3): p. 1992-2000.

75. Zougman, A., P.J. Selby, and R.E. Banks, *Suspension trapping (STrap) sample preparation method for bottom-up proteomics analysis.* Proteomics, 2014. **14**(9): p. 1006-0.

76. Cox, J. and M. Mann, *MaxQuant enables high peptide identification rates, individualized p.p.b.-range mass accuracies and proteome-wide protein quantification.* Nat Biotechnol, 2008. **26**(12): p. 1367-72.

77. Yu, F., et al., *Fast Quantitative Analysis of timsTOF PASEF Data with MSFragger and IonQuant.* Mol Cell Proteomics, 2020. **19**(9): p. 1575-1585.

78. Cox, J. and M. Mann, *1D and 2D annotation enrichment: a statistical method integrating quantitative proteomics with complementary high-throughput data.* BMC Bioinformatics, 2012. **13 Suppl 16**(Suppl 16): p. S12.

79. MacLean, B., et al., *Skyline: an open source document editor for creating and analyzing targeted proteomics experiments.* Bioinformatics, 2010. **26**(7): p. 966-8.

80. Emmanouilidi, A., et al., *Oncogenic and Non-Malignant Pancreatic Exosome Cargo Reveal Distinct Expression of Oncogenic and Prognostic Factors Involved in Tumor Invasion and Metastasis.* Proteomics, 2019. **19**(8): p. e1800158.

81. de Graauw, M., et al., *Annexin A1 regulates TGF-beta signaling and promotes metastasis formation of basal-like breast cancer cells.* Proc Natl Acad Sci U S A, 2010. **107**(14): p. 6340-5.

82. Pessolano, E., et al., *Annexin A1 May Induce Pancreatic Cancer Progression as a Key Player of Extracellular Vesicles Effects as Evidenced in the In Vitro MIA PaCa-2 Model System.* Int J Mol Sci, 2018. **19**(12).

83. Xing, X., et al., *ANXA2(Tyr23) and FLNA(Ser2152) phosphorylation associate with poor prognosis in hepatic carcinoma revealed by quantitative phosphoproteomics analysis.* J Proteomics, 2019. **200**: p. 111-122.

84. Chaudhary, P., et al., *Serum exosomal-annexin A2 is associated with African-American triple-negative breast cancer and promotes angiogenesis.* Breast Cancer Res, 2020. **22**(1): p. 11.

85. Maji, S., et al., *Exosomal Annexin II Promotes Angiogenesis and Breast Cancer Metastasis.* Mol Cancer Res, 2017. **15**(1): p. 93-105.

86. Rocha, M.R., et al., *Annexin A2 overexpression associates with colorectal cancer invasiveness and TGF-ss induced epithelial mesenchymal transition via Src/ANXA2/STAT3.* Sci Rep, 2018. **8**(1): p. 11285.

87. Esposito, I., et al., *Tenascin C and annexin II expression in the process of pancreatic carcinogenesis.* J Pathol, 2006. **208**(5): p. 673-85.

88. Mitra, A.K., et al., *Ligand-independent activation of c-Met by fibronectin and alpha(5)beta(1)-integrin regulates ovarian cancer invasion and metastasis.* Oncogene, 2011. **30**(13): p. 1566-76.

89. Ryu, S.H., et al., *Selumetinib Inhibits Melanoma Metastasis to Mouse Liver via Suppression of EMT-targeted Genes.* Anticancer Res, 2017. **37**(2): p. 607-614.

90. Rich, S., N. Van Nood, and H.M. Lee, *Role of alpha 5 beta 1 integrin in TGF-beta 1-costimulated CD8+ T cell growth and apoptosis.* J Immunol, 1996. **157**(7): p. 2916-23.

91. Hurwitz, S.N. and D.G. Meckes, Jr., *Extracellular Vesicle Integrins Distinguish Unique Cancers.* Proteomes, 2019. **7**(2).

92. Garmy-Susini, B., et al., *PI3Kalpha activates integrin alpha4beta1 to establish a metastatic niche in lymph nodes.* Proc Natl Acad Sci U S A, 2013. **110**(22): p. 9042-7.

93. Bhowmick, N.A., et al., *Integrin beta 1 signaling is necessary for transforming growth factor-beta activation of p38MAPK and epithelial plasticity.* J Biol Chem, 2001. **276**(50): p. 46707-13.

94. Odaka, H., et al., *CD63-positive extracellular vesicles are potential diagnostic biomarkers of pancreatic ductal adenocarcinoma.* BMC Gastroenterol, 2022. **22**(1): p. 153.

95. Ai, Y., et al., *Syntenin and CD63 Promote Exosome Biogenesis from the Plasma Membrane by Blocking Cargo Endocytosis.* bioRxiv, 2023.

96. Raiborg, C. and H. Stenmark, *The ESCRT machinery in endosomal sorting of ubiquitylated membrane proteins.* Nature, 2009. **458**(7237): p. 445-52.

97. Williams, C., et al., *Assessing the role of surface glycans of extracellular vesicles on cellular uptake.* Sci Rep, 2019. **9**(1): p. 11920.

98. Pupjalis, D., et al., *Annexin A1 released from apoptotic cells acts through formyl peptide receptors to dampen inflammatory monocyte activation via JAK/STAT/SOCS signalling.* EMBO Mol Med, 2011. **3**(2): p. 102-14.

99. Yang, T., et al., *TGF-beta receptor inhibitor LY2109761 enhances the radiosensitivity of gastric cancer by inactivating the TGF-beta/SMAD4 signaling pathway.* Aging (Albany NY), 2019. **11**(20): p. 8892-8910.

100. Bhatta, B. and T. Cooks, *Reshaping the tumor microenvironment: extracellular vesicles as messengers of cancer cells.* Carcinogenesis, 2020. **41**(11): p. 1461-1470.

101. Vestad, B., et al., *Size and concentration analyses of extracellular vesicles by nanoparticle tracking analysis: a variation study.* J Extracell Vesicles, 2017. **6**(1): p. 1344087.

102. Corso, G., et al., *Systematic characterization of extracellular vesicle sorting domains and quantification at the single molecule - single vesicle level by fluorescence correlation spectroscopy and single particle imaging.* J Extracell Vesicles, 2019. **8**(1): p. 1663043.

103. Kilinc, S., et al., *Oncogene-regulated release of extracellular vesicles.* Dev Cell, 2021. **56**(13): p. 1989-2006 e6.

104. Hanelova, K., et al., *Protein cargo in extracellular vesicles as the key mediator in the progression of cancer.* Cell Commun Signal, 2024. **22**(1): p. 25.

105. Tiwari, P.K., et al., *Extracellular Vesicular miRNA in Pancreatic Cancer: From Lab to Therapy.* Cancers (Basel), 2024. **16**(12).

106. Blume, K.E., et al., *Cleavage of annexin A1 by ADAM10 during secondary necrosis generates a monocytic "find-me" signal.* J Immunol, 2012. **188**(1): p. 135-45.

107. Bonowicz, K., et al., *Mechanism of Extracellular Vesicle Secretion Associated with TGF-beta-Dependent Inflammatory Response in the Tumor Microenvironment.* Int J Mol Sci, 2022. **23**(23).

108. Pillalamarri, N., et al., *Exploring the utility of extracellular vesicles in ameliorating viral infection-associated inflammation, cytokine storm and tissue damage.* Transl Oncol, 2021. **14**(7): p. 101095.

109. Doyle, L.M. and M.Z. Wang, *Overview of Extracellular Vesicles, Their Origin, Composition, Purpose, and Methods for Exosome Isolation and Analysis.* Cells, 2019. **8**(7).

110. Lee, Y.X.F., et al., *Considerations and Implications in the Purification of Extracellular Vesicles - A Cautionary Tale.* Front Neurosci, 2019. **13**: p. 1067.

111. Rodrigues-Junior, D.M., et al., *Extracellular Vesicles and Transforming Growth Factor beta Signaling in Cancer.* Front Cell Dev Biol, 2022. **10**: p. 849938.

112. Johnson, S.M., et al., *Large Extracellular Vesicles Can be Characterised by Multiplex Labelling Using Imaging Flow Cytometry.* Int J Mol Sci, 2020. **21**(22).

113. Soe, Z.Y., E.J. Park, and M. Shimaoka, *Integrin Regulation in Immunological and Cancerous Cells and Exosomes.* Int J Mol Sci, 2021. **22**(4).

114. O'Grady, T., et al., *Sorting and packaging of RNA into extracellular vesicles shape intracellular transcript levels.* BMC Biol, 2022. **20**(1): p. 72.

115. Kreimer, S., et al., *Mass-spectrometry-based molecular characterization of extracellular vesicles: lipidomics and proteomics.* J Proteome Res, 2015. **14**(6): p. 2367-84.

116. Hung, Y., et al., *The exosomal compartment protects epidermal growth factor receptor from small molecule inhibitors.* Biochem Biophys Res Commun, 2019. **510**(1): p. 42-47.

117. Kranich, J., et al., *In vivo identification of apoptotic and extracellular vesicle-bound live cells using image-based deep learning.* J Extracell Vesicles, 2020. **9**(1): p. 1792683.

118. Boudna, M., et al., *Strategies for labelling of exogenous and endogenous extracellular vesicles and their application for in vitro and in vivo functional studies.* Cell Commun Signal, 2024. **22**(1): p. 171.

119. Jin, Y., et al., *Extracellular signals regulate the biogenesis of extracellular vesicles.* Biol Res, 2022. **55**(1): p. 35.

120. Yue, M., et al., *Extracellular vesicles remodel tumor environment for cancer immunotherapy.* Mol Cancer, 2023. **22**(1): p. 203.

121. Yan, R., H. Chen, and F.M. Selaru, *Extracellular Vesicles in Hepatocellular Carcinoma: Progress and Challenges in the Translation from the Laboratory to Clinic.* Medicina (Kaunas), 2023. **59**(9).

122. Marchisio, M., et al., *Flow Cytometry Analysis of Circulating Extracellular Vesicle Subtypes from Fresh Peripheral Blood Samples.* Int J Mol Sci, 2020. **22**(1).

I List of abbreviations

AFB1	Aflatoxin B1
AFP	α-Fetoprotein
ANXA1	Annexin A1
ANXA2	Annexin A2
BCLC	Barcelona Clinic Liver Cancer
BMI	Body mass index
BMPs	Bone mophogenic proteins
BSA	Bovine serum albumin
CAFs	Cancer-associated fibroblasts
CCM	Concentrated conditioned medium
CI	confidence Interval
CM	Conditioned medium
CRC	Colorectal cancer
DMSO	Dimethyl sulfoxide
DTT	Dithiothreitol
ECL	Enhanced Chemiluminescence
ECM	Extracellular matrix
EE	Early endosome
EMT	Epithilial-mesenchymal-transition
ER	Endoplastmatic reticulum
ESCRT	Endosomal-sorting-complex-required for transport
EVs	Extracellular Vesicles
FCS	Fetal calf serum
FGF1	Fibroblast growth factor 1
FN	Fibronectin
GDFs	Growth and differentiation factors
GFP	Green Fluorescent Protein
HCC	Hepatocellular carcinoma
HGDN	high-grade dysplastiv nodules
HGF	Hepatocyte growth factor
HSCs	Hepatic stellate cells
HUVECs	Human umbilical vein endothelial cells
ICB	Immune checkpoint blockade
ICI	Immune checkpoint inhibitors
IFN	Interferon

ILV	Intraluminal vesicles
IM	intrahepatic metastasis
INTa5	Integrin α5
INTβ1	Integrin beta 1
LAP	Latency associated peptide
LGDN	low-grade dysplastic nodules
LT	Liver transplantation
MC	multi-centric occurence
MEK	mitogen-activated protein
MET	Mesenchymal-epithelial transition
MIF	Migration Inhibitory Factor
MMP	Matrix metalloproteinases
MVB	Multivesicular bodies
MVs	Microvesicles
NAFLD	Non-alcoholic fatty liver disease
NASH	non-alcoholic steatohepatitis
NTA	Nanoparticle tracking analysis
P/S	Penicillin/Streptomycin
PAA	Polyacrylamide
PBS	Phosphate-buffered saline
PDAC	Pancreatic ductal adenocarcinoma
PI3K	Phosphoinositide 3 kinase
PMN	Pre-metastatic niche
Pros1	Protein S1
PS	Phosphatidylserine
RFA	Radio-frequency ablation
RR	Relative Risk
RT	Room temperature
RTKs	Receptor tyrosine kinases
SCC	Single cell clone
SD	Standard deviation
SDS	Sodium dodecyl sulfate
SLC	Small latent complex
β-ME	beta-mercaptoethanol
TACE	transarterial chemoembolization
TGF-β	Transforming growth factor beta

Tim4	T-cell immunoglobulin-and-mucin-domain-containing molecules 4
TME	Tumor microenvironment
TNC	Tenascin C
TNFR1	Tumor necrosis factor receptor 1
WT	Wild-type

II List of tables

III List of figures